NTNU

Norwegian University of
Science and Technology

# Timing and Mechanism of magmatic sill emplacement in the Vøring Basin, Norwegian Sea

Christiana Odonkor

Petroleum Geosciences
Submission date: December 2017
Supervisor: Ståle Emil Johansen, IGP
Co-supervisor: Kamal Omosanya, IGP

Norwegian University of Science and Technology
Department of Geoscience and Petroleum

**Abstract**

The Vøring Basin is a magma-rich basin, which has several voluminous magmatic sill complexes emplaced within during Paleocene/Eocene continental rifting and break-up in the NE Atlantic. This intrusive event has had a significant impact on deformation, source-rock maturation and fluid flow in the basin. Magmatic sheet intrusions contribute significantly to the upper crustal magma transport network in the basin. The emplacement mechanism of the magmatic sheets controls the final geometry of the intrusions and the characteristics of host rock deformation. The aims of this study are to understand the emplacement mechanism and timing of magmatic event in the Vøring Basin and the effects of the intrusions on the hydrocarbon system in the area. These aims were achieved through seismic interpretation of a Zero-phased, high-resolution, reversed polarity three-dimensional seismic data, petrophysical analysis of borehole data and statistical analysis of the magmatic sills and structures associated with the intrusions (Faults, forced-folds and hydrothermal vents).

Magmatic sills were identified as high-amplitude anomalies with similar polarity to the seabed reflection. Twelve (12) magmatic sills were interpreted mainly at the intermediate to deep levels of the Vøring Basin. The intermediate sills have areas ranging from $1.20 \times 10^8 m^2$ to $6.64 \times 10^8 m^2$ and lengths of 164 km to 171 km. The area coverage and lengths of the deeper sills range from $0.52 \times 10^8$ $m^2$ to $12.8 \times 10^8 m^2$and 77 km to 253 km respectively. Aspect ratio (length/width), A for the magmatic sills ranges from 0.19 – 0.56. The deep sills dominated the area and were mainly layer-parallel and basin-saucer shaped. Other sill facies like the saucer-shaped, transgressive, fault-plane, bowl-shaped and the eye-shaped were interpreted, mainly in the intermediate levels of the basin.

The mechanical strength of the host rock (brittle or ductile) plays a major role is the type of deformation caused by the emplacement of the sills. Ductile deformations are mainly force-folding and formation of magma figure whereas brittle structures are mainly hydrothermal vent complexes and bridges. Forced folding and hydrothermal vent structures associated with sill emplacement were used to constrain the timing of the magmatic evets by interpreting the bounding (upper and bottom) stratigraphic stratas in which these structures are accommodated. Two main phase of magmatic emplacement from the Late Paleocene to Earliest Eocene were identified in the Vøring Basin

## Preface

This thesis is submitted in partial fulfilment of the award of MSc degree in Petroleum Geosciences, specialization in Petroleum Geophysics at the Norwegian University of Science and Technology. The main objective of this thesis is seismic interpretation petrophysical analysis and statistical analysis of magmatic sills in the Vøring Basin to evaluate the emplacement mechanism and timing of the intrusion and their subsequent implication on the hydrocarbon propectivity in the study area.

Christiana Odonkor

**Dedication**

I dedicated this work to God Almighty, my family and loved ones who never gave up on me but supported and motivated me in every aspect of my existence.

**Acknowledgement**

My utmost appreciation goes to God Almighty for seeing me through and bringing me this far. I deeply thank my main supervisor Dr. Kamal'deen Olakunle Omosanya and co-supervisor Prof. Ståle Johansen for their patience and time for not giving up on me, but supported and assisted me throughout the work. I want to further appreciate and acknowledge Dr. Kamal'deen Olakunle Omosanya, Lisbeth Hultmann and Lars Espen Bjørgum for their motivation and time. I appreciate Marfo, George, Giannis Zervas and Siregar, Einstein for assisting me when I had some challenges during the work. Last but not the lease, I thank the Norwegian Government for the Quota Scheme Program that funded my study, Norwegian University of Science and Technology (NTNU) and the Department of Geoscience and Petroleum and Schlumberger for providing me with the Petrel software I used in the work.

**Contents**

**Figures**

# CHAPTER 1: INTRODUCTION

## 1.1. Background of the study

Most hydrocarbon prospective basins contain magmatic sheets intrusions and accompanying hydrothermal vent complexes (Planke et al., 2005; Jamviet et al., 2004). Most of these magma-rich basins are located along the Atlantic margins, the Arctic, and offshore Australia as shown in Fig 1.1 below. Due to the delicate nature of hydrocarbon exploration, investigation and assessment of oil and gas in magma-rich basins call for reliable ways for identification and interpretation of these intrusive complexes on seismic data (Planke et al., 1999; Rohrman, 2007). Use of other geophysical data from gravity and magnetic methods integrated with seismic data helps to understand volcanic processes and deposits and their impact on play assessment in a sedimentary basin (Rohrman, 2007).

Magma-rich basins are classified as sedimentary basins intruded by large volumes of magma (Planke et al., 2005). The processes and deposits associated with magmatism may have robust influence on the geometry and geodynamic growth of the continental margins and supplementary sedimentary basins (Planke et al., 2005; Svensen et al., 2003; Rodriguez Monreal et al., 2009; Schutter, 2003a, 2003b; Holford et al., 2012; Rohrman, 2007; Omosanya et al., 2017). Example of basins affected by voluminous magmatic complex emplacement as shown in Fig. 1.2 is the frontier Vøring and Møre Basins (Skogseid et al., 1992; Skogly 1998; Brekke, 2000; Gernigon et al., 2003). These basins were affected significantly by magmatic events, which included deformation, source-rock maturation and fluid flow (Planke et al., 2005; Svensen et al., 2003; Omosanya et al., 2017). Thus, it is important for hydrocarbon explorationists to identify magmatic deposits and evaluate their impacts on continental margins and how their presence affect the petroleum system in neighboring basins (Planke et al., 2005).

Magmatic intrusions have normally been seen to be associated and interact with fault planes by climbing along faults into the top levels of the basin (Thomson and Schofield, 2008; Magee et al. 2013c). Magmatic sills have been observed to feed themselves without the need for prevailing dykes, as increasing evidence would suggest that the rim of a lower sill can feed the base of an upper sill (Thomson and Hutton, 2004; Cartwright and Hansen, 2006). As a result, sill complexes are formed in an interconnected sequence of intrusions which can flood widely through a basin fill in all directions both vertically and horizontally. Hydrothermal vent complexes are formed if sufficiently large pressures are generated to fracture the overburden in low permeability sequences. The vent complexes commonly originate from the upper

terminations of transgressive sill segments, and consist of a pipe connecting the aureole to a crater at the paleo-surface (Planke et al., 2005). Magmatic sill emplacement may yield in the formation of forced fold in the overburden strata.

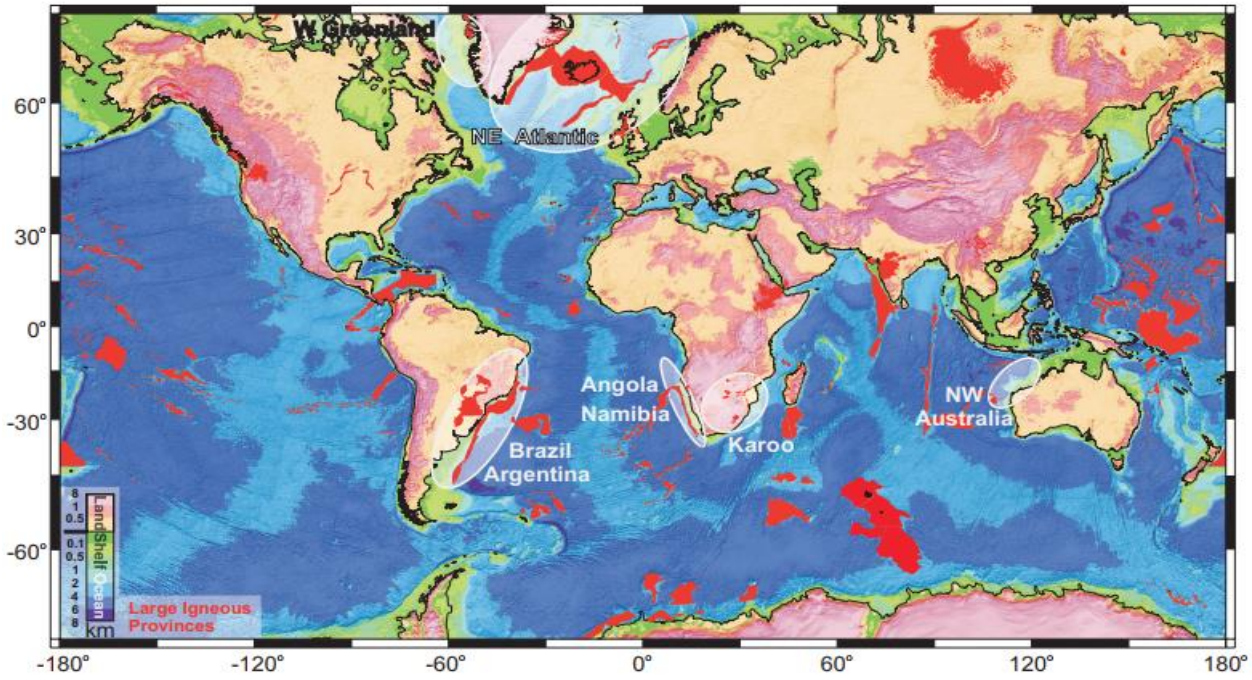


Fig 1.1: Magma-rich basins found along many of the world's prospective rifted margins, particularly the North and South Atlantic oceans (Gray Ellipses on the map) (Coffin and Eldholm., 1994; Planke et at., 2003).

Furthermore the emplacement of magmatic sills, may have a major impact on basin history and petroleum systems. The implication of sill emplacement may be temporal or permanent (Planke et al., 2005 and Rohrman, 2007). Temporal (short-term) effects may include heating of host rock, deformation, uplift, metamorphism of adjacent rocks, petroleum maturation and boiling of host-rock fluids, possibly leading to the formation of hydrothermal vent complexes (Plank et a., 2005 and Rohrman, 2007). The permanent (long-term) effects may include compartmentalization, directional fluid flow and shielding of the sedimentary sequence by the formation of solid dolerite and hornfels, and differential compaction. These effects are being studied and investigated by combined seismic reflection imaging and interpretation example in NE Atlantic margins, fieldwork in the well-known volcanic basin, the Karoo basin, South Africa; central-east Greenland and geodynamic modelling which includes magma emplacement, heat transport, maturation and boiling activities (Svensen et al. 2003; Jamtveit et al. 2004; Malthe-Sørenssen et al. 2004).

Metamorphic reactions during sill emplacement into the host rock strata may lead to the formation of large volumes of greenhouse gases such as methane and carbon dioxide, or ozone-depleting gases such as chlorinated and brominated halocarbons if evaporite basins are intruded. Svensen et al., 2004, suggested that rapid release of such gases to the atmosphere may have triggered rapid global warming and mass-extinction events several times during Earth history. The igneous intrusions also have an impact on the petroleum and mineral prospectivity of sedimentary basins. The sill complexes may represent long-lasting barriers to fluid flow, whereas fracture contact zones and hydrothermal vent complexes may lead to focused fluid flow. The permeable zones are good targets for water exploration drilling in dry regions such as the Karoo of South Africa (Chevallier and Woodford 1999).

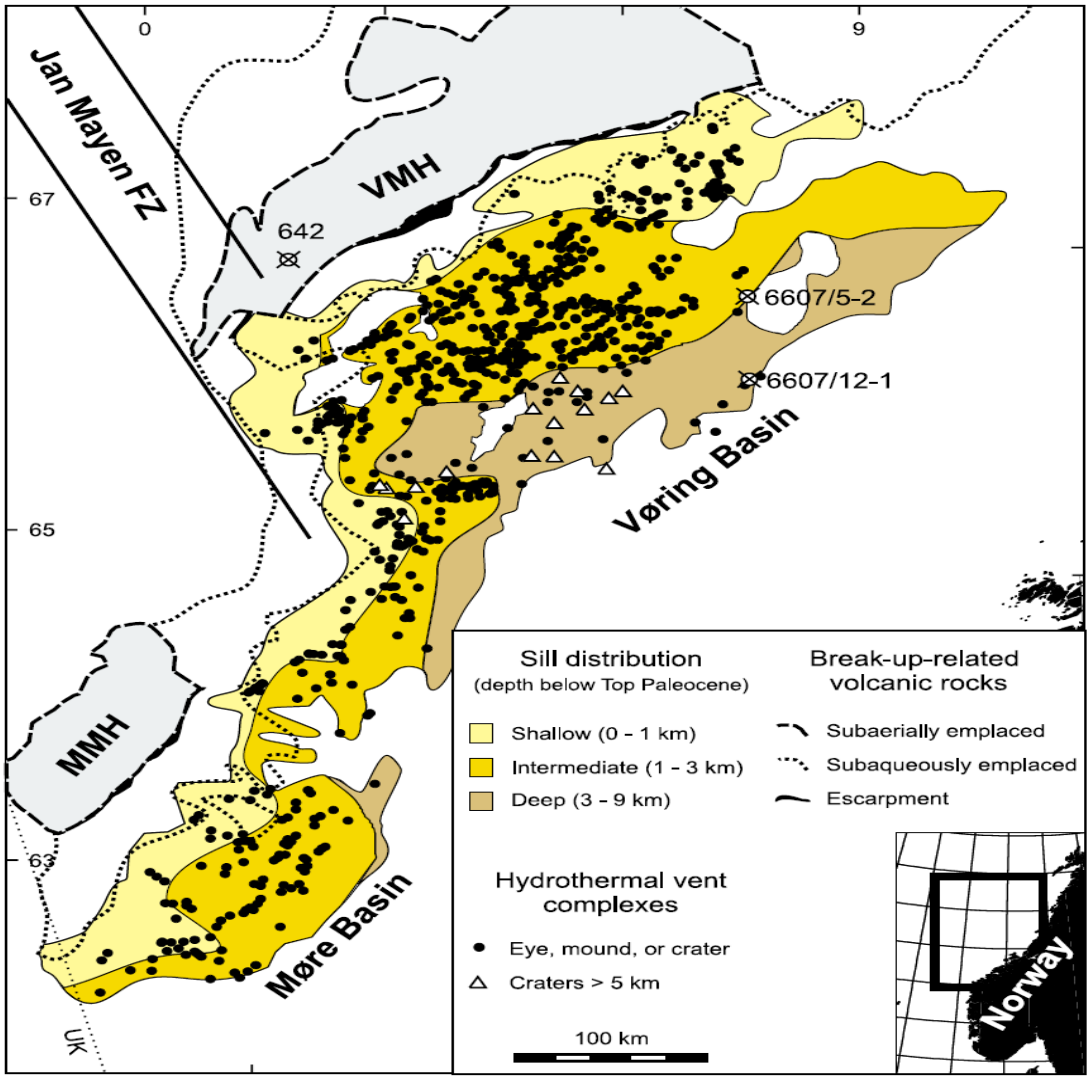

Fig 1.2: Distribution of sill intrusions and location of hydrothermal vent complexes in the Vøring and Møre basins. MMH, Møre Marginal High; VMH, Vøring Marginal High; FZ, Fracture Zone (Planke et al., 2005)

Conventionally, dating of intrusion event of sills in sedimentary basins has been subjected to only radiometric dating, even though, igneous intrusions have been studied for more than a century and their basic geometries and emplacement mechanisms are well known (Bradley, 1964; Du Toit, 1920; Pollard and Johnson., 1973) and this method has proven to have some inaccuracies. Radiometric dating may be subject to errors due to alteration or poor sampling, as is the case in many subsurface sills penetrated by boreholes (Gibb and Kanaris-Sotiriou., 1988 and Trude et al., 2003). Trude et al., 2003, proposed a new dating technique use to constrain magmatic sill emplacement by interpreting forced folds and hydrothermal vents structures associated with the igneous bodies in sedimentary basin. Three-dimensional seismic interpretation is an ideal means with which to analyze sill emplacement because of the high spatial resolution of igneous bodies and their associated deformational and hydrothermal structures (Davies et al., 2002 and Trude et al., 2003; Planke et al., 2005). 3D seismic data have the potential to identify new features not previously recognized at outcrop because of scale and resolution limitations and most critically their lack of three-dimensionality. Interpretation of 3D seismic data has already led to many novel discoveries including polygonal fault systems (Cartwright 1994; Cartwright and Dewhurst 1998), large-scale density inversion structures (Davies et al. 1999), giant pockmarks (Cole et al. 2000), dyke-fed submarine volcanoes (Davies et al. 2002), and flow structures in a shallowly emplaced igneous sill (Trude 2004). Numerous models have been published to account for the geometry and emplacement of igneous intrusions at shallow level (duToit 1920; Bradley 1965; Leaman 1975; Francis 1982; Lister and Kerr 1991; Kerr and Lister 1995; Chevallier and Woodford 1999) as well as the nature of associated hydrothermal systems (Einsele et al. 1980; Boulter 1996).

## 1.2. Aim and Objectives

The aims of the thesis are to;

- Understand the origin and mode of emplacement of magmatic sills in the study area.
- Interpret sill geometries and their influence of pristine basin structures and their host strata

The main objectives of this research work are as follows:

- To evaluate the mechanisms of sill emplacement.
- To investigate how sill interact with geological structures such as faults, forced – folds and hydrothermal vents in the area.
- To characterize magmatic sills based on their morphometries
- To establish the timing of emplacement of the magmatic sills.

### 1.3. Location of the Study area

The Vøring Basin is a sedimentary basin that formed during and subsequent to a major Late Jurassic-Early Cretaceous extensional episode (Skogseid et al., 1992). The Vøring basin is located between 64ºN- 68ºN and 2ºE - 10ºE (Fig 1.3) and consists of grabens, basins and structural highs (Blystad et al. 1995). To the north and south of the Vøring Basin are the Brivost and Jan Mayen Lineaments, respectively (Blystad et al. 1995). The Vøring Basin is bounded in the east by the Kristiansund-Bodø Fault Complex and the basement highs forming the extension of the Lofoten trend (Bukovics and Ziegler, 1985). The Vøring basin is bounded in the west and northwest by the Vøring Plateau Escarpement (Bukovics and Ziegler, 1985).

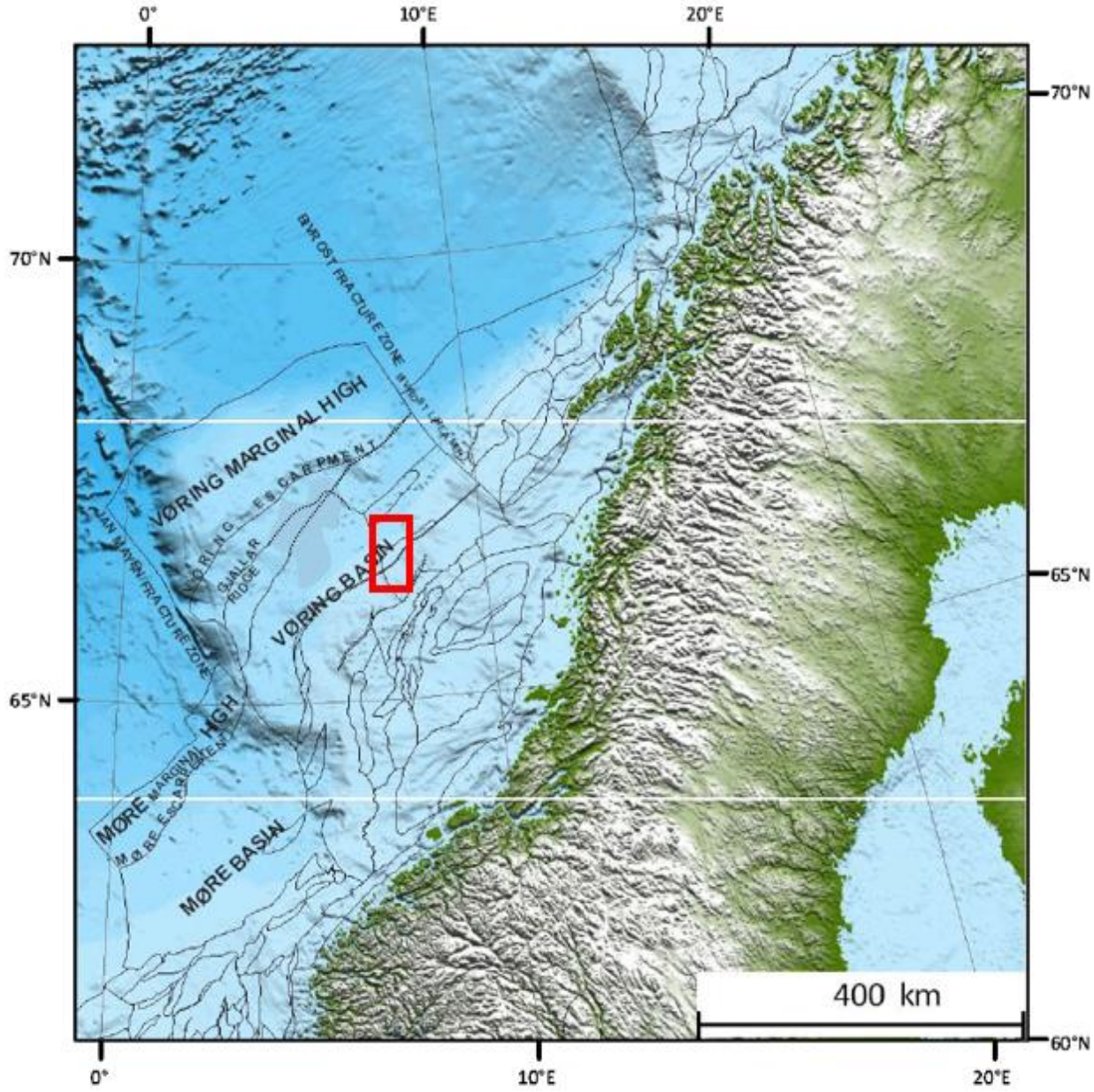


Fig 1.3 Bathymetric map of the Norwegian Sea showing the location of the study area in the red box (Modified from Njone, 2014)

The southeastern part of the Vøring Basin represents a deep Cretaceous depocentre, whereas the northwestern part (the Fenris and He1 Graben) is dominated by Cenozoic subsidence resulting from Late Cretaceous-Paleocene extension and subsequent break-up (Skogseid and Eldholm. 1989). The Surt Lineament which is parallel to the Jan Mayen and Brivost Lineaments divides the basin as follows (Blystad et al. 1995): a central anticline occurring in the Vøring Basin in the Cretaceous along the Fles Fault Complex is flanked by two synclines, south of the Surt Lineament; the basin is divided into three synclines in the north of the Surt

Lineament into Træna Basin (east), Någrind Syncline and Hel Graben (west) separated by the Utgard and Nyk Highs.

### 1.4. Thesis structure

The thesis is divided into five chapters as shown in Table 1. Chapters 1 is about the introduction to the research. Chapter 2 is the literature review which includes the geological setting of the study area and main concept of the study (Magmatic sills). Chapter 3 includes the various methods I employed in the research to attain the interpretation and results in Chapter 4. Chapter 5 includes the discussion and conclusion to back the results from the study.

Table 1. The Structure of the thesis

| Chapter | Content |
|---|---|
| 1 | Introduction |
| 2 | Literature Review |
| 3 | Data and Methods |
| 4 | Results and Interpretation<br>- Horizon interpretation<br>- Magmatic sill Interpretation |
| 5 | Discussion and Conclusion |

# CHAPTER 2: LITERATURE REVIEW

## 2.1. Geological history of the Norwegian Sea

The Norwegian Sea continental margin is dominated by two major basins with a very thick Cretaceous basin fill: the Vøring and Møre Basins (Brekke, 2000). These basins are flanked by the uplifted mainland and the Cretaceous Trondelag Platform to the east and by the More and Vøring Marginal Highs capped by Eocene lavas to the west (Brekke, 2000). The tectonic development of the area is controlled by two structural trends mainly in the NE-SW and NW-SE parts. Tectonically, the Norwegian Sea has been active since Carboniferous to Late Pliocene time with the main tectonic phases in Late Palaeozoic, late Mid-Jurassic-Early Cretaceous and Late Cretaceous-Early Tertiary time (Brekke, 2000). The overall tectonic development included a period of extension and rifting that ended in Early Eocene time by major volcanism, subsequent sea-floor spreading and continental separation, in the Norwegian-Greenland Sea (Brekke, 2000). The extensional tectonics were related to within-plate continental rifting during the Carboniferous to Early Cretaceous time (Brekke, 2000).

According to Brekke, 2000, the tectonics of the Late Cretaceous and the Tertiary periods were controlled by the relative movements along plate boundaries and the general NE-SW structural grain is established by faults and basin axes that perhaps was initiated in Late Palaeozoic time and were active during all subsequent tectonic phases. The transverse NW-SE trend is expressed as major lineaments that probably reflect the old, Precambrian grain of the basement (Brekke, 2000). Two of these lineaments are the continuation into the continental crust of major oceanic fracture zones, which controlled the tectonic activity during Cretaceous and Tertiary time and developed the boundaries between the major structural provinces of the area (Brekke 2000). The extension phase during the late Mid-Jurassic-Early Cretaceous brought about the differentiation into the Cretaceous basins and the bounding platforms and marginal highs (Brekke 2000). The remarkably thisckness of the basin resulted from the succeeding Cretaceous subsidence, where the basin flanks formed by flexuring rather than faulting (Brekke, 2000). In the Vøring Basin the Cretaceous development comprised an early thermal subsidence phase and a post-Cenomanian phase of tectonically driven subsidence involving intermittent phases of normal faulting and compression and folding (Brekke, 2000).

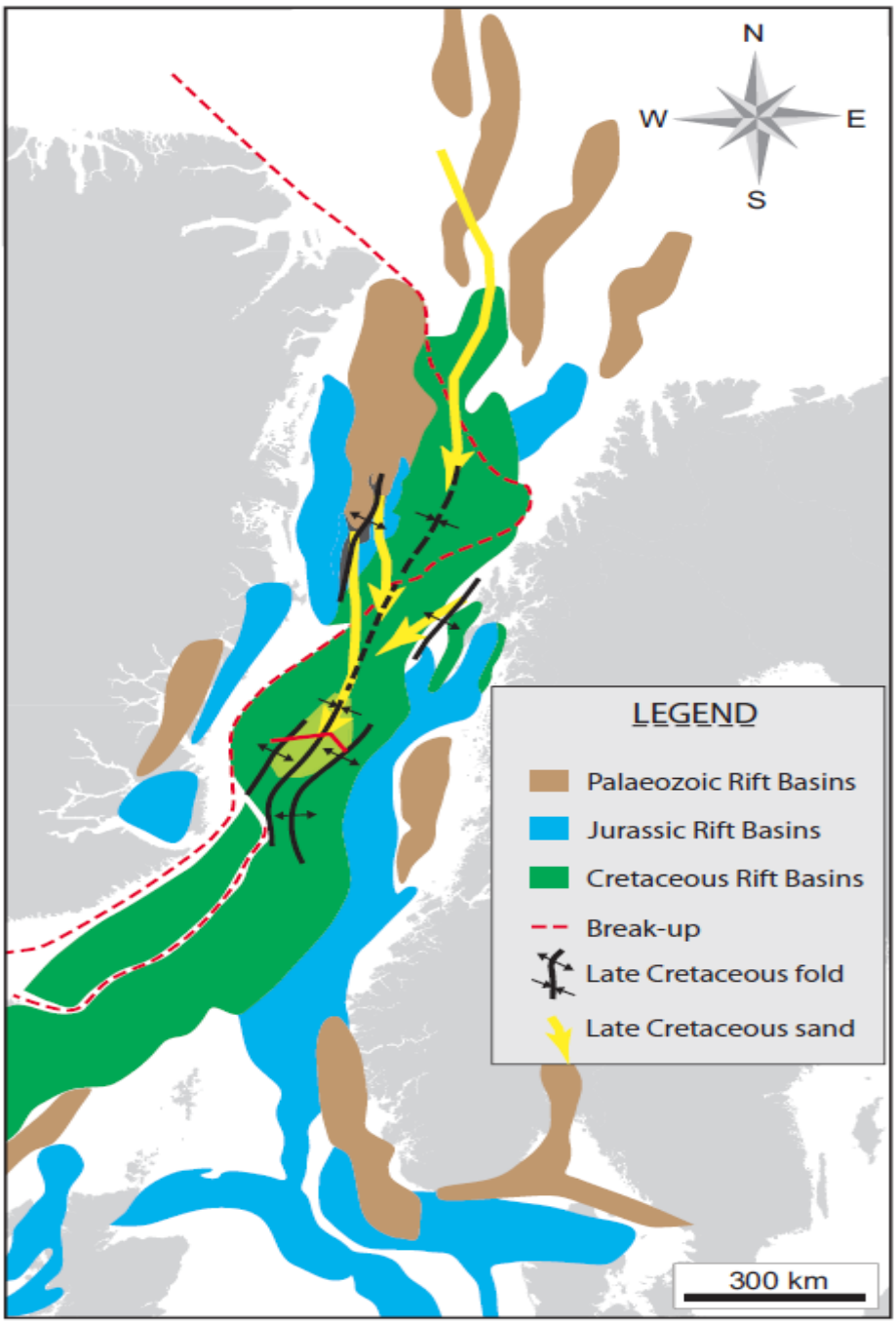


Fig 2.1. Pre-break plate reconstruction to 53 Ma, showing how younger rifts overprints older at an oblique angle (Lundin et al., 2013)

### 2.1.1. Tectonic Framework

According to Raum et al., 2002, two main plate tectonic episodes including the Caledonian collision and the break-up forming the North Atlantic occurred in the Norwegian Sea and the tectonic history can be divided into three epochs. Namely:

- Pre - Mid-Devonian: Final closure of the Iapetus Ocean during the Caledonian Orogeny

- Mid-Devonian to late Paleocene: A series of mainly extensional deformation episodes, culminating with the continental separation between Greenland and Eurasia.
- Early Eocene to present: Active seafloor spreading in the North Atlantic between Eurasia and Greenland

Raum et al., 2002 suggested that, the first epoch ended with the final closure of the Iapetus Ocean (proto-Atlantic Ocean) during the Caledonian orogeny in the late Silurian and early Devonian time and was followed by the epoch where an periodic extensional deformation culminating with the separation between the Eurasian and the Greenland plates during late Paleocene to early Eocene) took place.

The major basin development was initiated during the extensional episode from late Jurassic to early Cretaceous. This episode is most commonly subdivided into three phases; the late Bathonian/Callovian phase, the Kimmerian phase and the Neocomian phase. During the first two phases, the southern part of the Trøndelag Platform constituted the tectonically most active parts of the Platform (initiating formation of the Fles Fault Complex), and pronounced flexing and faulting took place along the eastern flanks of the Møre and Træna basins (Blystad et al., 1995). During the Neocomian phase, the separation between the Platform and basins became more distinct. In the period between the Neocomian rift phase and the end of Cenomanian, the Vøring and Møre basins experienced thermal subsidence, although pronounced expansion of the lower Cretaceous strata in the Ribban, Træna and Rås basin indicate faulting activity along boundary faults during Albian/Aptian time (Blystad et al., 1995). The post-Cenomanian subsidence was also the main period of subsidence in the Någrid syncline and Hel Graben, controlled by the Surt Lineament. This tectonic episode may have been related to rifting in adjacent areas, such as seafloor spreading in the Labrador Sea (Srivastava and Tapscott, 1986).

The uplift and eastward tilting of the westernmost part of the Vøring Basin initiated the formation of the Gjallar Ridge. This resulted in onlap of the post-Cenomanian on the eastward sloping upper interface of the Cenomanian along the Gjallar Ridge. A mirror image of this onlap may be seen on the Trøndelag Platform, especially across the Frøya High (Dewey, 1982). Renewed rifting, block faulting and an increased subsidence rate in the Vøring basin immediately followed this tilting of the basin flanks during the Turonian–Campanian time. Faulting was concentrated along the eastern flank of the late Cretaceous Vøring Basin, but some faulting is also observed along the Gjallar Ridge at the western flank of the basin (Blystad et al., 1995).

The final intra-continental rifting episode between the Greenland and Eurasian plates probably lasted from Campanian/Maastrichtian times until continental separation at the Paleocene/Eocene boundary. The rifting had its centre west of the Møre and Vøring Escarpments, but major mobile zones to the east (like the Jan Mayen Lineament, Fles Fault Complex and the Surt Lineament) were apparently reactivated, leading to local folding in the Vøring basin along the Fles Fault Complex (Blystad et al., 1995; Bjørnseth et al., 1997). The late syn-rift period of the Maastrichtian–Palaeocene episode involved central rift uplift that strongly affected western parts of the margin and areas north of the Jan Mayen Fracture Zone (Dore and Lundin, 1996). This caused erosion of the Møre and Vøring Marginal Highs together with highs and ridges in the Vøring basin. Increased clastic sediment input also indicates uplift and erosion of the mainland at that time. Additional uplift may have affected the outer margin areas due to emplacement of igneous material at the base of the crust, whereas widespread volcanic activity characterizes the phase of continental break-up and initiation of sea floor spreading (Skogseid et al., 1992).

The subsidence of the northeastern Atlantic margins following break-up indicates that significant lithospheric extension affected an approximately 300 km wide area along the final break-up axis (Skogseid, 1994). In the Vøring basin, the region west of the Fles Fault Complex shows extensional deformation by normal faulting, pronounced Cenozoic subsidence and igneous activity, indicating spatial correlation between areas affected by crustal and lithospheric thinning and melt generation.

Active spreading started in the earliest Eocene at about anomaly 24B (Skogseid and Eldholm, 1987), and from this time the regional stress regime changed from extensional to weakly compressional. This new stress regime resulted in the formation of major anticlines in the Vøring basin: Modgunn and Helland Hansen Arches together with the Vema and Nagelfar Domes. The mechanism behind this compressional process is not established. The last important tectonic period started in the Neogene, possibly in the latest Miocene to early Pliocene time, with strong differential tilting and asymmetric uplift of the mainland (Dore and Lundin, 1996). The uplift initiated strong erosion of the sedimentary cover and basement rocks of Scandinavia, creating an up to 1500-m-thick Pliocene/Pleistocene prograding succession across the shelf. This is clearly observed across the Helland Hansen Arch as a sedimentary wedge thinning towards the Fles Fault Complex.

2.1.1.2. Stratigraphic Framework

From Brekke et al., 1999, well data analysis show that the post-Lower Triassic stratigraphy of the platform and terrace sequences is made up of sedimentary rocks of Permian and possible Carboniferous age on top of crystalline basement, as in East Greenland (Surlyk et al. 1984; Surlyk, 1990) and are well identified (Dalland et al. 1988). Three conventional exploration wells tested wells ( (6607/5-1, 6607/5-2 and 6607/12-1) from the Northeastern part of the Vøring basin ended in the very thick Upper Cretaceous stratigraphic sequence, mainly comprising of deep marine clays. Reservoir sandstones in the Campanian and Coniacian can be identified in wells 6607/5-1 and 6607/5-2 drilled on the Utgard High and well 6707/10-1 on the Nyk High

The pre-Cenomanian sequences within the Vøring and Møre basins are still unknown, but extrapolation from the platform and terrace area to the east suggest a Lower Cretaceous basin fill of mainly deep marine shales (Brekke et al., 1999). The Paleocene and Eocene was a period of rapid shifts in palaeogeography and sedimentation patterns and the nature of the lithologies is largely speculative Deep Sea Drilling Project (DSDP) and Ocean Drilling Program (ODP) wells (Brekke et al., 1999). These wells have only penetrated to the Miocene and indicated a succession of Upper Pliocene sandy claystone overlying Miocene siliceous ooze and minor claystone in the Norwegian Sea continental margin (Talwani et al. 1976; Eldholm et al. 1987; Brekke et al., 1999).

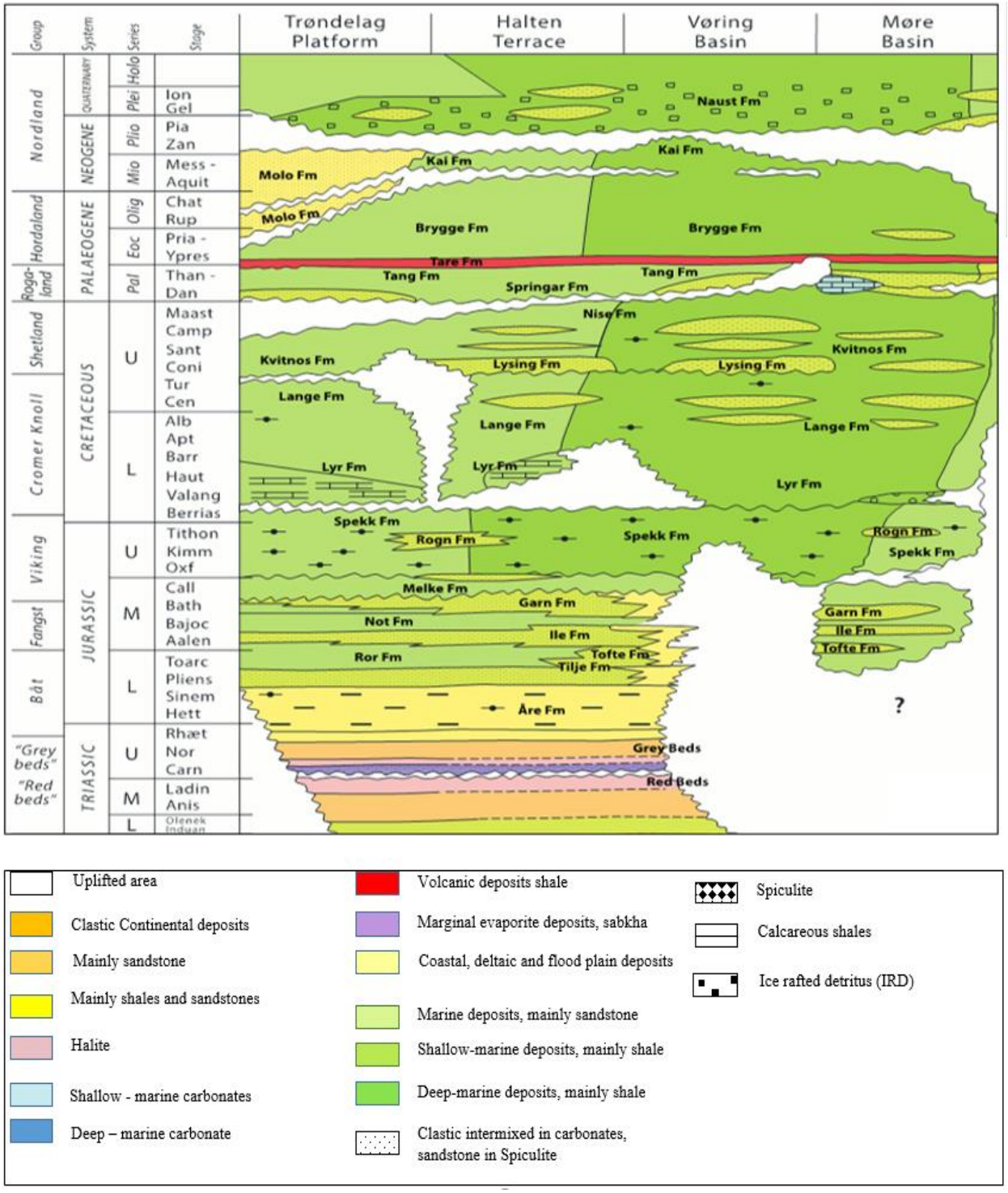


Fig 2.2. Lithostratigraphic summary of the Norwegian Sea shelf area (NPD, 2017)

According to Brekke et al., 1999, nine main local unconformities are known in the area's stratigraphy and these were evident in wells as shown in Fig 2.2 above. The platform regions have the three oldest unconformities and they are data with the East Greenland based on exploration well data and analogies (Surlyk et al. 1984). The other six younger local unconformities are identified on seismic data in both the basin and platform/ terrace areas (Brekke et al., 1999). All these unconformities may be tied to wells in the Halten and Donna

terraces and are supported by regional biostratigraphical studies (Eidvin and Riis 1991, 1992; Eidvin et al. 1993; Rundberg et al. 1995; Gradstein and Backstrom 1996).

### 2.1.2. The Tectonic Framework and Structural development of the Vøring Basin

Earlier researchers suggest that the Vøring Basin has a compound and complex extensional history. The youngest and most prominent extensional structures in the basin are of Palaeocene age (c. 65 Ma), immediately predating continental break-up west of the basin at around the Palaeocene–Eocene boundary (57.5 Ma, Skogseid et al. 1992a). These youngest faults are superimposed on older, more poorly imaged, structures of Jurassic and/or Cretaceous age. Direct analogy with the Halten Terrace area suggests a Late Jurassic age. The studies of Skogseid et al, 1992a and Walker et al. 1997, have used a Late Jurassic age for the earlier structures, but Lundin and Doré 1997 have suggested an alternative tectonic model with greater emphasis on Cretaceous extension (Brekke, 2000).

Structurally, the Vøring Basin can be divided into two sub-provinces by the Fles Fault Complex which is mainly a Late Jurassic–Early Cretaceous feature, but reactivated during the Late Cretaceous–Paleocene rifting (Brekke et al, 2000). The eastern sub-province comprises the Træna and Rås basins, whereas two prominent structural highs, the Gjallar Ridge and Nyk High, separate, respectively, the Vigrid and Någrind synclines from the Fenris and Hel grabens in the western sub-province. The Vøring Basin was tectonically active also during Tertiary time with the main phases of strike-slip-compression coinciding with the Alpine orogenies in Late Eocene and Mid-Miocene time (Brekke, 2000).

The Vøring Basin, bounded by the Bivrost and Jan Mayen lineaments of Blystad et al.1995, developed by regional subsidence subsequent to the Late Jurassic–Early Cretaceous extension episode (Skogseid et al., 1992b). However, the definition and the timing of the various tectonic events remain a matter of debate. For example, Brekke et al. 1999, suggested three main tectonic phases:

(1) Extension in late Middle Jurassic to late Cenomanian

(2) Extension and compression in late Cenomanian to early Paleocene, and

(3) Extension and compression from early Paleocene to the present.

On the other hand, Dore ´ et al., 1999 and Lundin and Dore ´, 1997 divided the Late Jurassic–Early Cretaceous extension episode into two separate tectonic phases (Late Jurassic and Early Cretaceous), suggesting that the Vøring Basin mainly formed by subsidence following Early Cretaceous extension. In addition to Late Cretaceous–Paleocene extension, a mid-Cretaceous extensional phase has been proposed (Dore ´ et al., 1999; Lundin and Dore ´, 1997).

- Late Mid-Jurassic to Late Cenomanian phase

The Fles Fault Complex probably originated as a Mid to Late Jurassic zone of normal faults with an eastward polarity along its northern NE-SW trending segment, and a westward polarity along its southern N-S trending segment. By several phases of reactivations, the Fles Fault Complex has played a central role in the tectonic development of the area since Early Cretaceous time. The Rås and Træna Basins were established as deep depocentres between the Fies Fault Complex to the west and the terraces to the east. The area to the west of the Fles Fault Complex, comprising the present Vigrid and Någrind Synclines, the Hel Graben and the Nyk High, probably constituted a single broad Early Cretaceous basin somewhat shallower than the Rås and Træna Basins. Researchers who prefer a shallower correlation for the base of the Cretaceous sequence to the west of the Fles Fault Complex have a regional high, informally termed the "Fulla Ridge', in place of the present author's western Early Cretaceous basin (Skogseid and Eldholm 1989: Skogseid et al. 1992).

The Gjallar Ridge, which is western part of the Vøring Basin was formed during Late Cenomanian-Early Turonian. To the north of the Gjallar Ridge, along the western margin of the Hel Graben, the Lower Cretaceous sequence is interpreted to thin in a similar way. This is taken to indicate that the western flank of the Early Cretaceous basin was situated more or less parallel to the present Gjallar Ridge, but probably offset to the west of the ridge along its central segments. This Early Cretaceous basin formation is believed to be the result of thermal subsidence after the major rifting episode in late Mid-Jurassic to Early Cretaceous time (Brekke et al., 1999)

- Late Cenomanian to Early Paleocene phase.

Through Cenomanian time the different depocentres of Early Cretaceous time and the Halten and Donna Terraces merged into one large basin, the Vøring Basin sensu stricto. This basin was mainly formed by the renewed tectonics that started in latest Cenomanian to earliest Turonian time and the associated subsidence that reached its maximum in Campanian time.

Hence, the Vøring Basin sensu stricto is defined at the post-Cenomanian Cretaceous levels (Blystad et al. 1995).

At the transition into Turonian time, the Gjallar Ridge started to rise and formed the western flank of the Vøring Basin. This is demonstrated by the thinning and onlap of the post-Cenomanian strata towards the tilted Top Cenomanian units on the eastern flank of the Gjallar Ridge. This Late Cenomanian-Early Turonian eastward tilting of the Gjallar Ridge is mirrored by a simultaneous westward tilt of the southern part of the Trøndelag Platform; across the Froya High and Froan Basin the post-Cenomanian sequence thins and onlaps the tilted Top Cenomanian units. This symmetrical basinward tilting of the basin flanks indicates that the development of the Vøring Basin started with a phase of renewed or accelerated subsidence. At the same time, or just afterwards, faulting activity started in the Gjallar Ridge and continued through Campanian time creating the complex pattern of strongly rotated fault blocks that characterizes the ridge (Brekke et al., 1999).

In the same period, renewed faulting activity took place in the Revfallet Fault Complex along the Nordland Ridge and on the eastern boundary faults of the Halten Terrace (the Bremstein and Vingleia Fault Complexes), across which the post-Cenomanian sequence demonstrates a marked growth. These fault complexes then acted as the eastern flank of the Vøring Basin, which implies that the Halten and Donna Terraces must be regarded as parts of the Vøring Basin sensu-stricto (Brekke et al., 1999).

In the northern part of the Vøring Basin, the Surt Lineament acted as a tectonic hinge zone in Late Cretaceous time. The post-Cenomanian sequence expands greatly to the north of the lineament. The lineament, including the Rym Fault Zone, constituted the southwestern flank of the Hel Graben in post-Cenomanian times and also marks the transition zone between the very thick post-Cenomanian deposits in the Någrind Syncline and the thinner post-Cenomanian succession of the Vigrid Syncline. The post-Cenomanian to Campanian thickness is more or less constant across the Någrind Syncline, Nyk High and the Hel Graben. This indicates that during most of the period from Cenomanian to latest Campanian-Maastrichtian time the area north of the Surt Lineament was a major depocentre before the formation of the synclines and highs.

The fact that the Late Cretaceous phase of subsidence in the Vøring Basin started slightly before the observed faulting activity, and that the maximum subsidence rate (in Campanian time) seems to have coincided with the maximum faulting activity, indicates that the formation

of the Late Cretaceous Vøring Basin was not the result of a simple sequence of rifting and consequent thermal subsidence. The Late Cretaceous subsidence was probably driven by active tectonic stresses rather than passive thermal relaxation. South of the Surt Lineament, the Vøring Basin seems to be regionally folded into a central anticline along the Fles Fault Complex, flanked by two synclines (Brekke et al., 1999).

The western syncline is termed the Vigrid Syncline, whereas the eastern syncline coincides with the Rås Basin. This regional folding suggests a probably regional compressional tectonic phase involving reactivation along the Fles Fault Complex. The role of the Fles Fault Complex is well demonstrated by the more intense internal folding of the Rås Basin to the east of the fault complex compared with the broad, open fold of the Vigrid Syncline to the west. The smaller scale internal folds of the Rås Basin have a NE-SW strike and may be seen on the map of the Top Cenomanian units. The folds are best developed in the regional bend where the strike of the fault complex changes from N-S to NE-SW, indicating space problems during the reactivation of the Fles Fault Complex. North of the Surt Lineament the Vøring Basin is folded into three NE-SW trending synclines (the Træna Basin, the Någrind Syncline and the Hel Graben) separated by two anticlines (the Utgard and Nyk Highs). The folds affect the whole of the Cretaceous sequence, but in the uppermost part of the Upper Cretaceous (Maastrichtian?) sequence the Någrind Syncline becomes progressively less tight, indicating a latest Campanian-Maastrichtian age for the folding. The Nyk and Utgard Highs show no internal onlaps and, therefore, must also have been formed in latest Cretaceous time. A possible minor growth of the uppermost Cretaceous sequence in the Hel Graben indicates that the faulting activity in the Nyk High and along the Rym Fault Zone that established the Hel Graben initiated just before the folding. This indicates that the overall anticlinal shape of the Nyk High and its position between the two synclines is the result of changing phases of both extension and compression.

Thinning of the Lower Cretaceous sequence indicates that the Utgard High was probably initiated as a marginal high along the Træna Basin already in Early Cretaceous time. However, its present shape as a faulted anticline between two synclines is the result of a combination of latest Cretaceous extension and subsequent compression similar to the development of the Nyk High. In addition to being a tectonic transfer and hinge zone, the Surt Lineament also probably marks a change in the substrate to the Cretaceous and latest Jurassic basin fill. South of the lineament the basin fill probably overlies Upper Palaeozoic to Jurassic strata, whereas to the north the basin fill rests directly on the crystalline basement or deeply eroded Upper Palaeozoic

rocks. In the north, this statement is based on a westward extrapolation of the geological relationships revealed by wells and seismic mapping of the northern part of the Trøndelag Platform. A westward thinning, caused by pre-Cretaceous erosion, of the basement cover across the platform edge and basin flanks indicates a very shallow basement also beneath the northern Vøring Basin. To the south, one may also argue for a shallow basement under the basin area from the erosional thinning of the basement cover in the Froya High and Sklinna Ridge along the platform and terrace edges. Influx of sand from the west into the western Halten Terrace during Mid-Jurassic time also indicates that the Vøring Basin area was subject to strong uplift and erosion then (Gjelberg et al. 1987).

However, the Jurassic and Triassic rocks are present in many parts of the basin margin along the terrace areas, indicating that Triassic, and perhaps Jurassic, deposits may also be present within the adjacent parts of the basin (Brekke at al. 1999). Sub-basin fill internal parallel reflectors in the Slettringen and Gjallar Ridges probably represent sediment layers. Across the whole of the Vøring Basin, the base of the Tertiary sequence is a regional angular unconformity constituting a generally even surface not involved in the folding of the underlying Cretaceous strata, substantiating the latest Cretaceous age for the folding. The major highs, such as the Gjallar and Nordland Ridges, the Nyk and Utgard Highs and the central anticline along the Fles Fault Complex, are seen to have been eroded. This means that the whole basin was uplifted at the end of the Cretaceous and beginning of the Tertiary period.

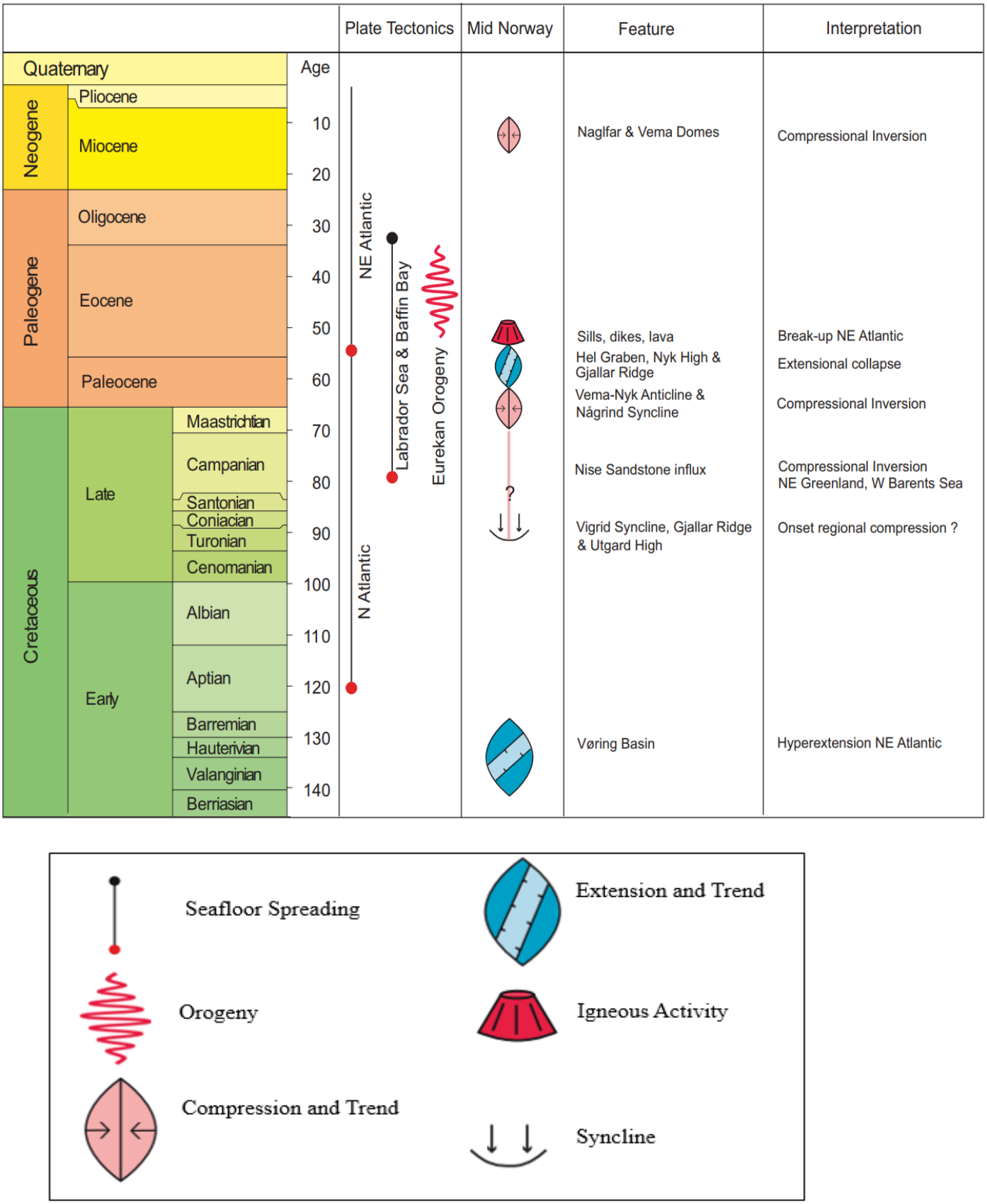


Fig 2.3. Tectonic events chat of the Vøring Basin (Modified from Lundin et al., 2013)

- Early Paleocene time to the present.

In the two large synclines, the Vigrid and Någrind Synclines, weak folding probably persisted into Paleocene time and the synclines were infilled by a Paleocene wedge that onlaps the syncline limbs. This indicates that the whole area stayed uplifted, giving erosion of the most elevated highs through most of Paleocene time. The uplift increased westwards so that the Gjallar Ridge was deeply eroded and was subsequently onlapped by the Paleocene sequence and progressively overstepped by early Eocene deposits. Even to the east some of the highest areas were also onlapped by the Paleocene sequence and overstepped by younger sediments; these areas include the Nyk High, the Nordland Ridge and an area in the northern R~s Basin close to the Surt Lineament flexuring along the Vøring Escarpment in the latest Eocene-Early Oligocene and Late Miocene times, respectively. This is indicated by the onlap of post-Eocene strata onto the flexure top of the Eocene sequence, and a similar relationship between the middle Miocene unconformity and Late Miocene strata. The same phases of movement are also recorded as the most important Tertiary reactivation phases on the major tectonic lineaments: the Jan Mayen and Bivrost Lineaments, the Fles Fault Complex and the Surf Lineament including the Rym Fault Zone. The activity resulted in large domes and arches that are well defined on the maps of the base Tertiary unconformity and of the Middle Miocene unconformity (Brekke et al., 1999).

Reverse reactivations of the Fles Fault Complex governed the growth of the very prominent Helland-Hansen Arch. A similar compressional structure, the Modgunn Arch, was controlled by reactivations on the Jan Mayen Lineament. South of 65~N the strata across the arch are continuous: this makes it possible to correlate the Cretaceous reflectors from well control in the east across the Fles Fault Complex into the western parts of the basin area. A study of the internal stratigraphic relationships of the Helland-Hansen Arch in this area supports the dating of the tectonic events. The Middle Miocene unconformity defines the present arch surface of the Helland-Hansen Arch. The Upper Miocene and Pliocene strata onlap and overstep this surface.

The unconformity is probably erosional and truncates the underlying strata. The oldest strata overlying this unconformity have been dated to latest Mid-Miocene time in nearby wells, and the youngest strata beneath the unconformity have been dated to Early Miocene time (Eidvin and Riis 1991). This implies that the latest phase of folding of the arch took place in Mid-Miocene time, according to the dating of Eidvin and Riis, 1991, 1992. (The dating of Gradstein and Backstrom, 1996 would place the event in Late Miocene time.) Flattening the unconformity

still leaves an arch structure at the Upper Eocene-Lower Oligocene surface. There are some indications of thinning and onlap onto this surface on the flanks of the arch, but these relationships are not conclusive. However, combined with the clear onlaps onto the flexure of the same surface along the Vøring Escarpment, these relationships indicate onset of folding of the arch already in latest Eocene to earliest Oligocene time.

In the northern part of the Vøring Basin, the Eocene and Miocene tectonics are controlled by the reverse reactivations along the Fles Fault Complex and the Surt Lineament, which initiated folding and doming of the Middle Miocene Unconformity. The Prominent Naglfar Dome is an inversion of the Hel Graben controlled by the Rym Fault Zone and the faults along the Nyk High. The Vema Dome is situated on the intersection between the Surt Lineament and the faults along the Nyk High. The Træma Basin was inverted along the Fles Fault Complex, giving rise to minor domes and arches.

In addition, the tectonic activity gave rise to further elevation of the Nordland Ridge, the Nyk and Utgard Highs. The Lower to Middle Miocene hiatus is recorded all over the Norwegian Continental Shelf (Eidvin and Riis 1989, 1991, 1992; Eidvin et al. 1993; Jordt et al. 1995; Gradstein and Backstrom 1996). This implies that just before the folding in Miocene time, there must have been a period of erosion or non-deposition to give the observed hiatus. As only deep-water faunas are recorded immediately below and above the unconformity, this must have been a submarine erosion, as an uplift of the whole basin area to above wave base seems excluded. However, Gradstein and Backstrom, 1996, stated that the basin flanks seem to have reached wave base and been considerably eroded. The mechanism behind this regional event of submarine erosion is not known. However, there is evidence of a regional uplift, lasting for about 7 Ma, of the whole continental margin and the surrounding mainlands in Early to Mid-Miocene time (Anderton et al. 1979; Jordt et al. 1995).

The Mid-Miocene folding created a significant submarine topography that lasted through Late Miocene time. The map of the Middle Miocene unconformity shows that the summit of the large domes and arches lies 1000-1800ms twt above the adjacent lows, corresponding to a sea-bottom topography of the order of 1000- 2000 m at that time. Substantial deposits of flat lying Upper Miocene sediments filled in the lows, onlapping and burying the tectonically created topography. A regional hiatus is also demonstrated at the base of the Upper Pliocene sequence along the continental margin (Eidvin and Riis 1989: Riis and Fjeldskaar 1992; Eidvin et al. 1993). On the mainland and in the shallow parts of the continental margin this hiatus is an unconformity related to uplift and deep erosion. In the deeper-water parts of the margin it is

mainly a surface of non-deposition, downlapped by the deposits of a huge sedimentary wedge prograding from the eroded mainland and shelf. However, in places this hiatus is an erosional unconformity also within the basin area.

In the Vøring Basin the Pliocene unconformity is relatively flat, and Upper Pliocene sediments overstep the Middle Miocene unconformity on the summit of the large domes and arches. In these elevated areas the Middle and Upper Miocene sequence is missing because of tectonic uplift, erosion and non-deposition: these areas include the Helland-Hansen Arch, the Naglfar and Vema Domes, the Nyk and Utgard Highs, the eastern edge of the Voting Marginal High, and areas involved in the Jan Mayen Lineament. The mechanism behind the regional, submarine erosion in Pliocene time is also unknown, but is clearly related to the onset of glaciations and rapid uplift of the surrounding mainland (Riis and Fjeldskaar 1992; Riis and Jensen 1992; Riis, 1996).

#### 2.1.2.2. Paleogeography

In the Norwegian continental margin, paleogeography can be categorized into pre- and post-continental breakup (Fig 2.4).

- Middle Jurassic

Understanding the development of the deep Møre and Vøring basins in the Cretaceous seems to be linked to the enigmatic influx of sand from the west into the western part of the Halten Terrace in the Middle Jurassic (Gjelberg et al. 1987 and Dore 1992). The sedimentology of the He and Garn formations there suggests the existence of an uplifted hinterland to the north and west large enough to sustain river systems capable of transporting fine to coarse sands. Brekke (in press) has suggested that the areas of the Møre and Vøring basins were at that time highly uplifted due to the early onset of increased heat flow and incipient faulting activity. Such a history implies that the Cretaceous and uppermost Jurassic basin fill rests unconformably on deeply eroded Lower Mesozoic and Upper Palaeozoic rocks; north of the Surt Lineament the substrate may even be eroded crystalline basement (Blystad et al. 1995; Brekke in press).

- Late Jurassic

In the late Middle Jurassic to earliest Cretaceous tectonic phase the crust beneath the Vøring and Møre basins became highly attenuated. The sea transgressed large parts of the area, though local highs on the shallow Trondelag Platform/Halten Terrace and along the More-Trøndelag

Fault Complex stayed emergent and were subject to erosion until the Kimmeridgian/ Volgian. During the Kimmeridgian, local shallow marine sands were deposited on the Trondelag Platform interbedded with the black shales of the Spekk Formation, an excellent source rock. At the same time the Vøring and Møre areas started to subside by down flexing of their basin flanks, leaving the shallow platforms along both sides (Brekke et al., 1999).

- Early Cretaceous

Sands and conglomerates of Hauterivian to Barremian age were deposited on the flanks of the emergent landmasses and islands as submarine fans and fan deltas (Surlyk 1990; Dore 1992; Jongpier et al., 1996). A regional transgression started in the Aptian and continued into the Late Cretaceous, slowly drowning the submerged land masses and islands (Brekke and Riis 1987; Surlyk 1990). Syntectonic submarine gravity flows - conglomerates and sands interbedded with Aptian and Albian deep marine shales - are found in East Greenland (Surlyk 1990). Submarine coarse elastics interbedded with deep marine shales are also recorded along elevated areas in the eastern Vøring and Møre basins (Hastings, 1987; Jongpier et al. 1996). These observations in surrounding areas suggest that sand was deposited as submarine gravity flows in the rapidly subsiding Vøring and Møre basins in Neocomian and Aptian-Albian times.

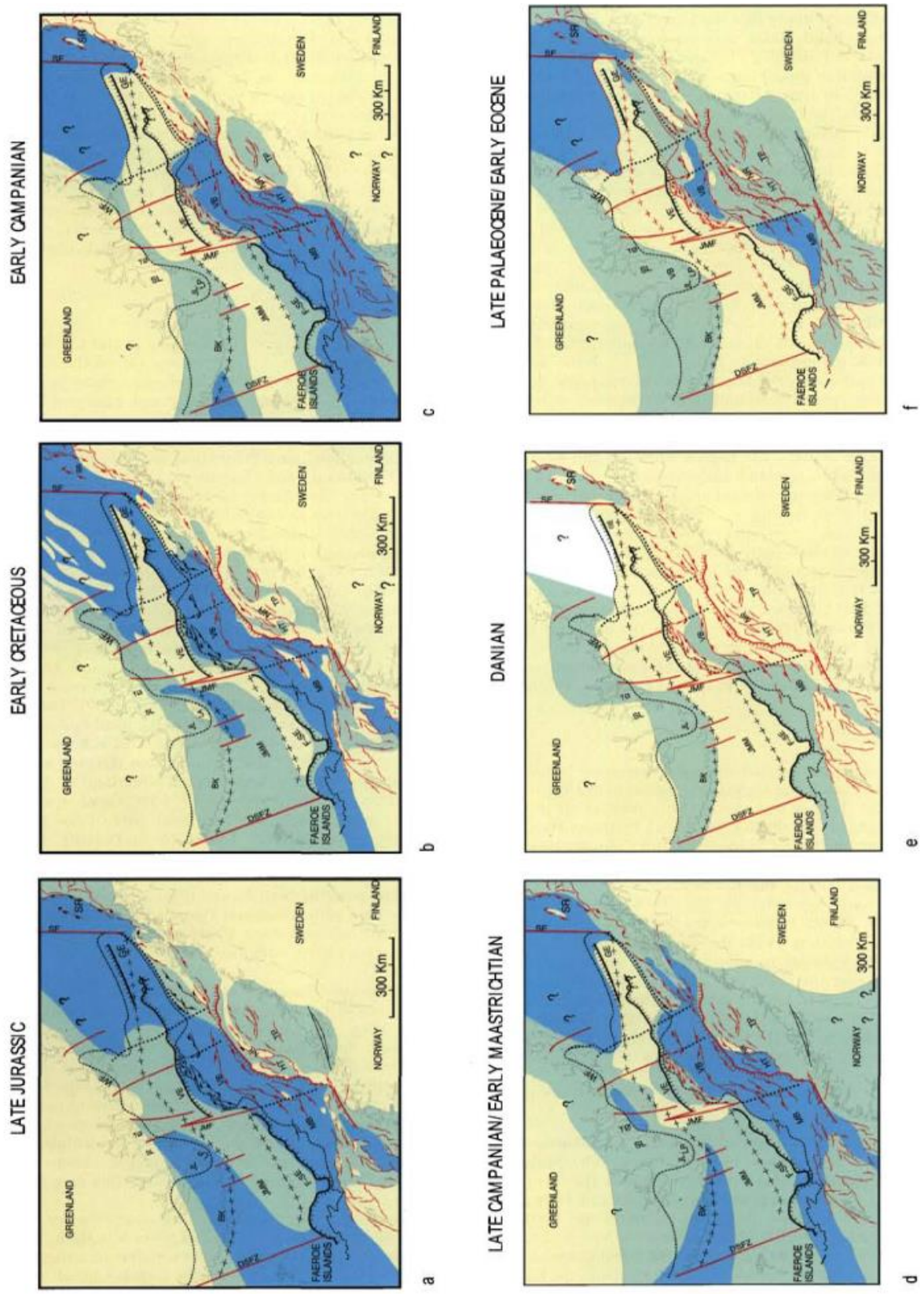


Fig 2.4. Possible reconstruction of Paleogeography of the Vøring basin. Red structures formed at or prior to the given time whereas black are yet to be formed (Brekke et al., 1999)

- Late Cretaceous

Late Cretaceous tectonic events, starting in end Cenomanian/ earliest Turonian times, were superimposed on the continued regional transgression. The onset of accelerated basin subsidence and conjugate uplift, tilting and emergence of the bounding platforms gave a base Turonian unconformity with basin flank onlaps and erosion. Local submarine sands of the Cenomanian Lange Formation, the Turonian/Coniacian Lysing Formation and Santonian Nise Formation are recorded along the flanks of the Nordland Ridge. The Lysing Formation is most likely derived from the local erosion of the Nordland Ridge, while the influx of the large volumes of sand in the northern part of the Vøring Basin (Utgard and Nyk highs) strongly indicates a substantial hinterland to the north and west in the Cenomanian to Late Campanian. This hinterland was probably the northern part of the emerged western bounding platform. This platform, running along the full length of both the Vøring and Møre basins, probably sourced similar Turonian to Campanian sands into the western parts of both basins (Brekke et al., 1999)

- Danian

Regional uplift in the latest Maastrichtian and Paleocene is recorded as a hiatus and erosional break across the Vøring Basin and the Vøring and Møre marginal highs. The Danian was therefore a period of dramatic shallowing of the Vøring and Møre and the emergence once again of the surrounding areas. In the Vøring Basin the bounding platforms, the basin flanks, highs and domes were eroded and sediments were deposited in the shallow Vigrid and Någrind synclines. These synclines may even have been temporary lacustrine basins. In the Vøring Basin the bounding platforms, the basin flanks, highs and domes were eroded and sediments were deposited in the shallow Vigrid and Någrind synclines. These synclines may even have been temporary lacustrine basins (Brekke et al., 1999)

- Late Paleocene and Early Eocene

Paleocene strata progressively filled the Vigrid and Någrind Synclines and then transgressed eastwards across the Trøndelag Platform and onto the mainland. Westwards, however, Paleocene strata never succeeded in over-stepping the eroded platform flank along the Gjallar Ridge. This was probably because of further uplift of the central platform area between Norway and East Greenland and the consequent eastward tilt of the western platform and basin, shifting the late Paleocene shoreline eastwards to the flanks of the Gjallar Ridge (Brekke et al., 1999).

- Post-Early Eocene

In the Vøring Basin, Eocene volcanoclastics and tuffaceous muds eventually overstepped the eroded Gjallar Ridge and the axis of the depocentre shifted westwards from the Vigrid Syncline in the Paleocene to the Gjallar Ridge. This indicates that the axial uplift had ended and the central landmass to the west had started to subside giving an increasing westward tilt to the whole margin. The main Early Eocene to Late Pliocene depocentre seems to have been to the west, bounded by the Surt and Jan Mayen lineaments, the Vøring Escarpment and the reversed Fles Fault Complex. A Lower to Middle Miocene hiatus is recorded on the Norwegian Continental Shelf (Eidvin and Riis 1989, 1991, 1992; Eidvin et al. 1993; Jordt et al. 1995; Gradstein and Backstrom 1996), but a mechanism to explain such widespread and profound submarine erosion or non-deposition is lacking (Brekke et al., 1999). Substantial deposits of flat-lying Upper Miocene muds and siliceous ooze filled in the lows, onlapping and burying the tectonically created topography (Brekke et al., 1999).

2.1.3. Lithostratigraphy of the study area

From the borehole data 6607/5-1, 6607/5-2 and 6607/2-1, the stratigraphy of the study area in the Vøring basin can be divided into five main groups with ages from Cretaceous to Quartenary.

2.1.2.1. Nordland Group

The group can be seen throughout the Mid Norwegian Shelf. It ages from the Early Miocene to recent. Sediments in the group were deposited in a marine environment under rapid subsiding basin, therefore characterized by significant westward prograding wedges (Dalland et al., 1988). The group is dominated by alternating claystone, siltstone and sandstone in the Norwegian Sea. The upper boundary of the Nordland group is the Seabed and made up of glacial to glacio-marine origin sediments. The group can be subdivided into the Kai and Naust formation from the wells in the study area (Dalland et al., 1988).

- Naust Formation

The Naust Formation is made up of mainly interbedded claystone, siltstone and sand. Grain size of sediments are occasionally coarse clastics in the upper part of the formation. The sediment in the formation are of marine origin but some transitional sediment from glaciomarine environments occur at the top part. The Formation is literally continuous across the Mid-Norwegian Shelf. Sediments were deposited during the Late Pliocene (Dalland et al., 1988, NPD 2017).

- Kai Formation

The Kai Formation is made up of alternating claystone, siltstone and sandstone with limestone stringers and the sand content differs locally. Shell fragments, Glauconite and pyrite are also common. The Formation was deposited in marine environment with variable water depths. The Kai Formation can be observed throughout the Haltenbanken area apart from the crest of the Nordland ridge. Sediments were deposited during Early Miocene to Late Pliocene (Dalland et al., 1988, NPD 2017)

2.1.3.2. Rogaland Group

The Rogaland group is dominated by sandstones interbedded with shales at the west. These sandstones form lobes which passes laterally into shales eastwards. In greatest part of the Norwegian region the group contains of argillaceous marine sediments. The buttom deposits usually consist of reworked limestones and marls and on the way to the top of the group the shales become progressively tuffaceous. The upper boundary of the Rogaland Group is marked by a change from laminated tuffaceous shales to more irregularly bedded sediments which are much less tuffaceous. The underlying chalk or marl sequences of the Shetland Group in contact with the Rogalnd group marks the base boundary. In the Norwegian Sea, the group is dated Danian to Late Paleocene and sediments were deposited in a deep marine environment. In the Norwegian Sea the Rogaland Group comprises the Tang and Tare Formations (Isaksen et al., 1989, Dalland et al., 1988).

- Tang Formation

The Tang Formation is made up of mainly dark grey to brown claystones with minor sandstone and limestone. The Formation is dated Danian to late Paleocene and deposition of sediments occurred in a deep marine environment. Laterally, the Tang Formation thins towards the northwest (Dalland et al., 1988, NPD 2017)

- Tare Formation

Dominated by dark grey, green or brown claystones with some thin sandstone stringers showing a variable content of tuff and increases at the base of the formation. The Formation was deposited during the Late Paleocene in a deep marine environment. Laterally, the formation is ubiquitous except near the crest of the Nordland Ridge and the tuff content decreases southwards (Dalland et al., 1988)

2.1.3.3. Hordaland Group

The Hordaland Group comprises of marine claystone with minor sandstone. The claystones are normally light grey to brown, fissile and fossiliferous. The base of the Group is sometimes marked by red and green claystone. Occurrence of thin limestones and streaks of dolomite can be observed. Fine to medium sandstones usually interbedded with claystones are established at various levels in the group. These sandstone content increases to the east. (Isaksen et al., 1989, Dalland et al., 1988). Deposition of sediments mainly occurred in a deep marine environment. The Group is dated Eocene to Early Miocene in the Norwegian Sea. In the study area the Hordaland group comprises of the Brygge Formation. (Isaksen et al., 1989, Dalland et al., 1988)

- Brygge Formation

The Formation is made up of mainly claystone with stringers of sandstones, limestones, siltstone and marl. The sandstone contain shell fragments, pyrite and glauconite. The Brygge formation is dated Early Eocene to Early Miocene and deposited in the marine environment (Dalland et al., 1988, NPD, 2017).

2.2.3.4. Shetland Group

The Group contains mainly chalk facies of chalky limestones, limestones, marls, and calcareous shales and mudstones with chert (flint) existing throughout the facies. The siliciclastic facies consists of mudstones and shales, partly interbedded with limestones. The shales and sandstones are slightly-very calcareous. Characteristically the lower boundary is the contact to the calcareous mudstones or marlstones of the Cromer Knoll Group (Dalland et al., 1988). The Group is overlain by Paleocene mudstones, marls or sandstones of the Rogaland Group. The Group is usually very thin on the Trøndelag Platform. The group ages from Turonian to Maastrichtian in the Norwegian Sea. Sediments deposition occurred in an open marine environment. From the wells in the study area, the Shetland Group is represented by four formations namely, the Kvitos, Nise, Springar and Delfin Formations (Dalland et al., 1988, NPD 2017).

- The Delfin Formation

The Formation consists of sandstones deposited during Early Campanian and Late Santonian age and is interpreted as a basin floor fan intercalated into shales of the Nise Formation. The Delfin Formation is named informally, no well type nor well reference sections have been established (Dalland et al., 1988, NPD 2017).

- Kvitos Formation

Made up of grey and greyish green calcareous claystones with carbonate and sandstone stringers. The Kvitos Formation is laterally continuous but absent on parts of the Nordland Ridge and on local highs along the western flank of the Trøndelag Platform; else the Formation is very thinly developed on the platform. Deposition of the Formation occurred during Turonian to Santonian age in an open marine environment (Dalland et al., 1988, NPD 2017).

- Nise Formation

The Nise Formation consists of grey and greyish-green claystones interbedded with carbonate and sandstone stringers. Similarly to the Kvitos formation, laterally the Nise Formation regionally extensive but missing on some parts of the Nordland ridge and on the local highs along the western flank of the Trøndelag Platform. The Nise Formation is dated Santonian and Campanian. Deposition of sediments in the Formation occurred in deep marine environment (Dalland et al., 1988, NPD 2017).

- Springar Formation

The Formation is made up of mainly greyish-green claystones interbedded with stringers of carbonates and sandstones. Laterally, the Formation is regionally extensive and missing only on parts of the Nordland Ridge. They are mainly open marine deposits and aged Campanian to Maastrichtian (Dalland et al., 1988, NPD 2017).

2.1.3.5. Cromer Knoll Group

The Cromer Knoll Group consists mainly of fine-grained, argillaceous, marine sediments with a varying content of calcareous material. Calcareous claystones, siltstones and marlstones dominate, but subsidiary layers of limestone and sandstone occur (Dalland et al., 1988, NPD 2017). The claystones are generally light to dark grey, olive-grey, greenish and brownish, repeatedly becoming light grey, light greenish-grey and light olive-grey marlstones and contain minerals like glauconite, pyrite and mica. Normally, marlstones become the more dominant lithology in both the upper and lower parts of the group. The Group is dated from Ryazanian to Turonian in the Norwegian Sea. The Group is absent on parts of the Nordland Ridge and on local highs along the western flank of the Trøndelag Platform (Dalland et al., 1988, NPD 2017).

- Lange Formation

The Lange Formation is predominantly light/medium grey to green and brown claystones consisting of stringers of carbonates and sandstones. Claystones in the Barremian-Aptian

interval are usually reddish-brown and are intermittently interbedded with tuffs. The formation is only missing from parts of the Nordland Ridge and on local highs along the western flank of the Trøndelag Platform. The Formation was deposited in marine environment from age Berriasian to Late Turonian (Dalland et al., 1988, NPD 2017).

- Lysing Formation

The Lysing Formation is predominantly made up fine to medium, seldom coarse grained, white-grey sandstones, partly carbonate-cemented and interbedded with shales. Deposition of formation occurred during the Late Turonian to Early Coniacian possibly in submarine fan environment from shallow to deep marine. (Dalland et al., 1988, NPD 2017).

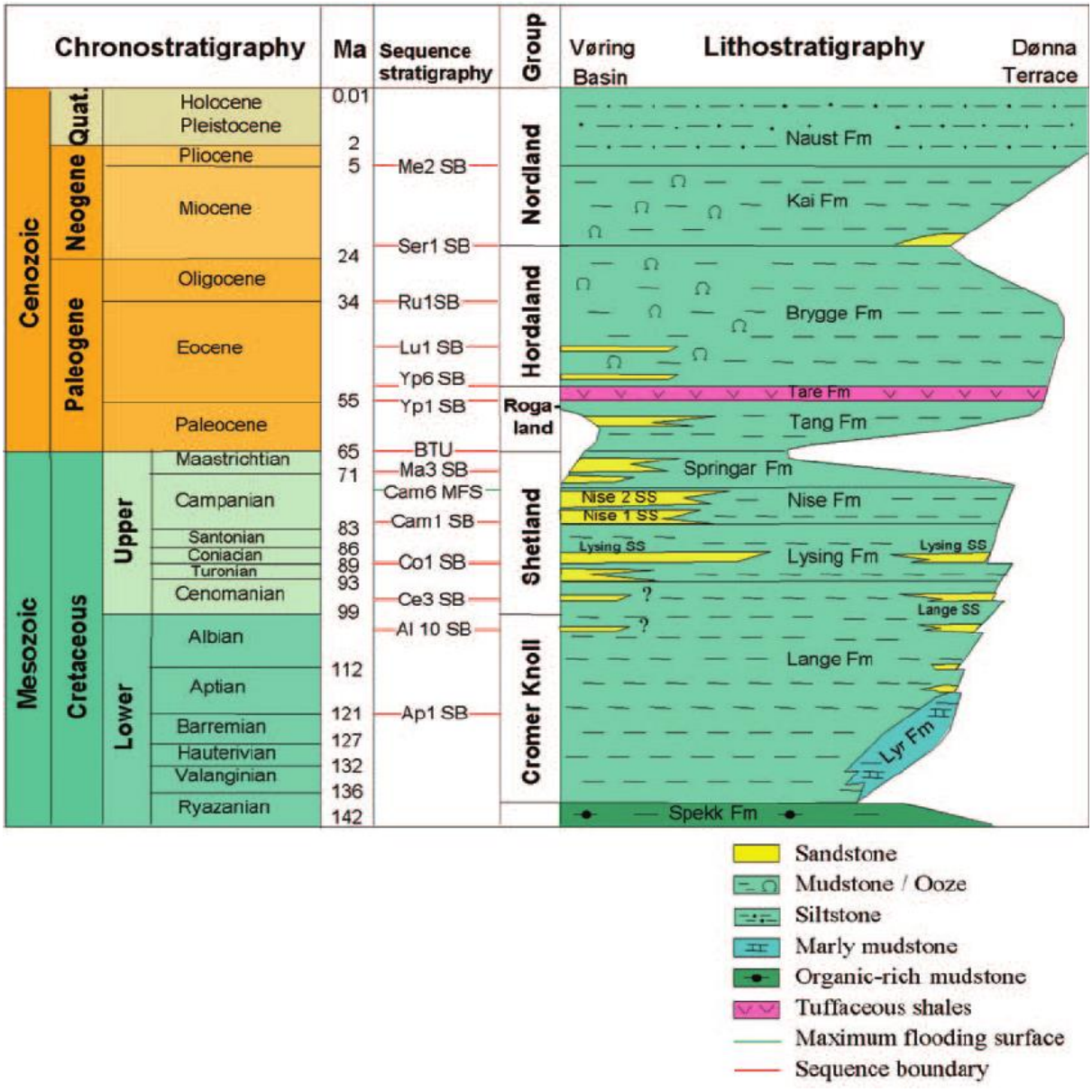


Fig 2.5. Summary of the stratigraphic coloumn of the Vøring Basin (Fjellanger et al., 2005)

### 2.1.4. Occurrence of Magmatic sills in the Vøring basin

The late rift phase was also associated with abundant intrusive igneous activity. Numerous sills and/or low-angle dykes appear as strong seismic reflections of good continuity terminating abruptly within the transparent and weakly layered pre-Tertiary sequences. The intrusions appear below the middle Campanian reflector, but become shallower in the stratigraphy and more abundant on the central Naglfar and Vema domes. In addition, the intrusions are fewer beneath the Gjallar Ridge and Nyk High, whereas they become abundant and thicker in the basinal areas, i.e. Hel Graben, Vigrid and Någrind synclines. Most intrusions follow the stratification, and commonly cut and/or follow the fault planes, suggesting a contemporaneous or later time of emplacement than the faulting.

According to Ren et al., 2003, the magmatic intrusions cut both the early and late rift phase faults, but they appear to follow early phase fault planes only. The sills are particularly abundant and thick in the Hel Graben, forming prominent complexes at 5 km depth (Berndt et al., 2000). The sill intrusions in the Vøring Basin have only been sampled in well 6607/5-2 on the Utgard High which penetrated three sills (Planke et al., 2005; Omosanya et al., 2016) Cuttings of the two lower sills (90 and estimated 150 m thick) show that they are coarse grained gabbroic mafic rocks with only little secondary alteration (Munz et al., 1997).The large amount of intrusives locally may have caused the observed pre-breakup doming and inversion of the Hel Graben, and amplified the rift flank uplift beneath the northern Vema Dome Sill intrusions east of the 'inner flows' the Cretaceous basin fill is intruded by numerous sills of probably latest Paleocene-earliest Eocene age. In the Vøring Basin the eastern limit of the sills generally coincides with the Fles Fault Complex. However, along the Jan Mayen and Bivrost Lineaments the intrusions are seen to extend further east, even into the flanks of the Trondelag Platform.

According to Brekke et al., 2000, the magmatic sills in the Møre and Vøring basins are mostly seen at their deepest position and lowest stratigraphic levels (Aptian?) to the east. These basins are generally stepping upwards towards the west to their highest levels (Maastrichtian) close to the front of the 'inner flows'; which is an indication that the sills originated from feeder dykes in the central parts of the basins (Brekke et al., 2000). Magmatic sills in the Gjallar Ridge found in the western parts of the Vøring Basin are semi-horizontal intrusions that cut across the eastward tilted bedding. Dykes from the west of the Fenris graben or the base of the Gjallar ridge might have been the main feeders to the sills present in the ridge (Ren et al., 2003).

## 2.2. Magmatic Sills

Magmatic basins are sedimentary basins with major components of intrusive and/or extrusive igneous rocks. Fig. 2.6 shows a sketch of a subvolcanic complex in a typical volcanic basin. Deep seated sills are dominantly layer parallel, whereas saucer-shaped sills are more common in the shallow intervals. The sills may form interconnected complexes, whereas dykes are less common (Skogseid et al., 1992; Planke et al., 2005; Cartwright and Hansen, 2006, Symonds et al., 1998; Magee et al 2013a, 2013b; Rohrman, 2013, 2015). .

Igneous intrusions particularly formed in rifted passive and volcanic basins are common in many sedimentary basins around the world. Rifting can result to melt production and is connected with Large Igneous Provinces (LIPs) and flood basalt emplacements in basins (Schofield et al., 2017). Most common intrusions are the sheet like intrusions observed in most sedimentary basins. They are predominantly mafic in composition, nevertheless ultramafic, andesitic, and felsic LIPs are also identified (Bryan and Ernst 2008; Bryan and Ferrari 2013). Tabular shaped sub volcanic sheet intrusions are dominant in most sedimentary basins, while laccoliths and plutons are less abundant (Planke et al., 2014) Studies have shown that most host rock units and associated properties have a serious impact on the emplacement and subsequent development of sills, resulting in a characteristic link between emplacement mechanisms and resultant sill morphology (e.g. Schofield et al. 2012a). The mechanical strength of the host rock at the moment of intrusion and the ability of the rock to act in a brittle or ductile (non-brittle) matter during the emplacement are the most dominant properties that affect the sill emplacement, growth and morphology. Sill emplacement is controlled largely by the form of consolidation and cementation in clastic rocks within the host rock during the time of emplacement (Schofield et al. 2012a). The several structures formed during volcanic intrusion depict the different mechanisms of magma emplacement (brittle and nonbrittle emplacement) and which can be used in outcrop to understand magma flow directions (Schofield et al. 2012a; Schofield et al., 2017).

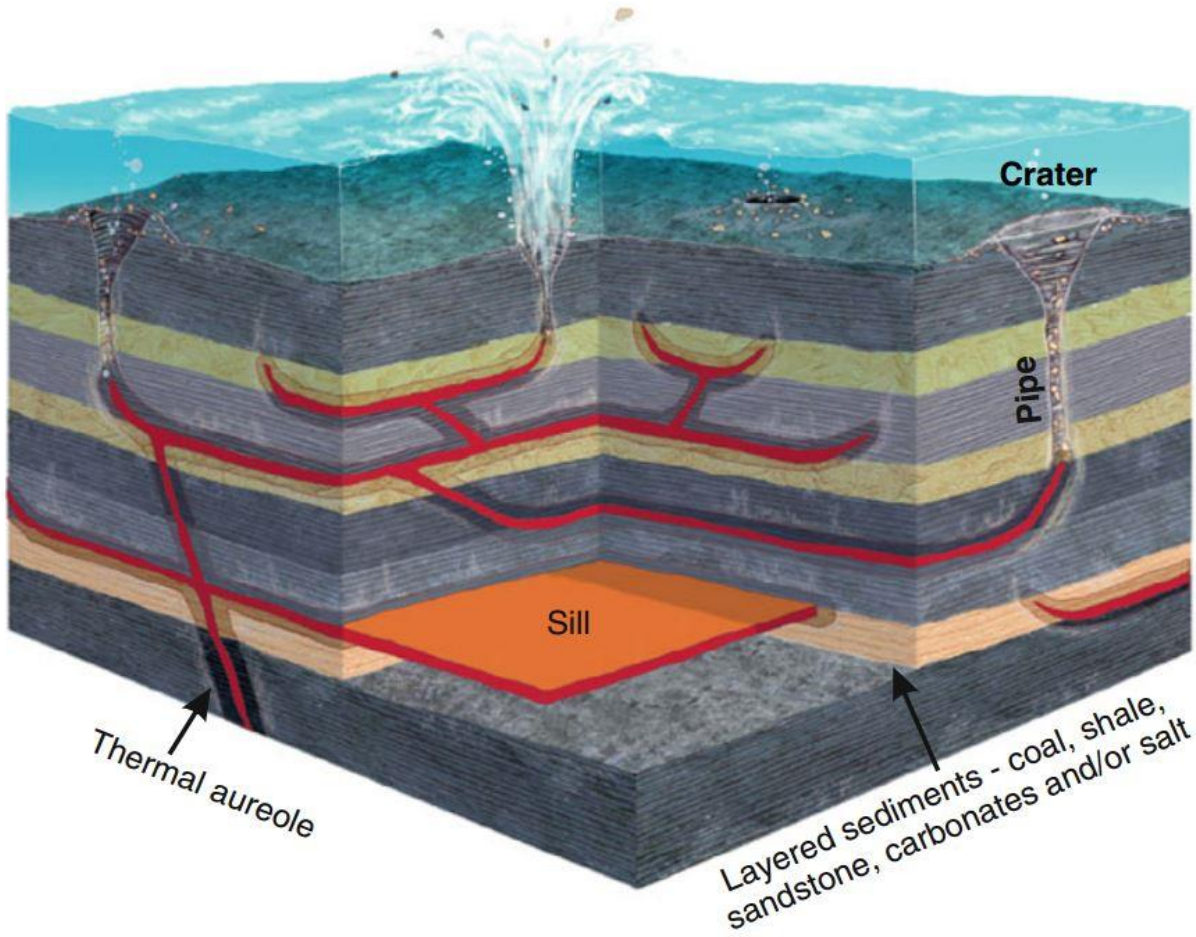


Fig 2.6. Sketch of a volcanic basin showing a sill complex (red), thermal aureoles and associated hydrothermal vent complexes. The vent complexes are typically located above the tip of transgressive sills, and consist of a vertical pipe and a crater at the seabed (Planke et al., 2014)

### 2.2.1. Models of sill emplacement (Post 3D seismic)

The uprising of information provided by 3D seismic data has led to a series of new models of sill emplacement

- **Thomson and Hutton (2004) and Bunger (1981)**

Thomson and Hutton, 2004 proposed a model of sill emplacement based on the laccolith emplacement model of Pollard and Johnson., 1973. Using opacity rendering to display relative thickness changes across saucer-shaped sills in the NE Rockall Trough, Thomson and Hutton (2004) defined lobe like features in the sills. By examining the branching patterns within these lobes, Thomson and Hutton, 2004 were able to infer paleoflow direction of the intruding

magma. Based on mapped out flow directions using these features they placed the feeder within the centre, or central axis of the saucer. Thomson and Hutton, 2004 proposed that the saucer-shaped geometry was the result of inflation of the inner sill causing uplift in the roof rocks allowing peripheral fracturing and intrusion of dykes to occur. This in turn enabled the magma to flow upwards and outwards away from the inner sill. Although the modified laccolith model of Johnson and Pollard ,1973 fits reasonably well with observations of upward magma flow, it does not account for the formation of flat outer rims, as seen in some saucer-shaped sills. In addition, field examples of saucer-shaped sills show no apparent evidence of having dykes cutting up through strata above the inner-dish, as predicted by the model (Chevalier and Woodford, 1999).

- **Malthe-Sørenssen et al. (2004)**

Malthe-Sørenssen et al., 2004, proposed a model of saucer-shaped sill intrusion based on 2D discrete element modelling. Within the model the sill began to propagate upwards
at the point that the length of the sill equalled that of the overburden thickness due to reorie tation of the stress field at sill tips, as a result of inner sill inflation. The re-orientation of the stress field at the sill tip led to brittle fractures being opened at an angle of approximately 45° to the horizontal, thus enabling the sill to climb upwards. The model was based on a nonviscous fluid, representing the magma, injecting into a homogenous elastic medium, representing the host rocks of a sedimentary basin. Within the Karoo basin, a general increase in inner sill diameter to the stratigraphically lower west region of the basin does occur (Chevalier and Woodford, 1999). This aspect is in agreement with the model of Malthe-Sørenssen et al.,2004 in that the inner sill needs to gain suitable diameter to allow rotation of the stress field at the tip of the sill. With increasing depth, the inner sill has to gain greater radius before the stress tips can reorientate.

The model of Malthe-Sørenssen et al., 2004, predicts a step-stair nature to the inclined transgressive sheet of saucer-shaped sills . This geometry is not ubiquitous across all saucer-shaped sills (Thomson and Hutton, 2004; Hansen and Cartwright, 2006: Thomson, 2007; Thomson and Schofield, 2008). Instead, in seismic and field observations the sills generally have a transgressive arcuate rim characterised by a curved sheet with generally increasing dip.

- **Goulty and Schofield, 2008**

Goulty and Schofield, 2008 employed elastic plate theory to explain the formation of saucer-shaped sills in a similar manner to Johnson and Pollard ,1973 who applied the same approach to laccoliths. Based on this, Goulty and Schofield, 2008 derived a relationship to predict the maximum radius of the inner sill based on the excess magma pressure and emplacement depth.

$$R = 2h\sqrt{\frac{E\varepsilon f}{3(1-v^2)\Delta\rho}}$$

R = Radius of Sill, h = Depth of emplacement, E = Young's modulus, _f = Radial tensile strain at failure, v = Poisson's Ration, p = magma pressure

In essence the relationship predicts that high tensile strains will develop at the sill periphery, and these will increase with increasing sill radius, so as the sill radius increases, eventually a point will be reached at the periphery were the tensile strain cannot be accommodated by the overburden, leading to failure. As a result increasing inner sill diameter will be expected with increasing sill depth, something which is seen in the Karoo basin (Chevalier and Woodford, 1999). Although the model of Goulty and Schofield (2008) does agree with observation of an increase in inner sill diameter with depth, the model has limitations. Goulty and Schofield ,2008, point out that the model is simplistic and only predicts up to the point of failure of the overburden, it makes no predictions in regard to the formation of the arcuate inclined sheet. In addition the fracture developed would initially be vertical, something which has not been documented in field or seismic data around the inner sill of saucer-shaped sills

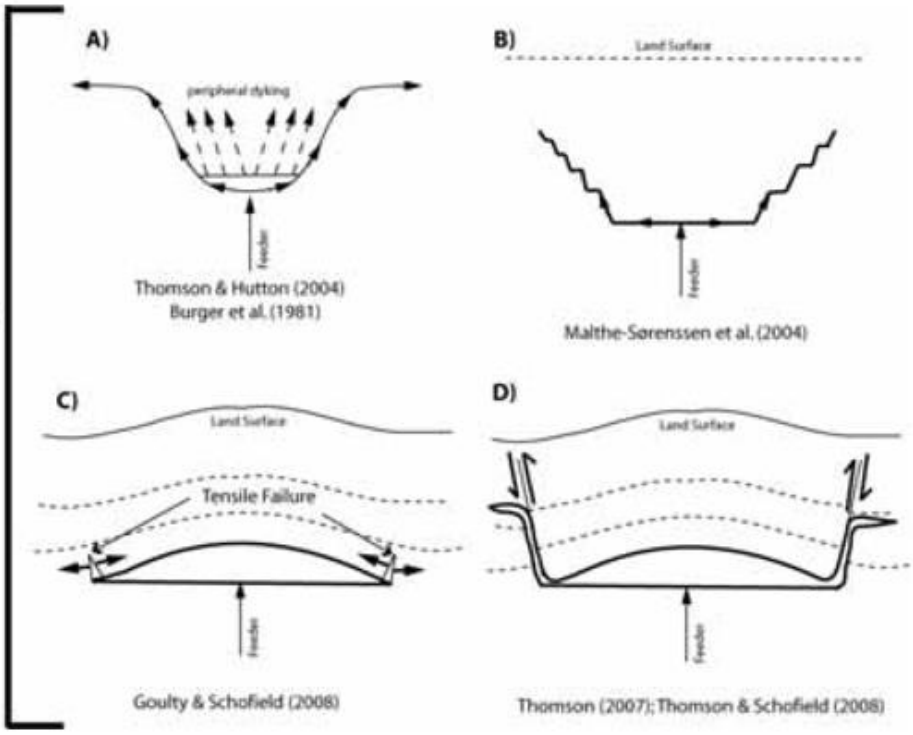


Fig 2.8. Sill emplacement models mostly derived from seismic data with exception of Burger et al. 1981. Note how the feeder is now placed beneath the centre of the base of the saucer, and not off to one side (Schofield et al.,2009)

2.2.2. Sill-Sill merger (Formation of Junctions)

Hansen et al., 2004, described three main junction classes, which are commonly observed in complex and compound sill geometries as shown in Fig 2.9 below. These definitions are based on seismically resolvable geometrical relationships.

- Class A junction (Fig. 2.9a): two sills are linked at their tips,
- Class B junction (Fig. 2.9b): one sill abuts against another. The junction may be at any angle and occur anywhere on either sill.
- Class C junction (Fig. 2.9c): one sill cross-cuts another leaving the two segments of the earlier sill displaced by the continuous, later sill.

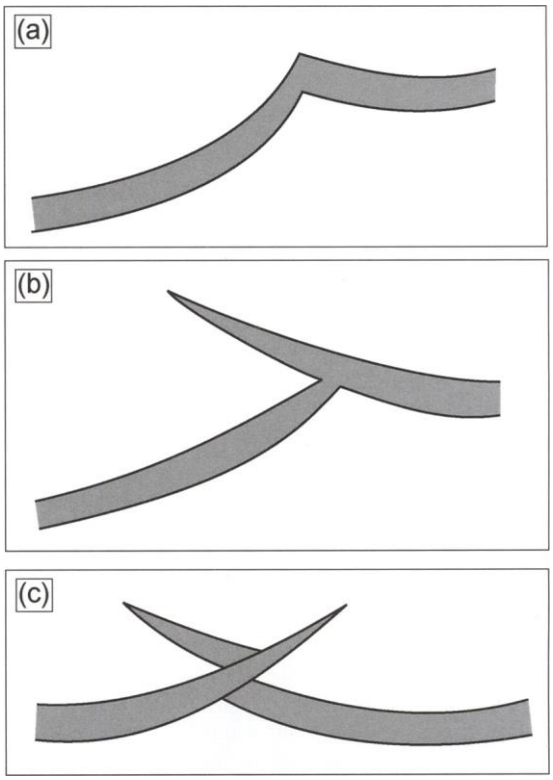


Fig 2.9. Classification of sill junction relationships: (a) Class A junctions form where the tips of two sills are linked. (b) Class B junction form where one sill abuts against another. (c) Class C junctions form where one sill cross cuts another (Hansen et al., 2004)

According to Cartwright and Hansen, 2006, the geometrical relationship of the sills in the crust can be classified into three main sill junctions as described below:

- Class A junctions

This type of junction shows two connected sill tips (Fig. 2.11). Three different characteristics are proposed to understand the development of this type of junction. The first model (Fig 2.11 a) describes that the connection occurs as the result of sills that propagate towards each other. The second model (Fig 2.11b) is when the sills from the source propagate in bi-directional way, whereas the third model (Figure 2.11c) occurs at the time that the secondary sill distributes from the adjacent early sill.

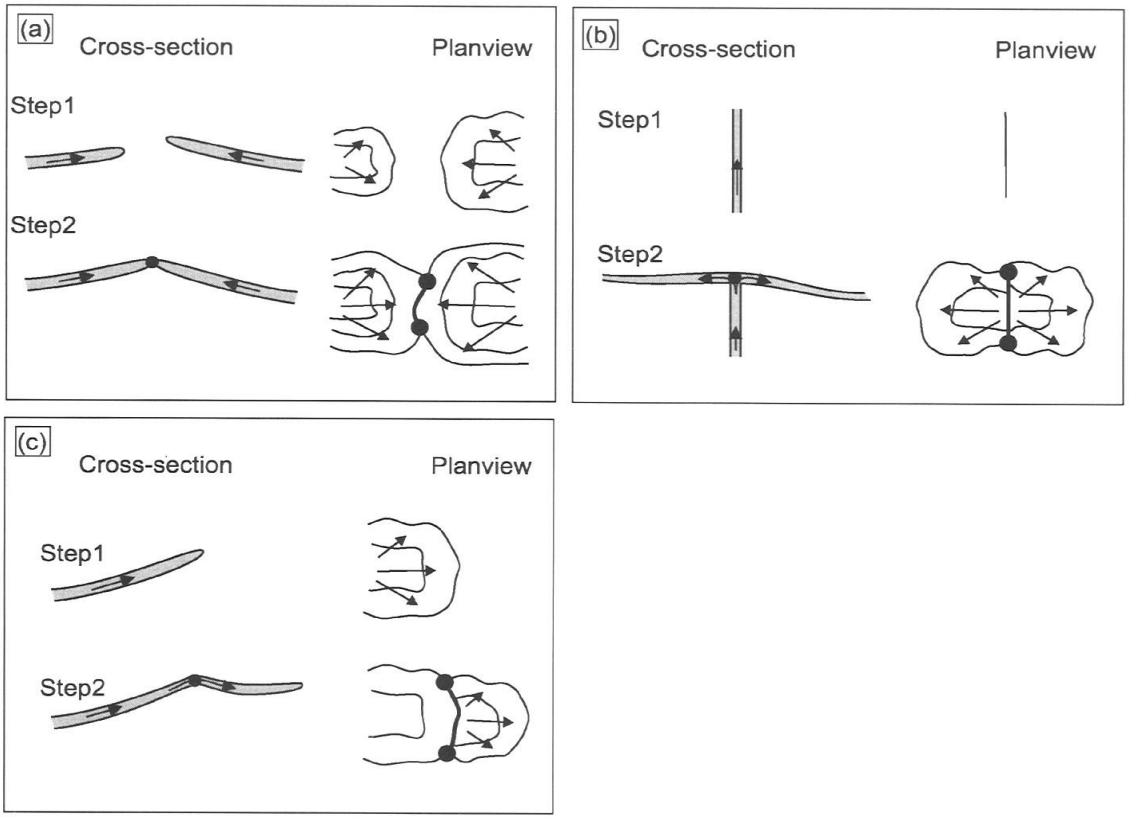


Fig 2.11. Models for the kinematic development of Class A junctions. Class A junctions might form as a result of (a) intersection of two independently propagating sills that intersect as a result of propagation towards each other, (b) bi-directional propagation away from a feeder source (dyke) that joins the sills at the line of junction, or (c) where a secondary sill spreads out from the edge of a primary sill (Hansen et al., 2004)

- Class B junctions

According to Hansen et al., 2004, this type is the most common geometry and the longest junction in sill complexes. The geometry displays a magmatic sill tip, which creates an angle to another sill body (Fig 2.12). Hansen et al., 2004, described junction in three models, with which the Class B junction can develop (Fig 2.12). The junction is likely to be formed by the propagation of the subsequent sill which is blocked by the early emplaced sill. In the second

model (Figure 2.12b), bi-directional parallel propagation out of a transgressive sill tip occurs because of formation compactness or due to a lithological obstacle. The third model is divided into two (Figure 2.12c): sill branching or splitting, which takes place because of mechanical and lithological heterogeneity. The splitting or branching is likely to be constrained by local stress that is related to sill propagation (Hansen et al., 2004).

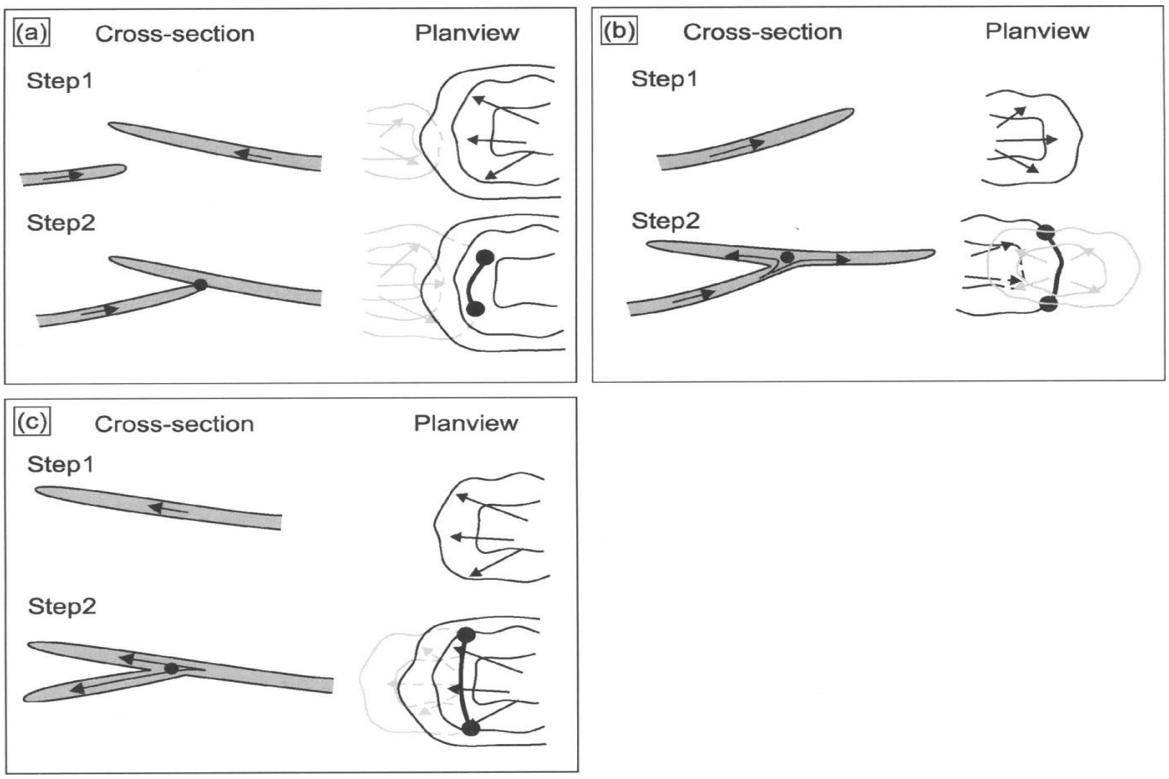


Fig 2.12. Models for the kinematic development of Class B junctions. Class B junctions might form as a result of (a) obstruction of the propagation path of a sill by a previously intruded sill, (b) bi-directional lateral propagation away from a transgressive sill tip, or (c) sill splitting and sill branching (Hansen et al., 2004).

- Class C junctions

According to Hansen et al., 2004, a Class C junction is considered most likely to form due to cross-cutting of an early sill by a later sill. The detached tip region is often structurally elevated to accommodate the added thickness provided by the thickness of the cross-cutting sill. Furthermore, the tip may be rotated slightly backwards as a result of drag induced during the forcible intrusion of the cross-cutting sill. This type of junction can be formed (kinematically feasible) when a Class B junction evolves in space (Hansen et al., 2004).

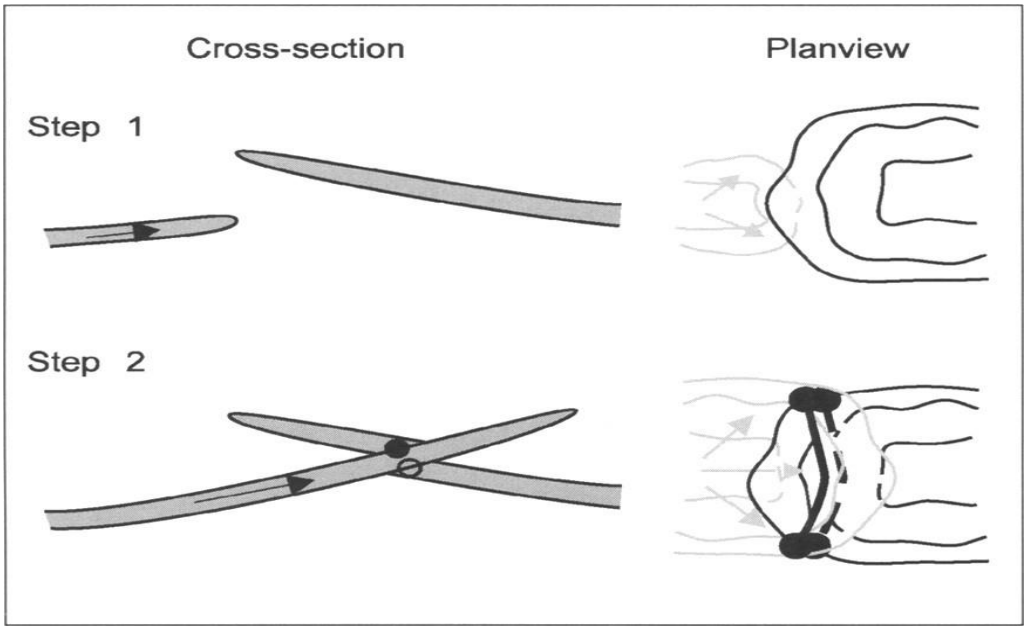


Fig 2.13. Class C junctions most likely form where an earlier emplaced sill is cross-cut by a later emplaced sill (Hansen et al., 2004)

2.2.3. Sill geometry in 3D seismic data

Sills (Fig. 2.14a) are generally characterized by continuous, very high-amplitude reflections that exhibit both concordant and discordant relationships with stratal reflections. They often have a simple three-dimensional geometry and a relatively smooth periphery. The development of compound sills can in most cases be shown to result from the junction of two or more saucer shaped sills (Hansen et al., 2004). They often have complex, irregular peripheries. The terms above are distinguished from sill complex (Fig 2.14c), which is used to refer to a highly interconnected network of sills and/or compound sills that developed through a succession of repeated intrusive events over discrete stratigraphic intervals (Hansen et al, 2004).

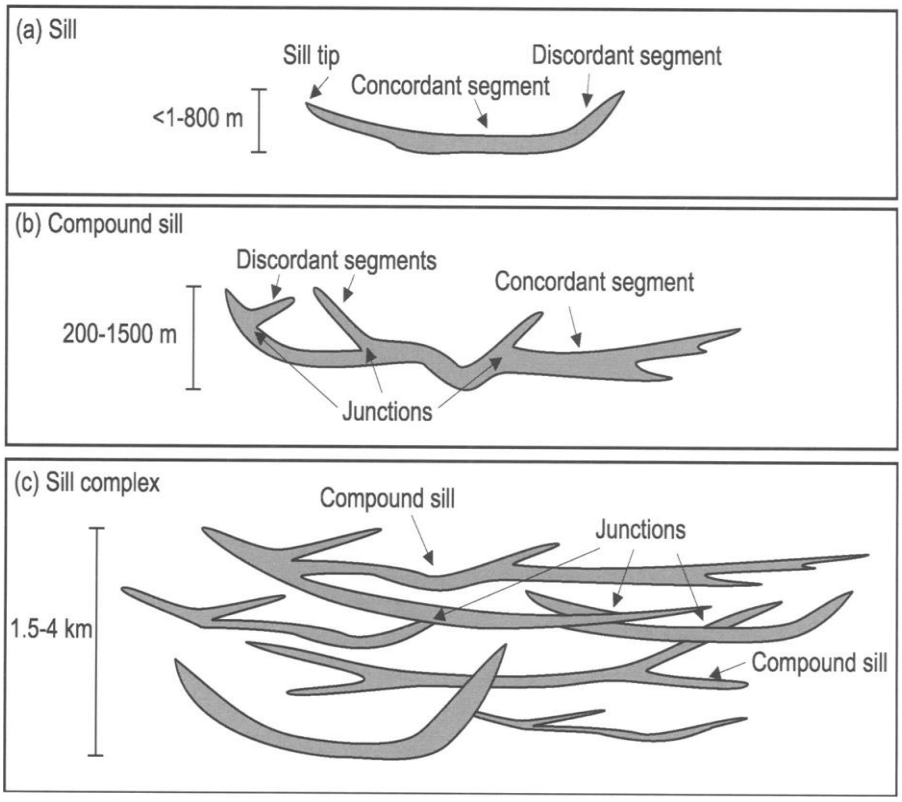


Fig 2.14. Schematic cross-sections showing different levels of the three- dimensional geometrical complexity of igneous bodies recognized on 3D seismic data: (a) Sill, (b) Compound sill, and (c) Sill complex (Hansen et al., 2004)

# CHAPTER 3: DATA AND METHODS

The workflow of the thesis involved retrieving of important geological information from seismic and well log data. Information extracted from the wells and seismic data were used to for seismic interpretation.

## 3.1. Data

### 3.1.1. Seismic data

The dataset for this study includes a high-resolution, three-dimensional (3-D), seismic survey and wireline logs from wellbore 6607/2-1, 6607/5-1 and 6607/5-2 all in the Vøring Basin, Norwegian Sea.

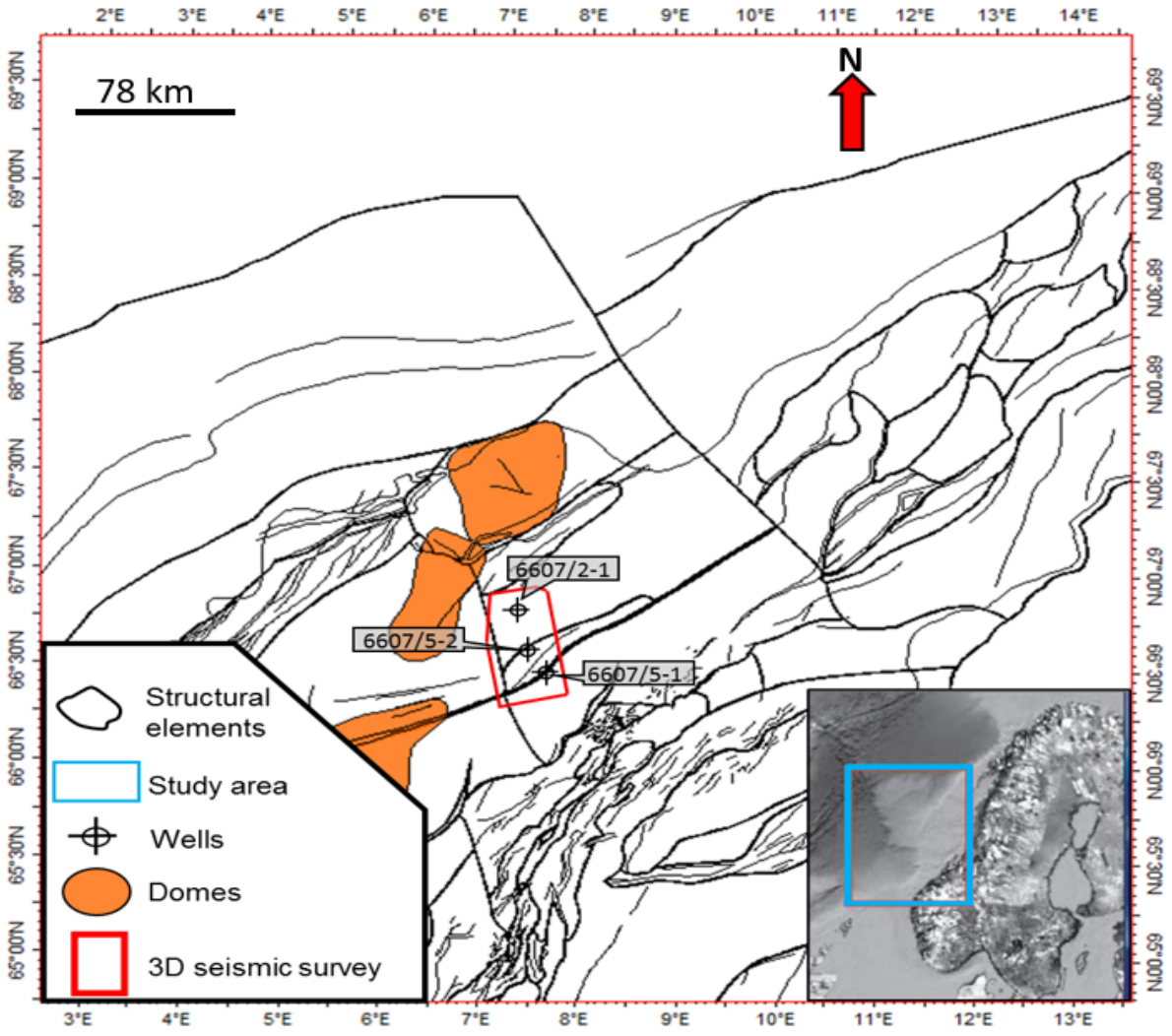


Fig. 3.1. Location map of study area showing both seismic and well data amidst the structural element in the Vøring Basin.

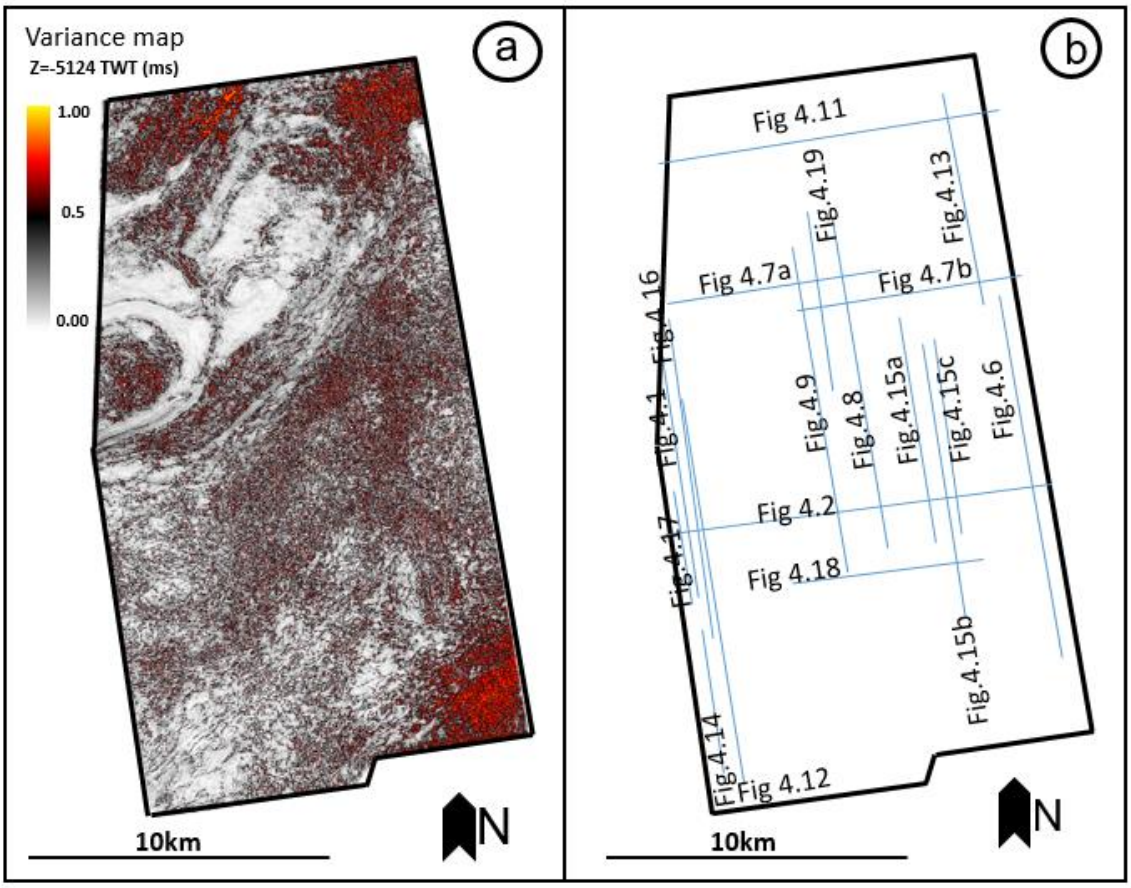


Fig 3.2. Extent of the study area showing the approximate location and direction where some of the seismic sections taken for detail interpretation and analysis in the as shown in Chapter 4.

The seismic data is in the time domain and shown in a zero-phase and “reversed” polarity (Fig 3.3). based on Society of Exploration Geophysicists (SEG) polarity convention. This indicates an increase in acoustic impedance with depth is represented by trough and a decrease is shown as peak (blue). A total of 2526 inlines (length 30.7 km) and 1230 crosslines (length 6.3 km). The inlines and crosslines trend N-S and E-W respectively. Inline and crosslines interval are approximately 25m and 25m (25m x 25m) respectively. In addition, the seismic data is recorded to a depth of 9s, vertical sampling rate of 2 ms giving rise to a Nyquist frequency of 250 Hz.

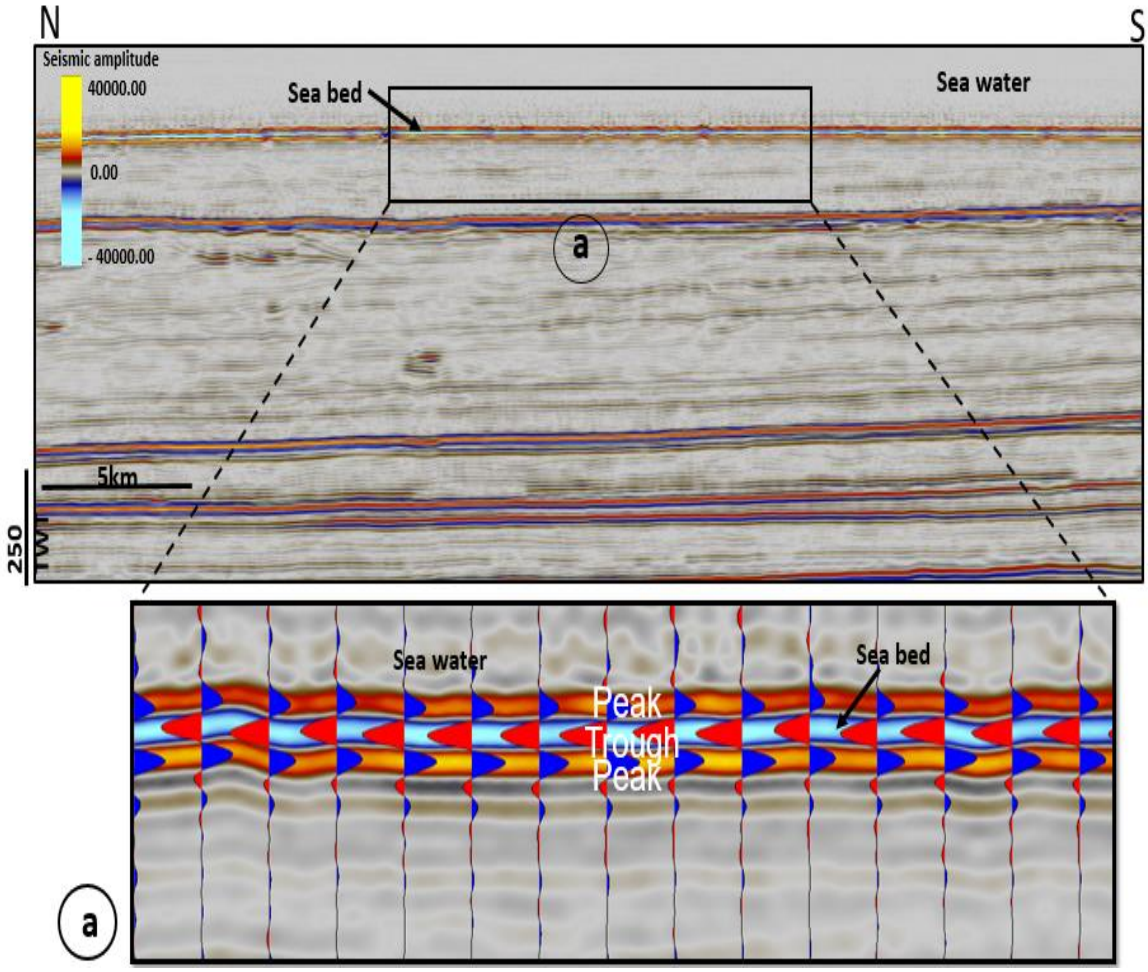


Fig 3.3. Seabed showing a reversed zero phase polarity of peak-through-peak

### 3.1.2. Seismic Resolution

Resolution may be defined at the ability to separate two narrowly spaced features with respect to depth and space. It is also the minimum separation of these two geological bodies before their individual identities are lost" (Sheriff and Geldart, 1991; Brown, 2004). In geological measurement, it is very important to consider resolution since usually geologic features in the subsurface exist in various extents and forms, in order to give a good representation of the geology (Herron, 2007). Each seismic dataset has unique characteristic resolving power, therefore it is essential to know the temporal and lateral limits of the resolution to include for a particular seismic interpretation (Sheriff, 2002). Because propagation velocity and the dominant frequency of the seismic signal change vertically and laterally throughout the subsurface, it follows that temporal resolving power will vary across a given area of

investigation (Herron, 2007). In seismic geophysics, resolution can be divided into two types; vertical and horizontal resolution.

The vertical resolution is considered as temporal and is the minimum in time between two reflections arriving at the surface that allows the detection of each reflector separately hence it helps to differentiate between the top and bottom of a bed. This enables one to differentiate between a bed of finite thickness from a single reflecting interface. Horizontal (or Lateral) resolution is the minimum lateral distance (spatial) between two close geologic objects that allows each feature to be imaged separately.

According to Brown, 2004, frequency (f), velocity (v) and wavelength (λ) are the main components that influence seismic data resolution with the latter being the major parameter (wavelength). Wavelength is an essential property of a wave which is the distance between consecutive points of its equal phase (e.g., crest to crest), completing one cycle. The wavelength equation incorporates both the velocity and frequency and is defined by the equation below;

$$\lambda = {}^{v}/_{f} \qquad (3.0)$$

Where 'v' and 'f' are the velocity and wave frequency propagating through the medium. From the equation above, the wavelength is directly proportional to velocity and inversely to frequency, hence, seismic resolution is better when wavelength is smaller usually at shallow depth and vice versa. At shallow depth, seismic wavelength is smaller as a results of reasonably lower velocity together with prevailing higher frequencies. In contrast, resolution declines with depth due to longer wavelengths due to increasing velocity and lowering of frequency at deeper level. There is a difference between resolution and detection capability. Resolution deals with clearly separate events, while detection exploits subtle interference effects to distinguish individual layers.

According to Sheriff, 2002, the thickness of a bed must be ¼ of the wavelength (1/4 λ) for it to be resolved (Rayleigh limit of resolution). This is a thickness which can influence interpretation criteria. Measuring the thickness of a bed that is thicker than the Rayleigh limit has to be based on features of the wave shape, whereas for one that is thinner it has to be based on amplitude measurements.

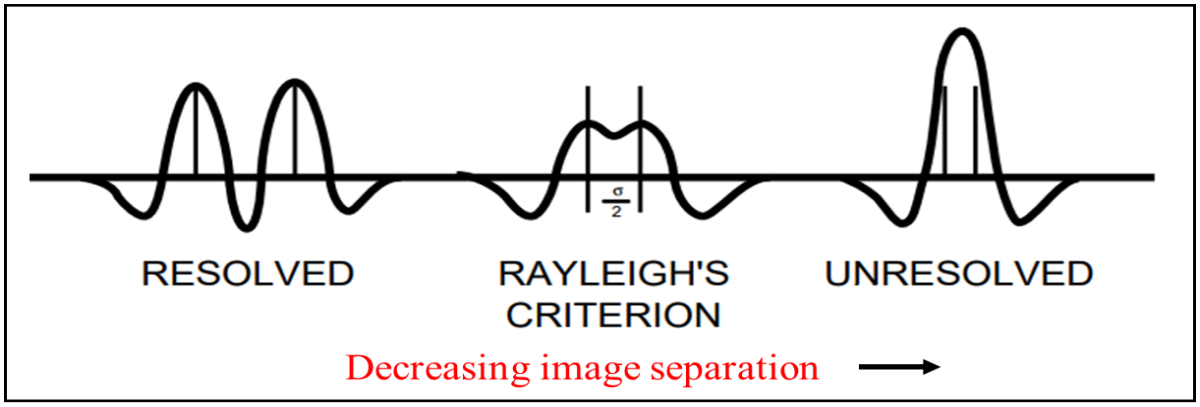


Fig 3.4. Showing Rayleigh's criterion for limit of Vertical resolution of thin beds on seismic data (Sherriff, 2002)

- Vertical resolution

For an observable single reflection to be achieved between two interfaces, the vertical resolution has to be good. The vertical resolution is the minimum vertical distance between the interfaces (Sheriff, 2002). Generally the vertical resolution is determined solely by the wavelength of the signal when the seismic data is noise-free (Brown and Fisher, 1980). Simm et al. 2014 provides an approach to solving or calculating the vertical resolution of the seismic data. Practically, the tuning thickness can be considered as vertical resolution (Simm et al., 2014). Basically, the tuning thickness is estimated by a simple relation between wavelength (λ) of the seismic pulse and the compressional velocity (v) of the wave. A first order approximation used for calculations is given by: tuning thickness.

$$\text{Tuning thickness} = {}^{1}/_{4}\,\lambda \qquad (3.1)$$

$$\lambda = \frac{\text{Vp}\left(\frac{\text{m}}{\text{s}}\right)}{\text{Fd(Hz)}} \qquad (3.2)$$

$$\text{Fd} = {}^{1}/_{\text{T}} \qquad (3.3)$$

Where λ wavelength (m), Fd = dominant frequency and T = 'period' (measured in seconds from trough to trough or peak to peak) on a seismic section (Simm et al., 2014)

Vertical resolution can be improved by shortening the wavelet shape, which is includes higher frequencies or shorter wavelength. The earth elongates and widen seismic wavelets passing through it, attenuating shorted wavelengths, hence increasing the number of longer wavelets over shorter ones. By deconvolution, one can remove some of the effects of the natural filtering resulting in the production of a shorter wavelet with a wave shape that is easier to interpret. The shorted wavelength creation helps to improve resolution. Additionally, frequency filtering

to remove low-frequency components can help, and intermittently removes the high-frequency components so that one can determine thickness from amplitude measurements (Sherriff, 2002 AAPG).

- Horizontal resolution

Not only vertical resolution limitations exist, but also in a horizontal direction there are restrictions. The lateral resolution is controlled by the trace spacing and therefore by the distance between the subsurface sampling points. The Fresnel zone is generally used to describe the lateral resolving power of seismic data. The Fresnel zone may be defined as the part of a reflector from which reflected energy can arrive at a sensor within one-half wavelength of the first reflected energy (Sheriff, 2002). The zone can be written as the following:

$$\mathrm{Fr} = \frac{\mathrm{v}}{2}\left(\frac{\mathrm{TWT}}{\mathrm{f}}\right)^{\frac{1}{2}} (3.4)$$

Where Fr is the radius of the first Fresnel zone, TWT represent the two-way-travel time of a reflector, v is the average propagation velocity and f is the dominant frequency. This relation indicates that that the Fresnel zone generally increases with depth due to increasing propagation velocity and decreasing dominant frequency (attenuation) with depth of signal (Sheriff and Geldart, 1995, Simm et al., 2014). The Fresnel zones are generally measured with respect to an unmigrated seismic data. Migration improves horizontal resolution just as deconvolution improves vertical resolution. Migration presumably moves reflections to the locations of the reflectors and it collapses point diffractions; the horizontal resolution of migrated data is taken as the horizontal distance over which the stacked diffraction is spread, which again depends on the dominant wavelength. Seismic migration collapses these zones; however, 2D migration collapses the zones only in the direction of shooting of the 2D line (Herron, 2007). Since the data has been time migrated well, the horizontal resolution is taken as the inline spacing distance which is 25m.

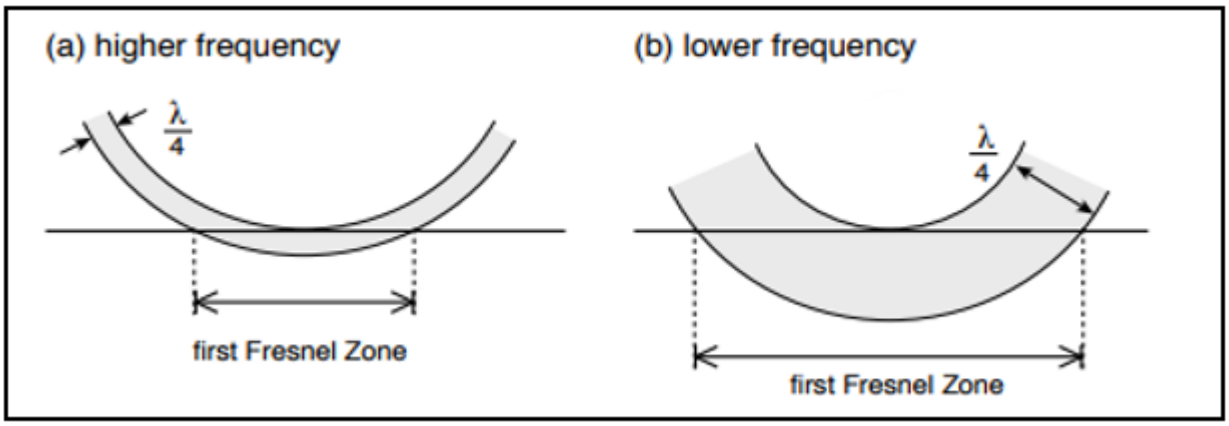


Fig 3.5. Illustration of the first Fresnel zone dependence on wavelength λ.Two wavefronts, a quarter wavelength apart, impinge on a horizontal surface.

3.1.3. Well data

Three exploration boreholes mainly 6607/5-1, 6607/5-2 and 6607/2-1 lie within the study area and these were used for petrophysical analysis and well correlation. Wells 6607/5-1 and 6607/5-1 are located on the Utgard High, whereas, 6607/2-1 is located between the Utgard High and the Nyk High within the Någard Syncline. A summary of well information is shown in table 1. (NPD, 2017). Wireline-logs from these boreholes that have been used in this study include bulk density ($g/cm^3$), gamma ray (API), sonic ($\mu s/ft$), neutron ($m^3/m^3$).

Wireline-logs from these boreholes that have been used in this study include bulk density (), gamma ray (API), sonic (), neutron ().The wells also contain check shot data used in the seismic to well tie process and synthetic generation. The markers and age of formation tops used for chrono-, litho- and seismic- stratigraphic correlation were derived from the wells in the study area.

Table 1. Summary of well information from NPD

| Wells | Total Depth (m) | Oldest Penetrated Age | Youngest Penetrated Formation | Oldest Penetrated Formation | Content | Location |
|---|---|---|---|---|---|---|
| 6607/2-1 | 3526.0 | Late Cretaceous | Naust Fm | Springar Fm | Dry | 66° 49' 20.18" N 7° 22' 15.5" E |
| 6607/5-1 | 3817.0 | Late Cretaceous | Naust Fm | Lang Fm | Dry | 66° 38' 9.67" N 7° 32' 21.38" E |
| 6607/5-2 | 4684.0 | Late Cretaceous | Naust Fm | Kvitnos Fm | Dry | 66° 41' 3.38" N 7° 21' 22.52" E |

## 3.2. Methods

The methods used for the research include seismic interpretation, which involved horizon mapping, interpretation of magmatic sills, faults, and hydrothermal vents. Statistical evaluation include the estimation of area, length, width and aspect ration for sills.Gridding of the 3D was done to facilitate automated contouring and to manipulate picked horizons (e.g., calculate the thickness of the interval between two horizons) as results, various maps including the isochronal map, structural map and surfaces were made to represent stratigraphy.

### 3.2.1. Seismic to well tie

Seismic to well tie is a key element to a successful and reliable seismic interpretation. The process enables the interpreter to compare the seismic data with well data since the seismic and well data are measured in vertical unit scale of 2-way travel time in seconds or milli-seconds and depth in meters or feet respectively. Seismic to well tie also provides a means to correlate horizon tops identified in a well with specific reflections on the seismic section (Simm et al., 2014). Density, sonic and checkshots data were used to generate synthetic seismograms to correlate seismic and well data and time shifts were applied where for reliable results.

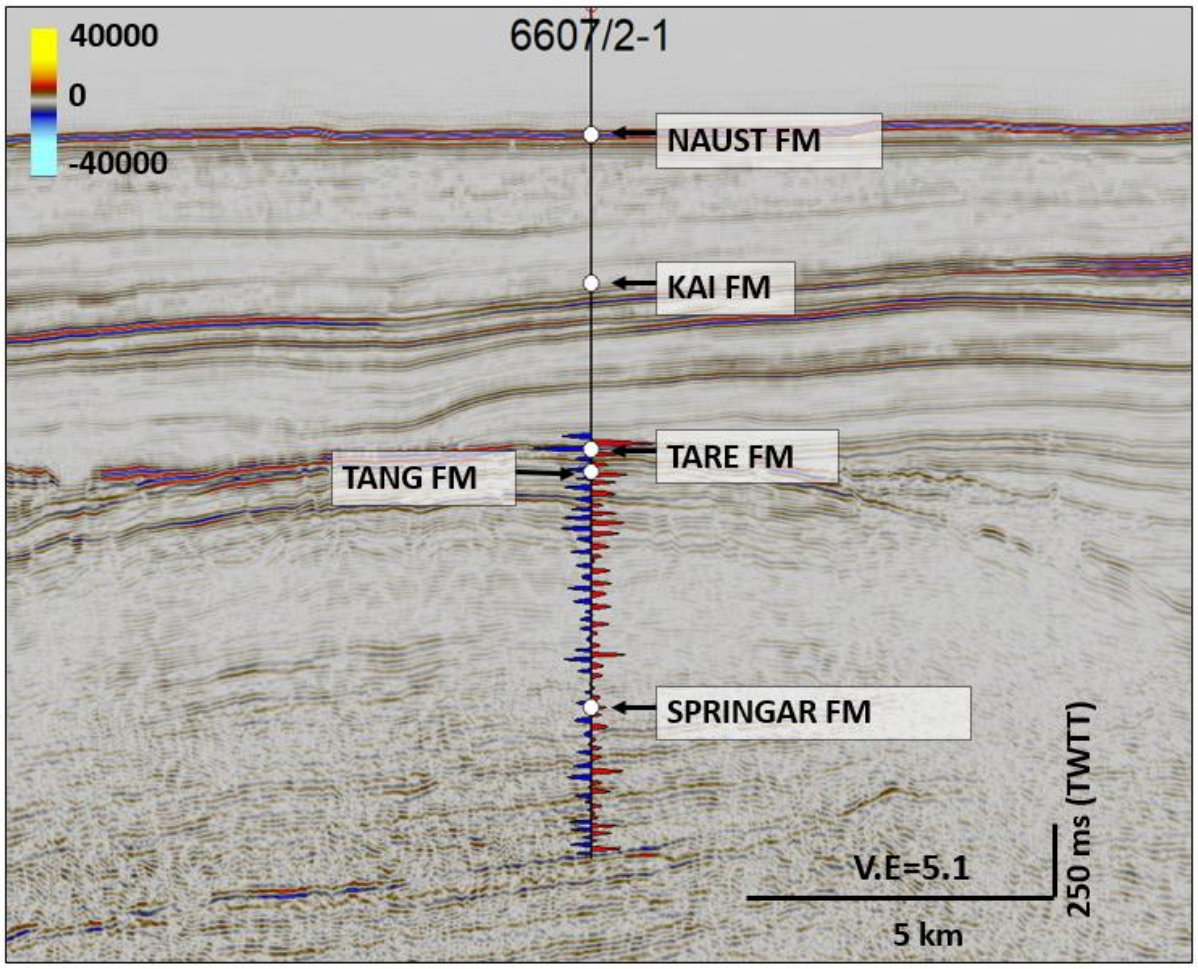


Fig 3.6. Image of seismic to well tie done to correlate horizon tops identified in a well with specific reflections on the seismic section

### 3.2.2. Seismic interpretation

Seismic interpretation method included horizon, magmatic sill and fault mapping together with seismic attribute analysis using Petrel® 2016.

- Horizon mapping

Seismic horizons indicate change in rock properties and are central in geoscience interpretation (Patel et al., 2010) Horizon mapping was an important aspect of the seismic stratigraphic interpretation process during the research. Horizons were mapped after the seismic to well tie was done. It was done by digitizing the horizons or outstanding reflections. Horizon mapping involved seeded 3D auto tracking beginning with a known stratigraphic top from the seismic and well data. They were then mapped as formation tops based on the well data. Even though

3D auto tracking was the main method used for the horizon mapping (high amplitude and continuous reflections), in areas where the seismic reflections were discontinuous or chaotic I employed both 2D auto tracking and manual picking. I carefully selected the right amplitude response to use for this which included both the peaks (red) and troughs (refer to Fig 3.2 above). The peak response was used for lithostratigraphic interpretation whilst the trough was used for the seabed and the magmatic sills. The inline picking interval used was 5 to 20 increments, which was greatly influenced by the data quality and the geological features I was looking out for based on literature.

A total of 9 horizons were mapped representing the stratigraphy of the area represented by H (H1 to H9) Horizons were then separated into units or packages based on similar seismic reflection patterns or configuration (Fig 3.7).

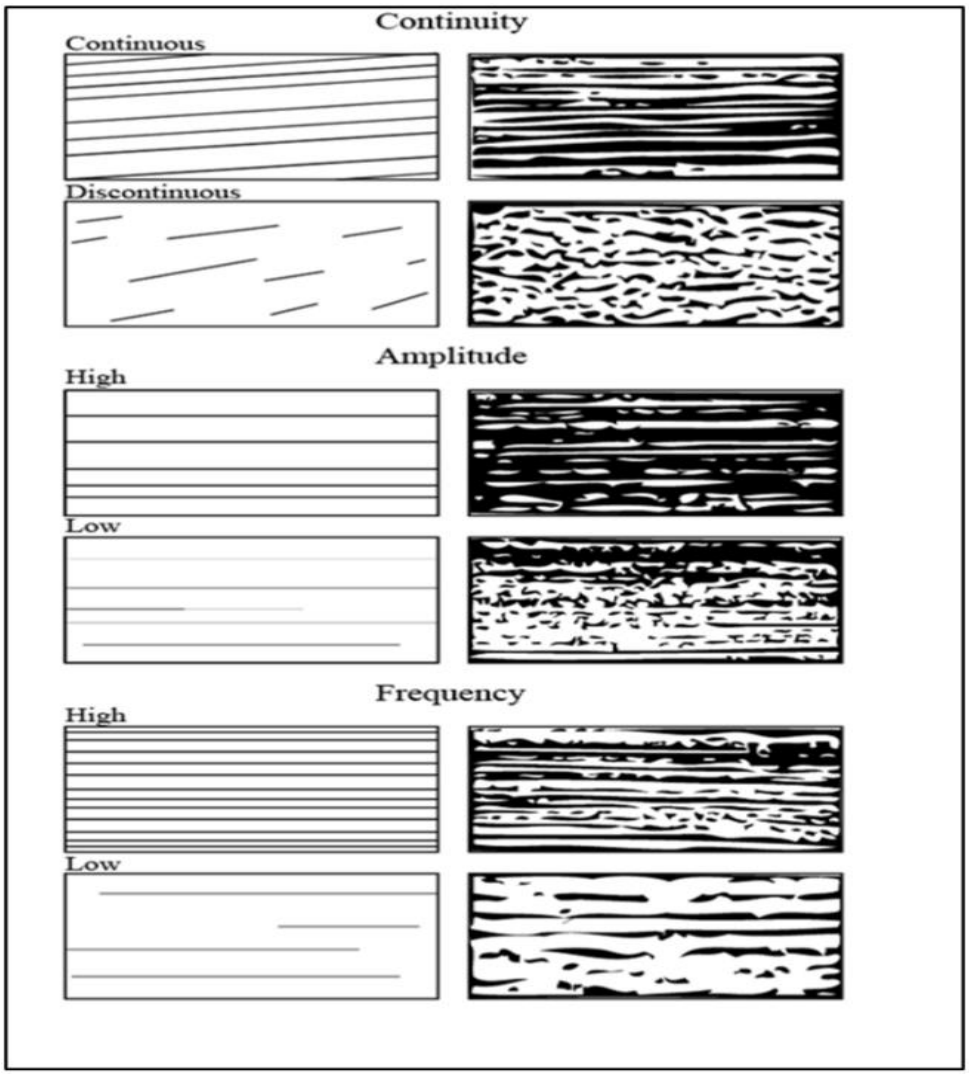


Fig 3.7. Illustration of seismic reflection configuration used for interpretation (Bradley. 1985)

#### 3.2.2.1. Interpretation of Magmatic sills

Interpretation of magmatic sill intrusions varies from conventional methods for time horizon mapping and it requests determination of lithology. Furthermore, magmatic sills may divide into several units and sometimes these units may join to form one unit. Sills can move up or down in the stratigraphy (transgression) and may contain holes. Due to the complex nature of magmatic sill intrusions, they are well-suited for 3D visualization techniques and ample new information about sill geometries and emplacement dynamics have been obtained using such methods over the past decade.

In this research, a combination of interpretation methods has been used: (1) interpretation of sill reflections, (2) seismic facies analysis; and (3) mapping of surfaces.

- Interpretation of sill reflections

In the quest to identify, interprete and map the seismic event as sill reflections, I used four main criteria: (1) high amplitude anomaly; (2) local transgression (cutting across stratigraphy); (3) saucer-shape; and (4) abrupt terminations. A reflection is identified as a possible sill reflection when there is abrupt increase in seismic amplitude (seismic anomaly) with respect to the background amplitude values. These seismic anomalies are localized brightening of positive amplitude values, which are complete or partial loop of 'peak-trough-peak' similar to the seabed reflection (Smallwood and Maresh, 2002). Additionally, if the seismic event locally cuts across stratigraphy whether up or down (transgressive), is saucer-shaped (because they are the most common geometries to observe in magmatic sills) and abruptly terminates at their edges. If the event transgresses, is saucer-shaped and/or terminates abruptly, then the reflection is interpreted as a probable sill reflection (Magee et al., 2015; Planke et al., 2000). During sill interpretation, morphometric characters such as area coverage, length, width and geometry of the sills were estimated to understand the spatial distribution of the sills.

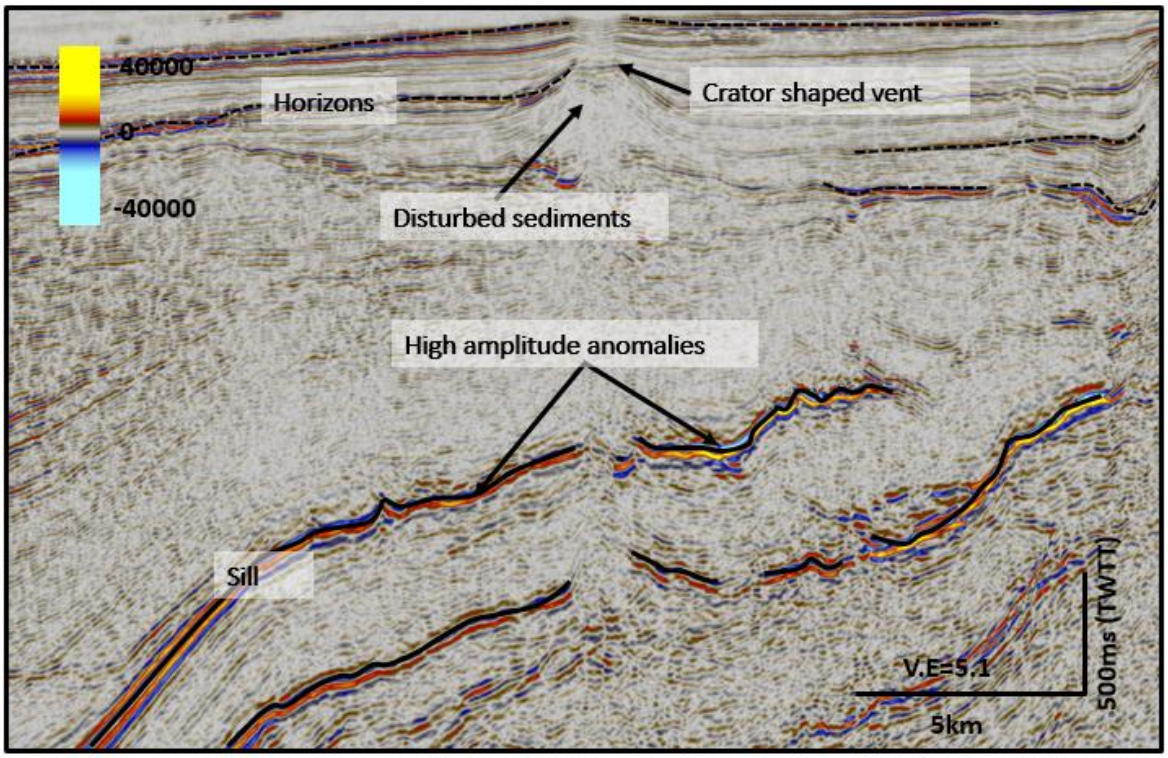


Fig 3.8. Seismic section showing magmatic sills, horizons, faults and vents in the Voring Basin.

- Seismic facies analysis and Surface mapping

Identified magmatic sill reflections were described and mapped using the concept of seismic facies analysis method, originally described by Vail and Mitchum, 1977. Seismic facies analysis can be defined as the description and geological interpretation of seismic reflection parameters, including configuration, continuity, frequency and interval velocity. It also involves the description and mapping of seismic facies units, which are the mappable three dimensional group of seismic reflections, whose reflection parameters differ from the neighboring facies units. Conventionally, seismic facies analysis is used mainly in sedimentary environment, nevertheless, it is also used in volcanic environments (e.g. Planke et al. 2000).

Seismic facies analysis method is appropriate for mapping magmatic sill intrusions (Skogly 1998), since the sills display an extensive range of geometries and reflection parameters. Sill facies units (seismic facies units) were identified on the seismic profiles and characterized based on their distinct geometries. Most of the sill facies units had boundaries that were not obvious, since they diffuse and overlap in some areas. The dominating facies unit was plotted on the map in areas where the overlapping sill reflections showed different seismic facies. If facies units merged, then the limit between the facies units was put at the center of the transition zone. All picked sill horizons were merged and the shallowest sill at each location was used to

make a gridded surface. The area distribution of the anomalies was computed for individual sill reflection and displayed in histograms and whisker-plots in order to understand their distribution with depth, areal extent, thickness and changes in their geometry.

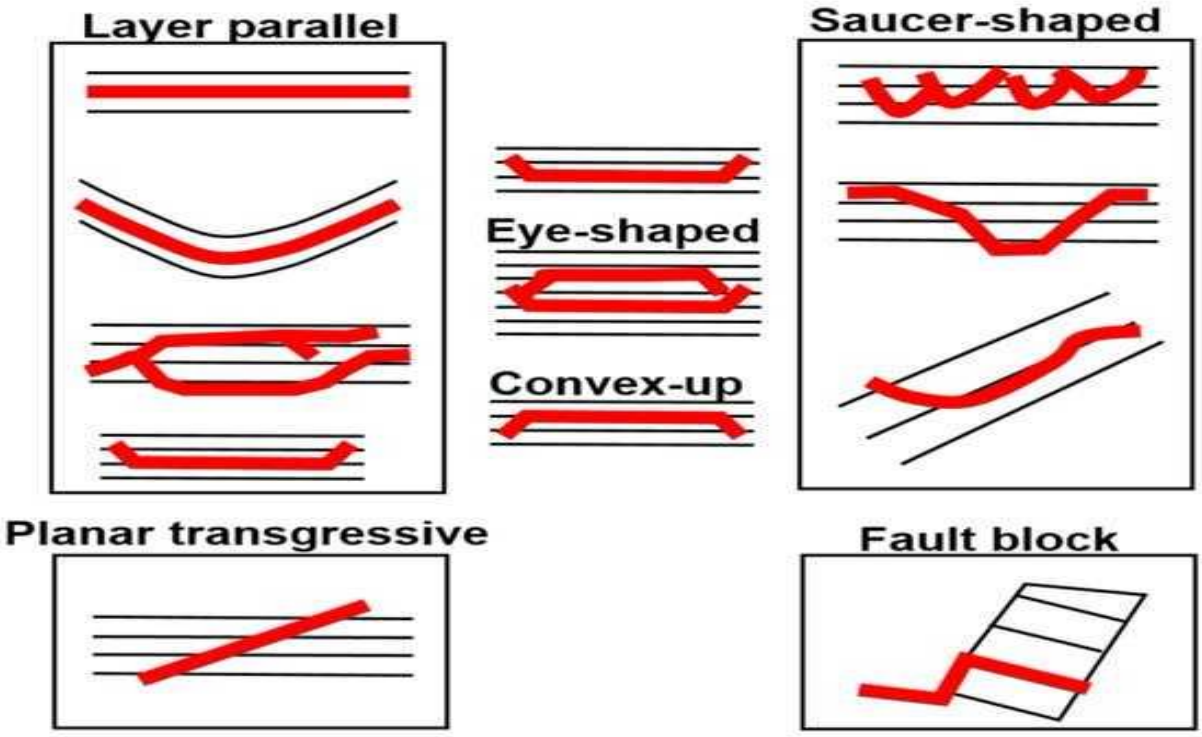


Fig 3.9. Sketch showing the configuration of magmatic sill facies units (Planke et al., 2005; Omosanya et al., 2016)

3.2.2.2. Interpretation of Hydrothermal vents complexes

Hydrothermal vent complexes are usually characterized by three main segments as revealed by a plethora of examples from 2-D and 3-D seismic reflection datasets across volcanic-rich margins: (a) lower part manifested as subvertical zones of disrupted reflection character ll: (i) the root-region located directly the sill tip termination and (ii) the neck of the vent structure, with a pipe- or chimney-like morphology and (b) the vent summit with a crater-like, eye-like of dome-like morphology arising from the seafloor or paleo seafloor extrusion extrusion of hydrothermal fluids and fluidized sediment and the subsequent build-up of the entrained sediments on the seafloor in case of the dome-like and eye-like end-members (Planke et al., 2005; Omosanya et al., 2017). Furthermore, seismic attributes like Variance and Chaos were used to identify the hydrothermal vents, distinguishing them from low amplitude reflection areas underlying the magmatic sills (Fig 3.11).

3.2.2.3. Fault interpretation

Faults were interpreted and mapped based using manual fault interpretation and Variance (seismic attribute). Faults represent trace-to-trace variability and mapped with a high variance coefficient compared to surrounding with low variance. They were identified as low amplitude zones with discontinuities in the seismic event. They had unique pattern of vertical displacement of reflectors and discontinuity, which helped to identify them on the seismic data.

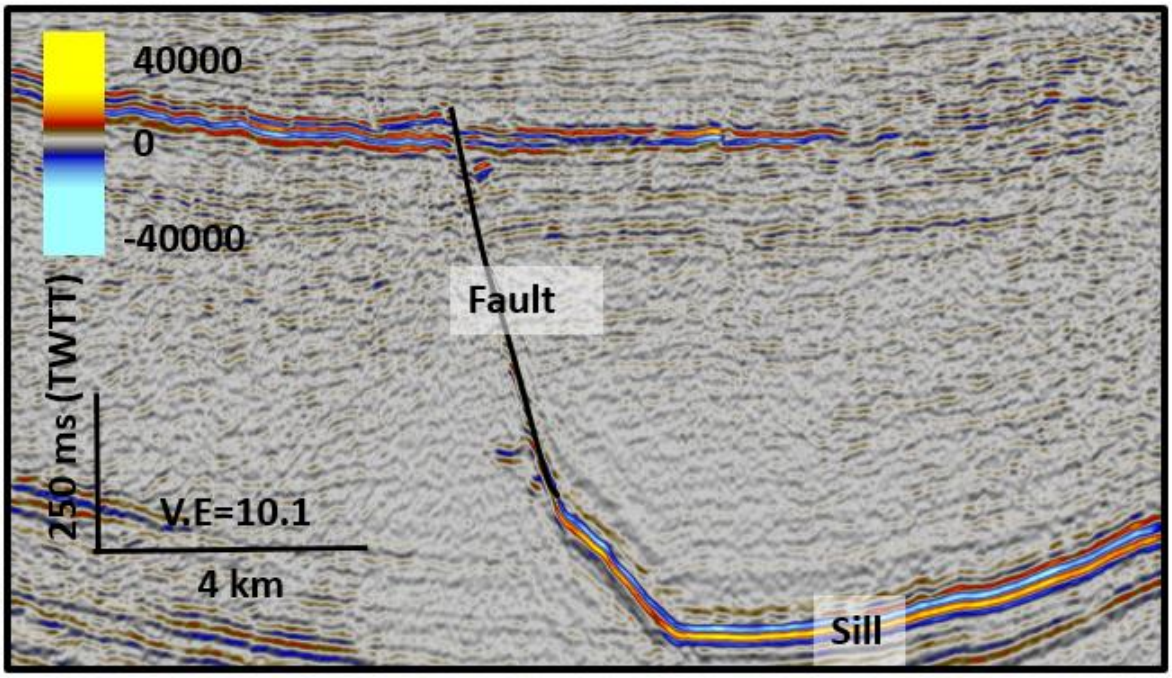


Fig 3.11. Interpretation of a reverse faults in the study area associated with the magmatic sill

3.2.3. Seismic attribute analysis

Seismic attributes have been increasingly used in petroleum exploration and production and have been integrated in the seismic interpretation process. Over the past decades, seismic attributes have been developed into many types ranging from structural attributes to stratigraphic attributes (Chopra and Marfurt, 2005). Conventional seismic reflection patterns (amplitudes) may sometimes be difficult to clearly image, some subsurface structures, as such, a combination with a variety of carefully selected attributes offer a better alternative (Brouwer and Huck, 2011). The essential attribute in data seismic data is the amplitude. However, seismic attributes can reveal characteristics, which are not easily observed in amplitude data themselves. Characteristically, seismic attributes provide information relating to the amplitude, shape, and position of seismic waveform, therefore extracting important information from

seismic data that is usually hidden in the data and have been used to identify prospects, determine depositional environments such as fluvial or deep water channels, carbonate buildups, detect and enhance faults and fracture sets to unravel structural history, and even provide direct hydrocarbon indicators (Koson et al., 2014).

In the study the two main categories of attributes mainly, physical and geometric attributes. The physical attribute is directly related to the wave propagation and lithology whereas the geometric attribute deals with the dip, azimuth and discontinuity of the seismic events (Subrahmanyam and Rao, 2008). Information extracted from the seismic attributes were used to interpret the magmatic sills, fluid flow conduits and faults in the seismic data. Seismic attributes used in the research are Variance, Root Mean Square (RMS) amplitude, Chaos, Envelop and Graphic equalizer as shown in Fig . The seismic attributes were made into vertical view and horizontal view (time slice) based on the location or position of an observable geological feature of interest.

- Envelope

The envelope or reflector strength is a trace attribute which shows acoustically strong (bright) events on both negative and positive seismic events. The complex trace of seismic signal used to highlights main seismic features helps to calculate the Envelope attribute. This attribute represents the instantaneous energy of the signal and is proportional in its magnitude to the reflection coefficient (Koson et al., 2014). The envelope is suitable in highlighting discontinuities, changes in lithology, faults, deposition variation, tuning effect, and sequence boundary. Bright spots (high amplitude reflection) from this attribute are important as they can indicate gas, especially in relatively young clastic sediments. The envelope attribute is independent of the phase or polarity of the seismic data which affect the apparent brightness. This makes it advantageous to use over the normal seismic trace values (Koson et al., 2014).

- Root Mean Square (RMS)

RMS amplitude resembles a smoother version of reflection strength. RMS amplitude provides a scaled estimate of the trace envelope. It is computed in a sliding tapered window of N samples as the square root of the sum of all the trace values x squared where w and n are the window values as shown in Equation 3.5 below (Koson et al., 2014)

$$x_{rms} = \sqrt{\frac{1}{N}\sum_{n-1}^{N} w_n x_n^2} \qquad (3.5)$$

It is applied to reveal the bright spots and amplitude anomalies in the seismic data. .This attribute is useful to highlight coarser-grained facies, compaction related effects in lithologies such as marl and limestone and unconformities (Koson et al., 2014). In the study, RMS was calculated as between the different magmatic sill horizons in order to extract high seismic amplitude anomalies, be it positive or negative (Koson et al., 2014).

- Variance

Variance attribute is an edge method which resemblance between waveforms or traces adjacent over given lateral and/or vertical windows. Hence, it is good for interpreting and imaging the discontinuity of the seismic data with respect to faulting or stratigraphy. It is an effective and efficient tool for describing faults and channel edges on both horizon slices and vertical profile from the seismic data. Variance is also helpful in imaging of faults and channels (Pigott et al., 2013) and aids in showing directly the major fault zones, fractures, unconformities and the major sequence boundaries (Koson et al., 2014). Variance attribute was used to interpret and map the sills, hydrothermal vents and faults in the seismic data from the study area.

- Chaos

According to Koson et al., 2014, chaos attribute is defined as measure of the "lack of organization" in the dip and azimuth estimation method. Hence, this attribute can detect chaotic textures displayed in seismic data, making visible the positions and location of the reflector disruption. Seismic facies with chaotic patterns or discontinuous character in seismic data such as coarse-grained sediments within channel infills are easily distinguished from surrounding seismic events. Therefore, it can be used to differentiate different sediment facies in lithology variation environments like sand and shale), zones of reflector discontinuities such as fault zones, angular unconformities, channel sand bodies and possible zones of fractures (Koson, 2014). Variance attribute was key in identifying, interpreting and mapping the magmatic sills, hydrothermal vents and faults.

- Graphic Equalizer

The Graphic Equalizer was used to interpret and map the magmatic sills in the seismic data, since it increases or decreases different frequency composition in order to adjust seismic resolution in various time ranges.

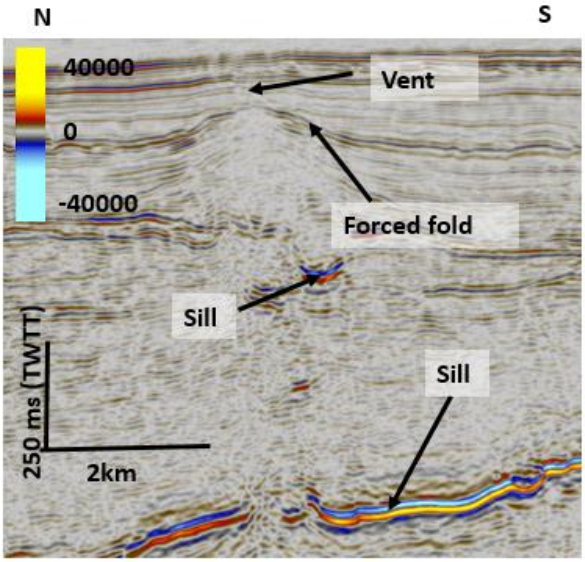


**Normal seismic**

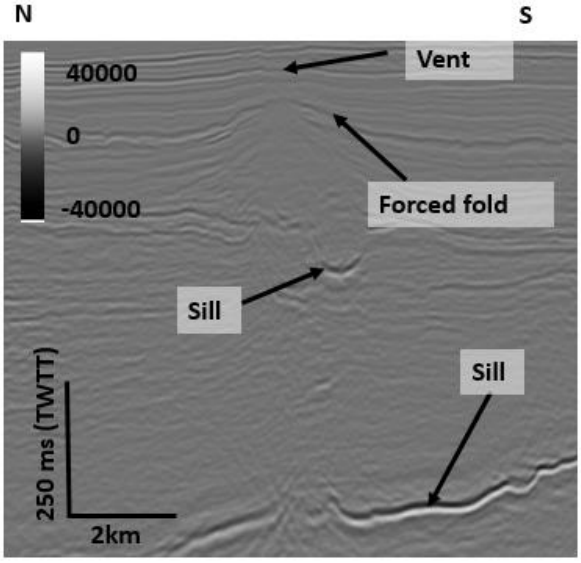


**Graphic Equalizer**

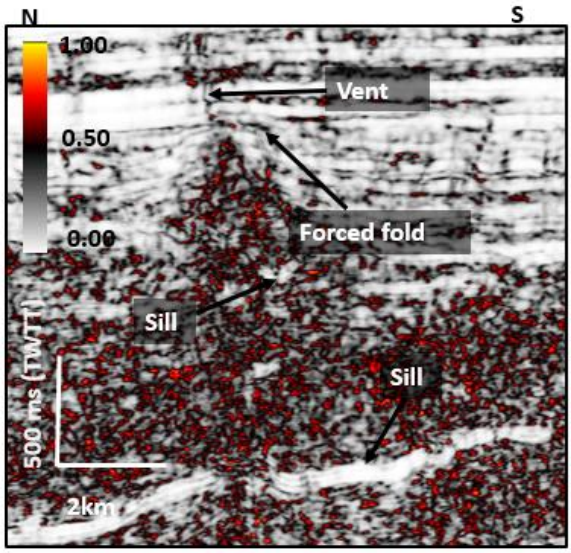


**Chaos**

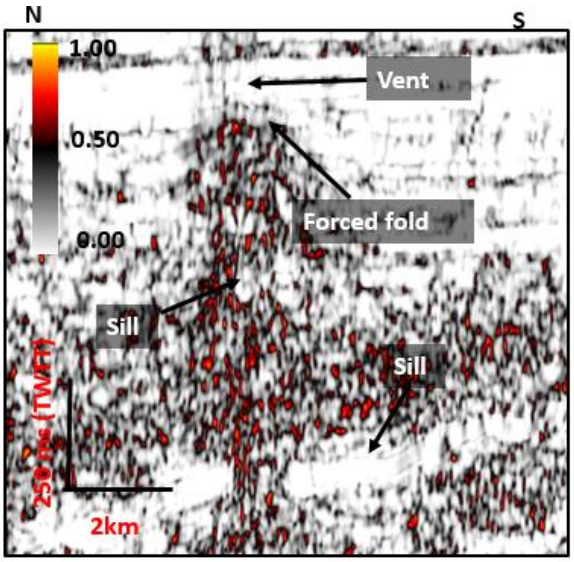


**Variance**

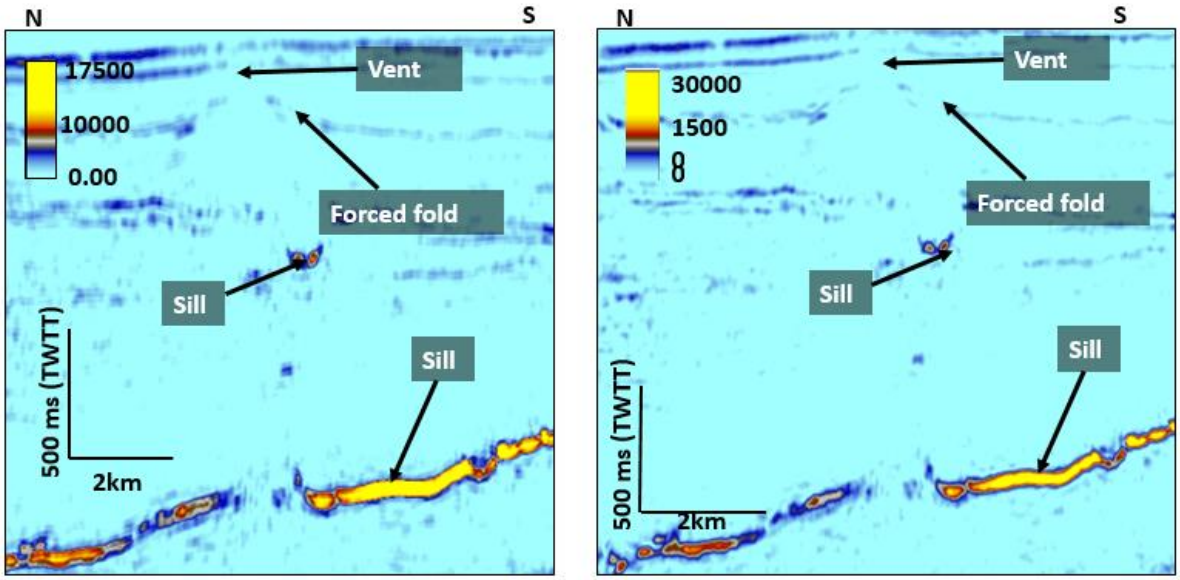


Root Means Square amplitude Envelop

Fig 3.12. Various seismic attributes used in the interpretation of the magmatic sills, hydrothermal vents and forced fold in the study area

### 3.2.4. Statistical analysis

During magmatic sill interpretation, morphometric characters such as area coverage, length, width, orientation and geometry of the sills were estimated to understand the spatial distribution of the sills. The length, area and width were calculated and extracted from the polygon and surfaces of the magmatic sills interpreted in the seismic data from Petrel. Histogram and whisker or box plot of the types, shape and their occurrences in the study area were made to understand their areal extent in terms of their spatial (location or position) and temporal distribution (relative to stratigraphy).

## 3.3. Seismic interpretation constrains in seismic data

A number of interpretational challenges and artefacts with special implications for interpretation of igneous intrusions on seismic data should be noted. There are only few examples of wells encountering sills within 3D seismic survey areas and well calibration of sills with 3D seismic datasets is therefore not often possible. This complicates the determination of the phase of the seismic wavelet, which again makes interpreting top and base of the sills difficult. Interpreting the top and base of a sill and estimating sill thickness is further complicated if the imaged sill is thinner than half the dominant wavelength of the seismic

wavelet because in such a case the seismic responses from the two intrusive contacts cannot be separated. In addition the seismic response from a series of thin sills separated by thin sedimentary sequences may be indistinguishable from the response from a single thick sill) (Badley 1965.

According to Magee et al., 2016, tuning reflection of magmatic sills is triggered by the interference of intrusion contact reflection initiated from an upper and lower intrusions resulting from the limit of separability of the vertical intrusion thickness and the visibility limit of the seismic data (Widess, 1973; Smallwood and Maresh, 2002; Brown, 2004; Hansen et al., 2008; Magee et al., 2015). This makes it difficult to differentiate between the actual geological features of sills and geological indicators in the seismic, caused by the uncertainty of the interpretation of exact intrusion geometry (Magee et al., 2016). The sill thickness and the number of sills are difficult to map. Tuning also made it difficult to measure the thicknesses of the sills, since their top and bottom could not be determined.

A seismic wavelet loses frequency when it encounters a high impedance boundary, such as a sill-sediment contact, resulting in a decrease in both vertical and horizontal resolution (Small-wood and Maresh 2002). As a result, the seismic response from geological features below sills is dimmed and they are poorly imaged, which complicates confident interpretation of deeper sills and thus the geometry of highly interconnected sill complexes (Hansen et al., 2004). Deeper sills are more difficult to image as the wave amplitudes decay across the uppermost sill due to transmission losses across the high-impedance boundaries at the top and the base of the sills. It is often possible to interpret several sill layers but the continuity of the deeper sills is commonly lost when the number of overlying sills increases.

Confident interpretation of sill terminations on seismic data is particularly challenging. If a sill gradually thins towards its tip interference between the reflections from the top and base sill boundaries could give rise to a tapering reflection amplitude and it would be difficult to locate the true termination.

Finally, dykes, which play an important role in vertical magma transport, are difficult to recognize on seismic data, as the reflection seismic method is unsuited to image near-vertical features (Badley 1965).

# CHAPTER 4: RESULTS AND INTERPRETATION

## 4.1. Interpreted seismic stratigraphy of the area

The various horizons interpreted and mapped as the stratigraphy of the stratigraphy of the area were done through the correlation of seismic data and wellbore data (seismic to well tie) as shown in Fig. 3.1 (Chapter 3). Additional help in identifying the lithologies making up the stratigraphy of the study area came from the data provided by NPD fact page on the wells and from previous research and literature on the Vøring basin. The different units or packages making up the stratigraphy of the area have been characterized based on seismic facies analysis and horizon interpretation and separated into different geological ages based on their time of deposition in the Vøring basin (Fig 4.1). A total of nine (9) horizons (H) were interpreted in the area as shown in Fig. 4.2.

Unit 1 (Seabed-H2)

Unit 1 is the Naust Formation and the youngest and topmost stratigraphic unit in the research area, dated late Pliocene. Naust Formation is made up of mainly interbedded claystones, siltstone and sand. At the upper part of the formation are occasional very coarse clastics, which are evident in the high amplitude reflection observed close to the uppermost part of the formation. Reflectors in the formation are generally parallel high to low amplitude, continuous and high to medium frequency seismic patterns (Fig. 4.3). The formation is undeformed, with variable thickness throughout the study area. The unit is thicker in the western part and thinner in the eastern and generally dips towards the north part of the area. The Naust Formation lies unconformably on the Kai formation forming the Base Pleistocene Unconformity (BPU), which occurred during the Pleistocene age. The unconformity is observed as high seismic reflection and hummocky reflection on the seismic data in the study area. The seabed and H2 marks the top and bottom of the Naust Formation respectively.

Unit 2 (H2-H5)

Unit 2 is the Kai Formation and consists of alternating claystone, siltstone and sandstone with limestone stringers deposited in the marine environment during the Early Miocene to Late Pliocene. The Formation is characterized by high to medium amplitude reflections that are mostly continuous and parallel. The Kai Formation includes package 3 (P3), 4 (P4) and 4B (P4B) (Fig 4.3). Package 3 represent the upper part followed by package 4 (the middle part) and package 4B. Package 3 is characterized by parallel, medium to high amplitude, continuous

reflectors. Package 4 on the other hand is characterized by medium to low amplitude reflectors. Some reflections are continuous to the east and discontinuous to the west of the study area. Package 4 is made up of low amplitude reflectors, generally continuous and parallel compared to surrounding reflectors. There are isolated high amplitude zones, generally to the western part of the area in the formation. These are likely gas charged zones as they are associated with fluid conduits in found in the formation. At the western part of the study area are series of polygonal faults. Hydrothermal vent is also present in the Kai formation through all the three packages (P3, P4 and P4B). The Kai Formation has variable thicknesses within the area and thins out towards the east and central part of the study area. In the central part of the area where well 6607/2-1 was drilled through the Någard syncline, the Kai Formation lies unconformably on the Undefined Formation and to the southeastern part in the Utgard High (wells 6607/5-1 and 6607/5-2), where the formation overlie the Brygge Formation.

Unit 3 (H5-H7)

Unit 3 is the Brygge Formation and interpreted between the base of the Kai and top of the Tare Formations. Brygge Formation is made up of sediments deposited in the marine environment during the Early Eocene to Early Miocene and these are mainly claystones with stringers of sandstone, limestone, marls and siltstone. The Brygge Formation is strongly uplifted in the eastern towards the central part of the study area (Fig. 4.3). The Formation is characterized by high to medium amplitude, which are continuous towards the west and east whereas in the center it is medium to low amplitude reflections, which are discontinuous and wrinkled. The Brygge Formation is severely deformed by structures such as hydrothermal vents and polygonal faults.

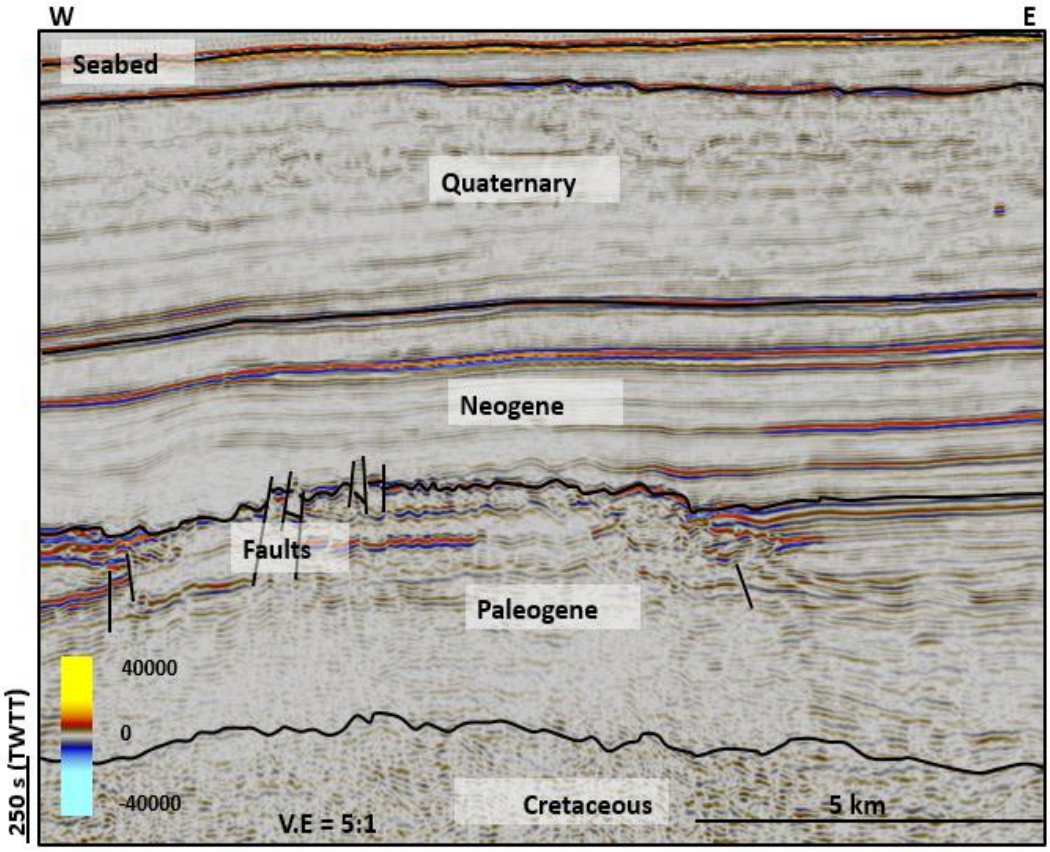


Fig. 4.1. Simplified stratigraphy of the study area based on time of sediment deposition in the Vøring basin.

Unit 4 (H7 to H8)

Unit 4 is the Tare Formation, comprising of dark grey, green or brown claystones with some thin sandstone stringers with variable content of tuff. Tare Formation is dated Danian to Paleocene. Reflections in the formation are characterized by medium to high amplitude, parallel reflectors, which are continuous to the west and discontinuous to the east of the study area. Reflections here are generally continuous but the formation is slightly disturbed with the by faulting (small faults) and some dipping events (Fig. 4.3). In the eastern part of the study area, the Tare formation is folded and underneath the folds are magmatic sill intrusions (Fig. 4.17). In the central part of the area, the topmost part of the Tare formation which is marked by the base of the undefined region is greatly deformed and some evidence of pockmarks and polygonal faults (Fig. 4.19). According to Cartwright et al., 2003, these polygonal faults are an array of layer-bound extensional faults within mainly fine grained stratigraphic interval that exhibits a diverse range of fault strikes which are represented as polygons in map view and as tiers in seismic data. They are almost randomly oriented.

Unit 5 (H8 to H9)

Unit 5 is the Tang Formation. In the central part of the area mainly in well 6607/2-1 is between the Undefined formation and the Tare formation whereas in the other parts it was not present both in well 6607/5-1 and 6607/5-2 in the study area. The Tang formation is predominantly dark grey to brown claystones with minor sandstones and limestone. Deposition of sediment occurred during Late Paleocene. The formation towards the northeastern part and is folded in the eastern and southern part of the study area. It is characterized by medium to low amplitude and discontinuous reflectors. Tang formation is highly faulted at the uppermost part and these are mainly polygonal faults. Reflection patterns in this formation are mainly chaotic towards the base. The Formation is folded in the eastern part of the study area (Fig. 4.3).

Unit 6 (Cretaceous)

Unit 6 represents the Cretaceous stratigraphic units, which is made up of cretaceous sediments deposited Vøring basin. The Unit overlie the basement rocks in the study area. The Cretraceous unit is the main area of interest since the area is heavily disrupted by magmatic sill intrusions. Magmatic intrusion are mainly in the No formal name and the Kvitnos formation as shown on the well log from well 6607/5-2 (Fig. 4.20). Aside the two formations mentions, the Springar, Nise, Delfine, Lange, Lysing Formations form part of the Cretaceous unit. The stratigraphic units mentioned above form the Upper Cretaceous layer in the study area. The Springer formation is the youngest unit, followed by Nise, Lang, Lysing, Delfin and Kvitnos Formation in the order of increasing age. The Cretaceous unit comprises of two main groups namely the Shetland group (Springer, Nise, Delfin and Kvitnos Formations) and the Cromer Knoll group (Lysing and Lange Formation). The Formations in the Shetland group in the study area consist of mainly greyish-green claystones (calcareous in the Kvitnos Formation) with stringers of sandstone and carbonate. The Cromel Knoll group on the other hand is predominantly fine to medium, randomly coarse grained, white-grey sandstones with some carbonate-cemented and interbedded with shales in the Lysing formation and light to medium grey to green and brown claystones with carbonate and sandstone stringers in the Lange Formation.

Generally the Cretaceous unit characterized by low to medium amplitude reflections, which are more chaotic towards the base of the units. The unit is greatly disturbed by faulting, causing it to be displaced in the study area. Low and medium amplitude reflectors are lying concurrently on top of one other towards the topmost part of the unit mainly in the Springer Formation. This type of reflection pattern indicates a succession of fine to medium-grained sediments (claystone and sandstone). The cretaceous sediment are intensely affected by magmatic activity mainly

sill intrusions. From well log data (mainly well 6607/5-2), the magmatic sills are observed in the Informal Name Formation and Kvitnos Formation. In the Lower cretaceous unit are the deep magmatic sill intrusions and deep-seated faults. Magmatic intrusions in the Lower Cretaceous unit are generally very high amplitude reflections.

Unit 7 (Basement)

The basement is the oldest unit in the study area and located at the base of the Cretaceous unit. It is represented by reflectors with high to medium amplitudes which are generally chaotic so no clear reflection responses were observed. The basement is also greatly affected by magmatic intrusions and these are marked by very high amplitude anomaly reflections.

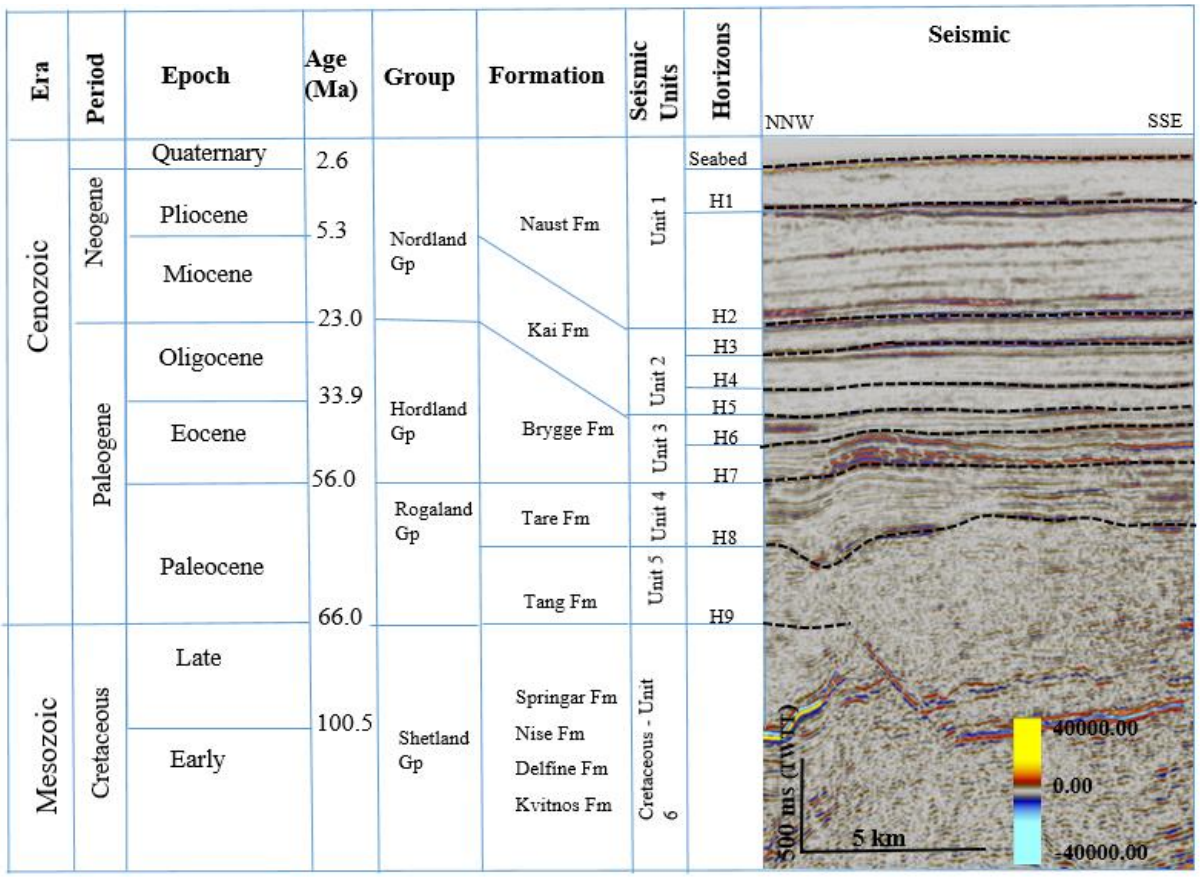


Fig. 4.2. Simplified lithostratigraphic column of the study area showing the ages of the interpreted horizons and their equivalent Formation tops. H-Horizon

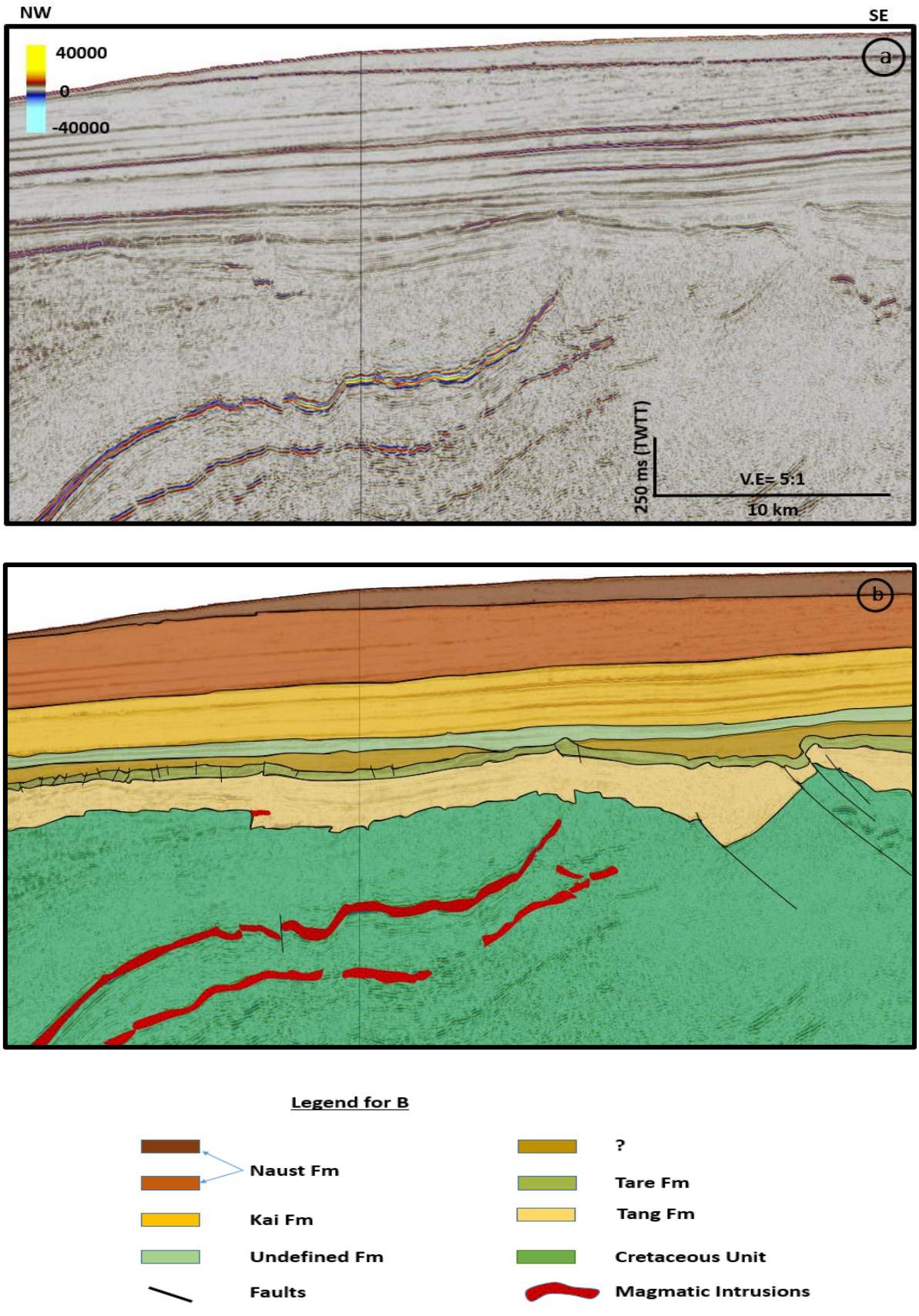


Fig. 4.3. Geological sketch of the lithostratigraphy of the study area. (A) Uninterpreted seismic section of the study area. (B) Interpreted seismic section of Fig 4.3a.

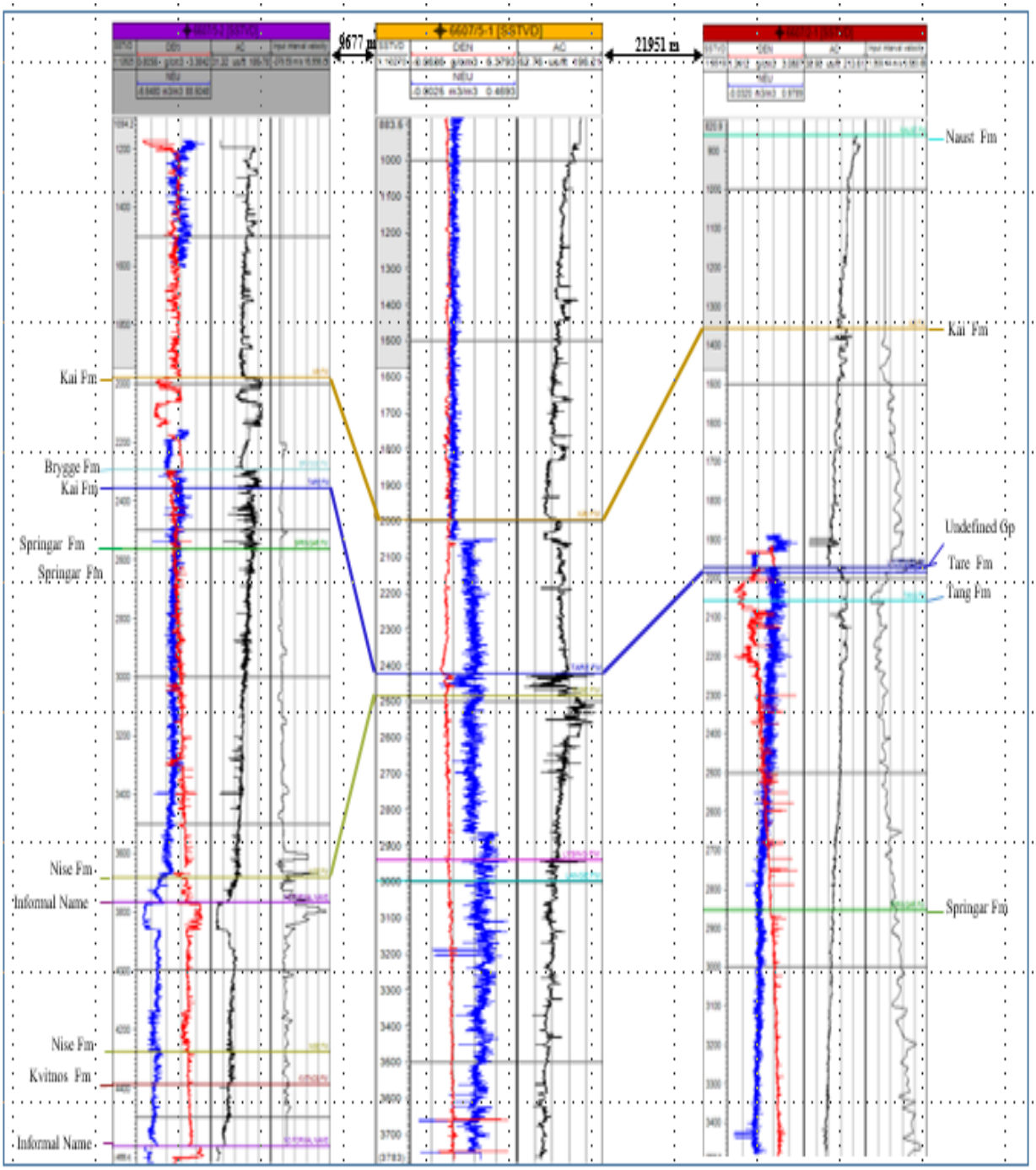


Fig. 4.4. Well correlation of the three boreholes in the study area, including 6607/5-1, 6607/5-2 and 6607/2-1. The sections also include the density log (red), neutron log (blue) and sonic log (black). (Petrel, 2016)

## 4.2. Magmatic Sill interpretation

The magmatic sill is conventionally defined as a tabular intrusive bodies of magmatic origin that are predominantly parallel with concordant surfaces of contact (Allaby and Allaby 1999) and thin compared to their lateral extent (Mudge, 1968; Lister and Kerr, 1991; Walker, 1993). Nevertheless, it is obvious from seismic mapping that sill-like igneous intrusions assume a wide range of geometries from fully concordant sheet-like bodies to highly complex discordant geometries (Hansen, 2004).
Magmatic sills are generally observed as extremely high amplitude reflections on seismic data due to a significant difference in acoustic properties between igneous material and sedimentary rocks they intrude (Badley, 1985).

In this section, magmatic sills in the study area are described based on their seismic characters, which includes high amplitude reflections, reflection continuity, abrupt termination of reflections, transgressive reflections (discordant relationship with stratal reflections), their geometries, areal of extent, position and how they interact with each other and other geological structures like folds, faults and hydrothermal vents in the region.

The magmatic sill intrusions in the study area appear as single and compound units in three dimensional complexity. The single unit sills are individual sills that are isolated without any connection to another sill whereas the compound sill units are sills with complex geometries that consist of a number of concordant and discordant segments as shown in Fig 4.5, where Sill 1 and Sill 2 are examples of such sills. These compound sills have complex and irregular edges.

In the 2 and 3- Dimensional view, the magmatic sill intrusions are highly interconnected to form a network of sills or compound sills that developed through a succession of recurrent intrusive events over discrete stratigraphic intervals.

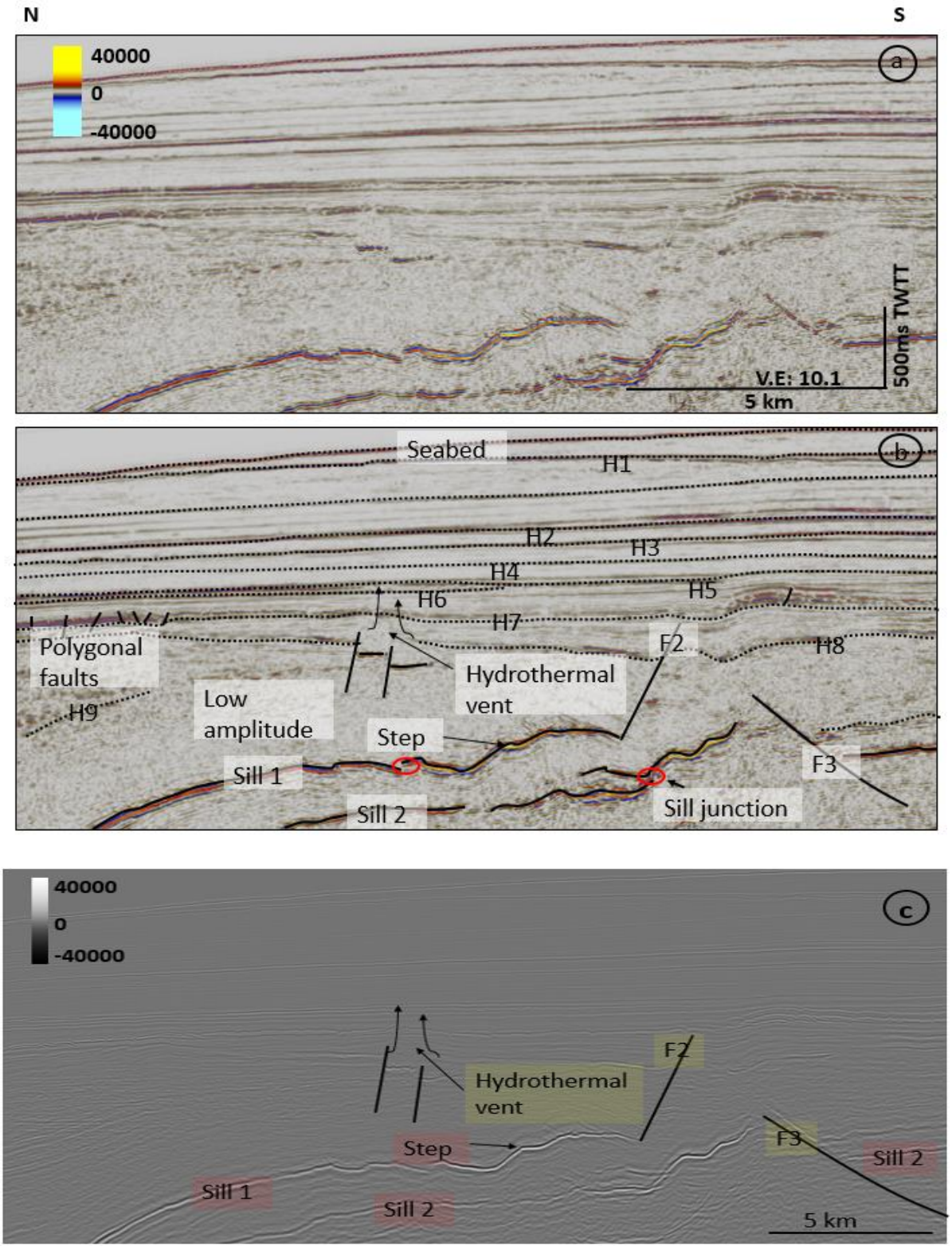


Fig. 4.5. Seismic interpretation of magmatic sills in the study area displaying high amplitude anomalies. Sills are showing various geometries and join to form compound units at sill-sill junctions. (a) Uninterpreted seismic section. (B) Interpreted seismic profile of Fig 4.5a and (c) Graphic equalizer showing that the sills appear brighter than surrounding features with low amplitudes. H - Horizons

4.2.1. The Magmatic Sill in the study area

Twelve major magmatic sills have been identified and interpreted from the study area based on the available 3D seismic data provided. The magmatic sills were interpreted at depths 3.1 s TWTT to 8.0 s TWTT as shown in Fig 4.5, At this depth, the magmatic sills are wide-spreading, forming sill complex of interconnected sills found mainly within the upper and lower cretaceous unit below Horizon 9 (Fig 4.5). Based on the depth of occurrence of the magmatic sills, they were categorized into three main groups, which are shallow, intermediate and deep sills. The shallow sills at depth less than 3.5 s (TWTT), intermediate sills at depth of 3.5-5.0 s (TWTT), and deeper sills at depth greater than 5.0 s (TWTT) accordingly.

The northern and southern part of the sill complex is defined by the Nyk High and the Utgard High respectively. The western extent of the sill complex is uncertain as the Cretaceous basin is poorly imaged here due to the presence of overlying volcanic extrusive rocks. The eastern extent of the sill complex is fairly well defined, except in the very northern and southern regions where high amplitude events are associated with major pre-Cretaceous faults.

The two main complex sills in the study area are Sill 1 and Sill 2 (Fig 4.5). These sills are extensive and seen in almost every part of the study area. They are continuous at the northwestern part of the study area and discontinuous towards the southeastern areas. This applies to most of the other sills present in the study area. The two complex sills in the study area are made up of combination of individual sills with several geometries and are interconnected by sill-sill joints (Fig. 4.5 and discussed below in details). Morphometrically, Sill 4 and Sill 2 are the two large sill complexes in the study area and cover approximately $10.60 \times 10^2 km^2$ and $12.80 \times 10^2 km^2$ respectively. Individual sills connecting to form the complex sills are both concordant and discordant sills (Fig. 4.5). The concordant and discordant sills are mainly layer parallel and saucer shaped respectively (Fig…). The approximate lateral extent of the sills in the study area ranges from 253.4 km (Sill 2) to 77.5 km (Sill 7) and the coverage area of the sills is between $12.80 \times 10^2 km^2$(Sill 2) and $5.20 \times 10 km^2$ (Sill 7). About 80% of all the magmatic sills observed in the study area are dipping NW with a few towards the SE part of the basin and are highly concordant to the host stratal reflection configurations.

The width of the sills can reach up to 426.4 km (Sill 2) (Table 2). The aspect ratio (A) (i.e., length/width) for the sills is expressed as $0.19 \leq 0.59$ (Table 2). Sills in the study area are composed of complex structural elements.

Between the intermediate and deeper levels of the study area are magmatic sill swarms. Sill swarms are sub-parallel to parallel arrangement of different sills, which are localized above highs (Fig. 4.7). Magmatic sills in the study area tuned seismic response, and sill thickness is estimated as being less than the vertical resolution (Smallwood and Maresh, 2002) and ranges from 40 m to 91m based on the velocity recording from the sonic log. Tuning reflections made it difficult to measure and estimate the actual thickness of the magmatic sills in seismic data. The sills are predominantly found in the Cretaceous unit and are mostly noticeable in the NW part and a few in the SE part of the study area. These sills exhibit complex geometries including saucer shaped, layer parallel, planer parallel and fault plane as shown in Figs Magmatic sills at the shallow level are planer parallel as compared to the intermediate sills which exhibit both saucer (mainly to the southern part of the area) and planer parallel shapes. Deep sills are lager and rise vertically further than those intruded at shallower levels, indicating the relationship between the vertical extent (Z) and the emplacement depth. In the northwestern part of the study area is a structure like volcanic edifice, piercing through H8 and H7. Sediments within the volcanic edifies are highly disturbed as shown in Fig. 4.6 below.

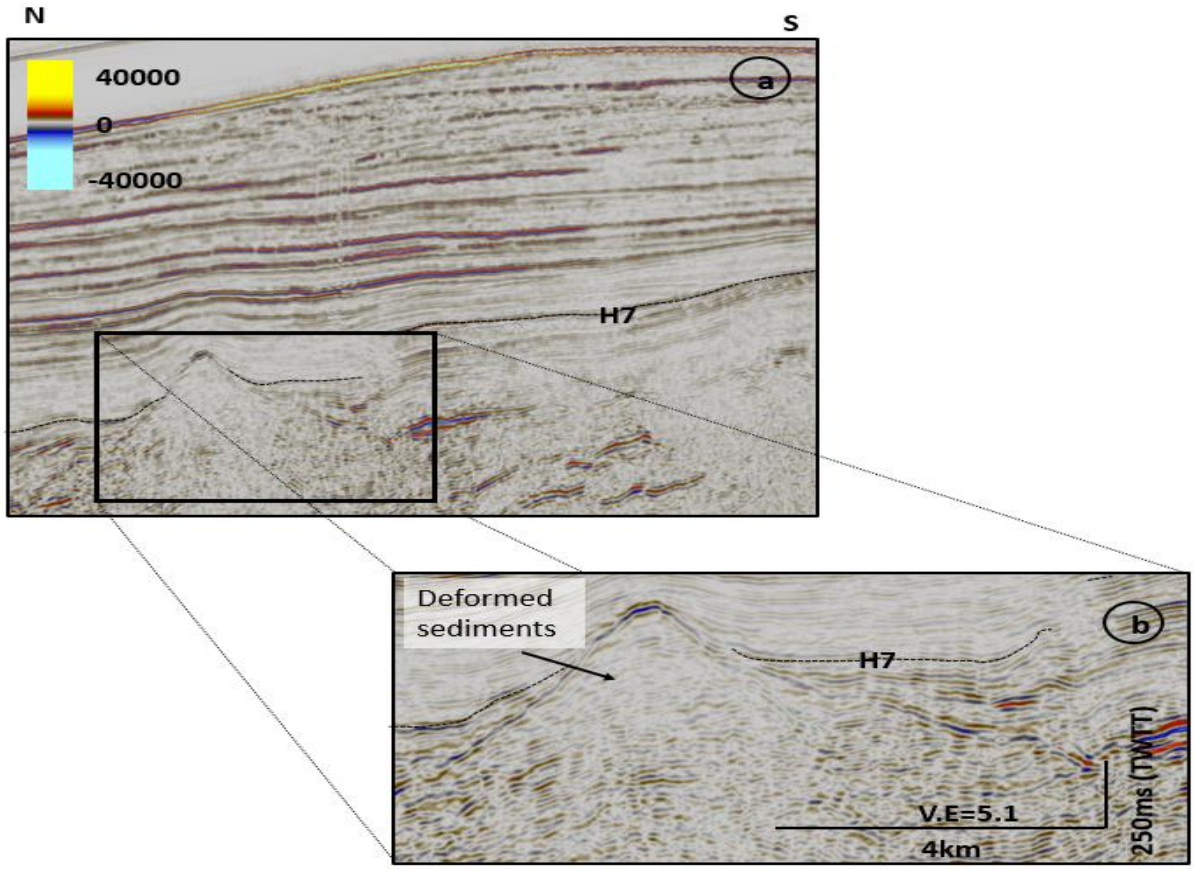


Fig. 4.6. An example of a volcanic edifice interpreted in the northwestern part of the study area and it has similar characteristics as a cinder volcano.

#### 4.2.1.1. Sill – Sill junction

A distinctive feature observed in the study area is that most sills connect with sills above and below through sill - sill junctions (Fig 4.7, 4.8, 4.9, 4.11 and 4.12). Hence indicating that these individual sills forming the junctions were emplaced as part of larger sill complexes as observed in the interpreted section in Fig. 4.5. The merging of sill complexes to form hybrid sill complexes (sill complexes made up of more than one sill facies) or the merger of flow units within a sill complex, results in the development of junctions due to the support of a sill or sill complex against a second sill or sill complex (Thomson and Hutton., 2004). Significantly, the sills forming junctions connect with shallower sills near their deepest point, which strongly implies that the shallower sills were intruded by magma fed via the deeper sills (Hansen et al., 2004).

Two main sill junctions were observed. Mainly the inclined and antiformal junctions, which developed as results of integration of individual sills to form complex sills (Thomson and Hutton, 2004). According to Thomson and Hutton., 2004, the inclined junction develops due to the support of an inclined sheet (Sill 1a) against another inclined sheet of an adjacent sill complex (Sill 1b) as shown in Fig. 4.7 below. The part of the inclined sheet terminating against the second complex sill prevents the sill from developing into an outer rim. The second sill complex is completely developed because it did not terminate against another sill (Fig. 4.9). The boundary between the two sill complexes forming an inclined junction progressively transforms into an antiformal junction in some areas in the study. The antiformal junctions develop between the tips of two inclined sheets (sills) from adjacent sill complexes and contrarily to the characteristic of the inclined junctions, both of the inclined sheets are equally developed and merge to form a tight antiformal closure (Fig. 4.7) with neither inclined sheets continuing upwards to form an outer rim (Thomson and Hutton., 2004).

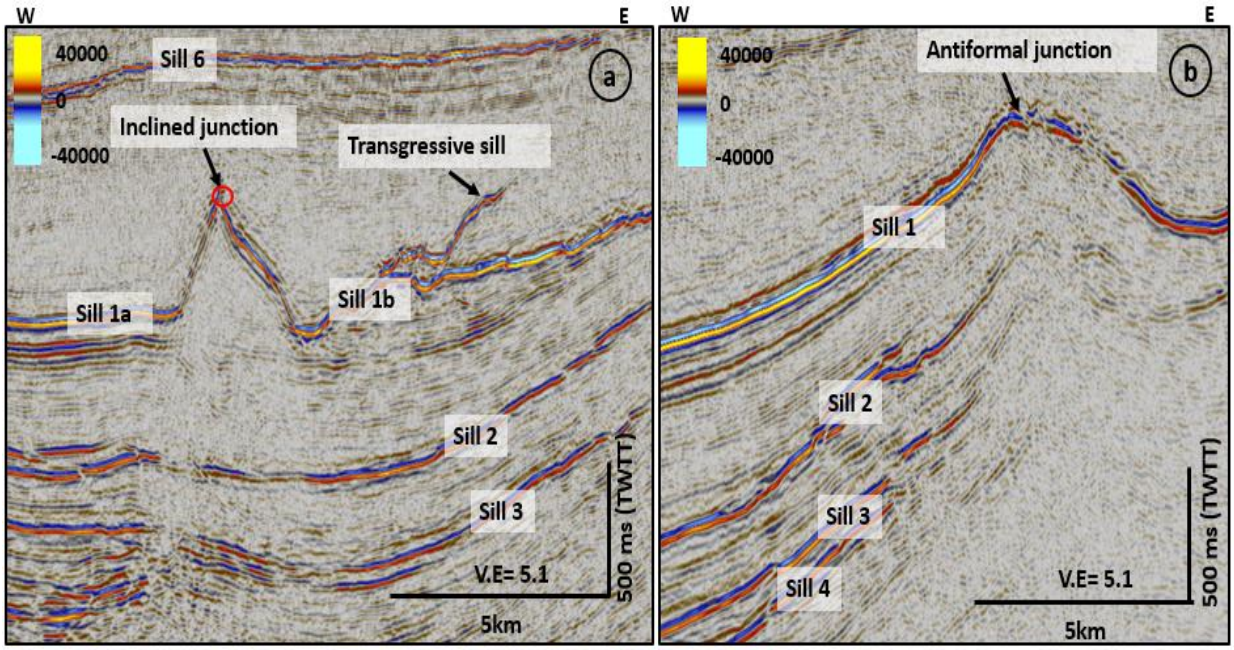


Fig. 4.7. Examples of sill-sill junctions in the study area. (a) Example of inclined junction formed by the joining of two inclined sheets and (b) Antiformal junction showing that both inclined sheets forming the junction are equally developed.

Hence, both sill complexes connected by an antiformal junction lack peripheral outer rims along the length of the antiformal junction as the inclined sheets mutually terminate. 'T' and 'F' shaped geometries were observed and they formed by the merging to magmatic sills in the study area (Fig 4.8 and 4.9).

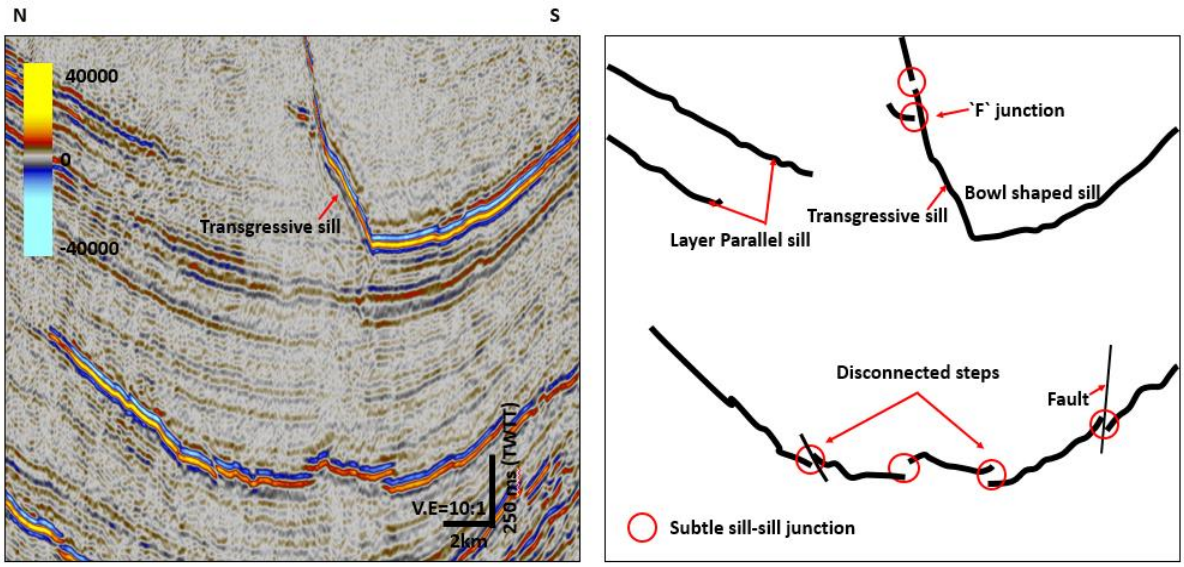


Fig. 4.8. Example of sill-sill junction forming sill complexes. Junctions formed the disconnected steps, the `F` junction and transgressive sill in the study area.

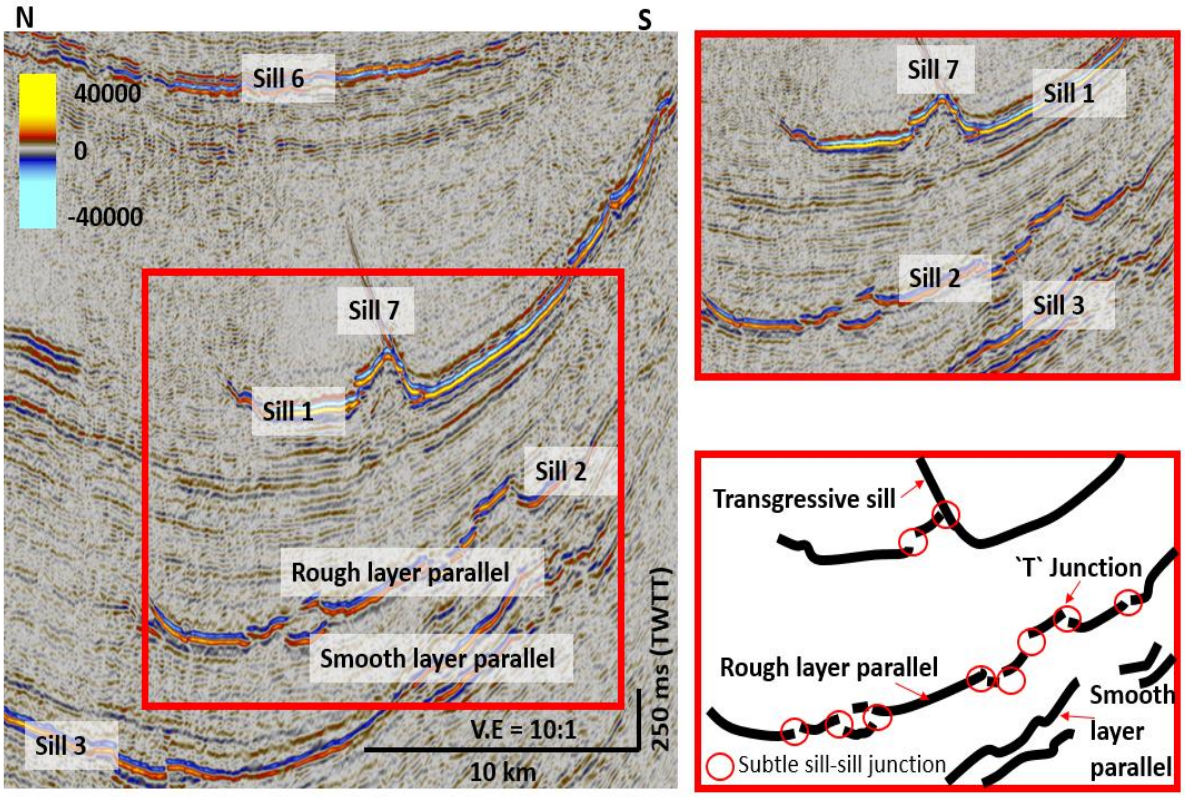


Fig. 4.9. Example of sill-sill junction mainly the T-junction. The rough layer parallel sill is noted to have series of sill –sill junctions hence making it discontinuous. The smooth layer parallel is made up of connected steps. In the image at the left Sill 6 is a smooth layer parallel sill without steps.

These unique sill-sill junctions form a complex structural feature termed as steps. The steps are generally found amongst the intermediate to deeper sills and they are more discontinuous (disconnected) than continuous (Fig 4.8, 4.11 and 4.12). Steps are described as flow indicators within magmatic sills, which are normally oriented parallel to the axis of sill emplacement (Pollard et al., 1975; Schofield et al., 2012a; Thomson and Hutton, 2004, Omosanya et al., 2017). Disconnected steps provide hint of original offset between magma segments at different stratigraphic levels, meaning, the increase of the segments was not sufficient to cause two adjacent steps to merge and form a continuous step (Schofield et al., 2012a and Omosanya et al., 2017).

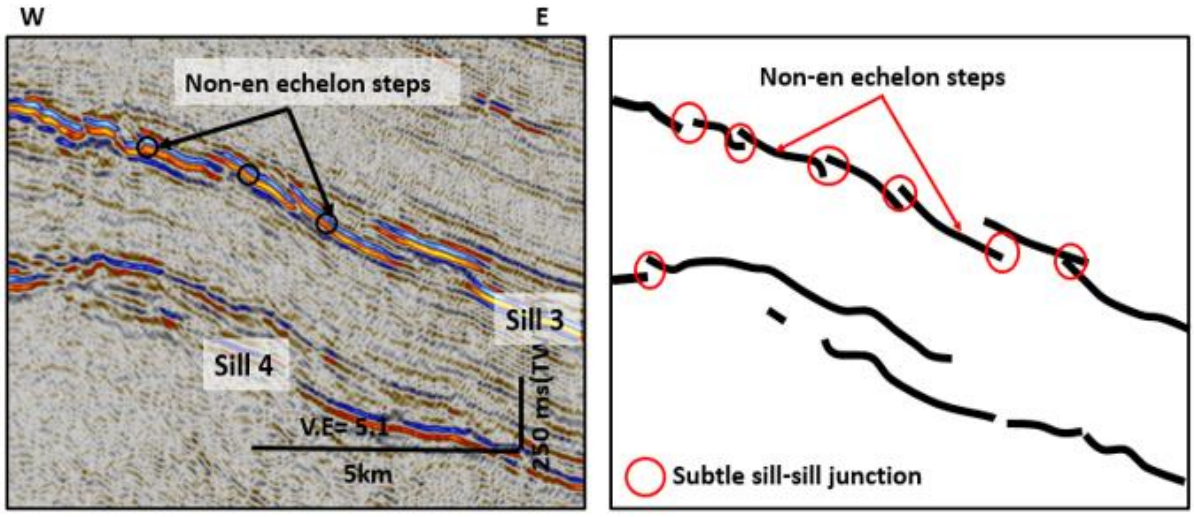


Fig. 4.11. Example of discontinuous steps forming a non-en echelon steps in the study area. The magmatic sills are discordant with respect to stratigraphy.

The magmatic sills show steps that are concordant and discordant with respect to their orientation (Fig. 4.11 and Fig. 4.12) The discordant steps are typically asymmetric and are developed as non-en echelon steps (Fig. 4.11) that move across stratigraphy suggesting they resulted from the preferential exploitation of different horizons in contrast to en echelon steps that are formed due to creation of a stepped fracture ahead of the sill tip (Schofield et al., 2012a, 2012b and Omosanya et al ., 2017). Symmetric steps along strike thus trend in one direction indicating the increase in offset between sill segments in a down-flow direction (Rickwood, 1990 and Omosanya et al., 2017).

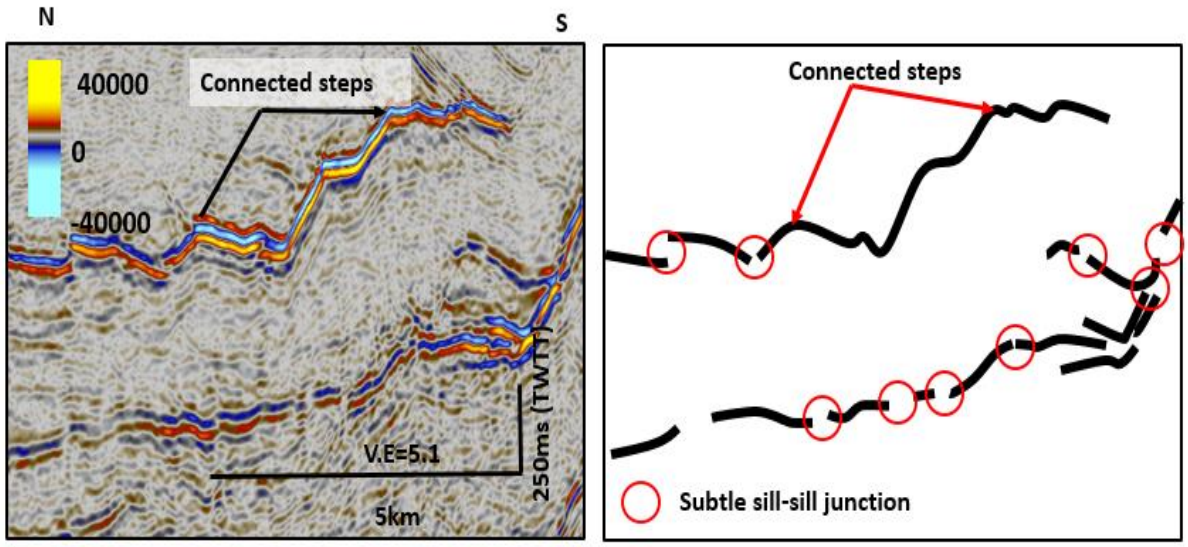


Fig. 4.12. Typical connected steps interpreted in the study area.

Apart from the sills forming steps or bridges, some magmatic sills are connected to structures like hydrothermal vents identified between H9 and H4, forced folds between H7 and H8.

#### 4.2.1.2. Sill facies Units

The seismic facies unit mapping of interpreted sill intrusions discloses several systematic variations in shape and geometry of the sill complexes. A more complicated sill facies unit distribution is present in the Vøring Basin. The magmatic sills are then categorized into 4 main sill facies units based on the size, geometry, smoothness, continuity and depth from the paleosurface of the interpreted sill reflections. The sill facies units are grouped into layer parallel, saucer-shaped, fault block and planar transgressive (Fig 4.7 and 4.15. The Saucer-shaped sills are a fundamental form and are most common in intermediate to deeper depths in undeformed basin segments. The deepest parts of the basins are characterized by layer-parallel intrusions. The central Vigrid Syncline is dominated by Layer-Parallel Rough sills, which merge into a Planar Transgressive sill. Layer-Parallel and Basin-saucer units dominate the inner parts of the basin (Figs. 4.9 and 4.14).These sill geometries are strongly influenced by structures and heterogeneities such as fault blocks, layering and deformed strata. Another form of sill geometry is the sill intrusions associated with faults and are described as fault block sills (Fig. 4.19).

- Saucer shaped sills

The Saucer-shaped sills are described by an inner sill, an inclined sheet and an outer sill (Fig. 4.15). They are widespread in the study area and they are characterized by high amplitude reflections and follow a down bending shape with edges terminating at different depth. In an instance, the upper part of the saucer shaped sill is associated with forced fold, indicating post depositional deformation of the bedding. Some of the saucer shaped sills are radially symmetrical and consist of a saucer-like flat inner sill at the base with inclined sheets connecting it to a gently inclined, commonly ragged outer rim (Fig. 4.15). Such geometries previously have been documented using 3D seismic data from Faeroe-Shetland Basin (Davies et al., 2002, Smallwood and Maresh 2002) and North Rockall Trough by Thomson and Hutton, 2004. These sills have a number of concentric magmatic intrusions like dykes rising from their inner saucer (Fig. 4.15). In some part of the area, the saucer shaped sill merges with a bowl-like shaped sill to form eye-shaped sills (Fig. 4.13). In this the saucer shaped sill is normally connected to the top of the bowl-shaped sill by sill-sill junction (Fig. 4.13).

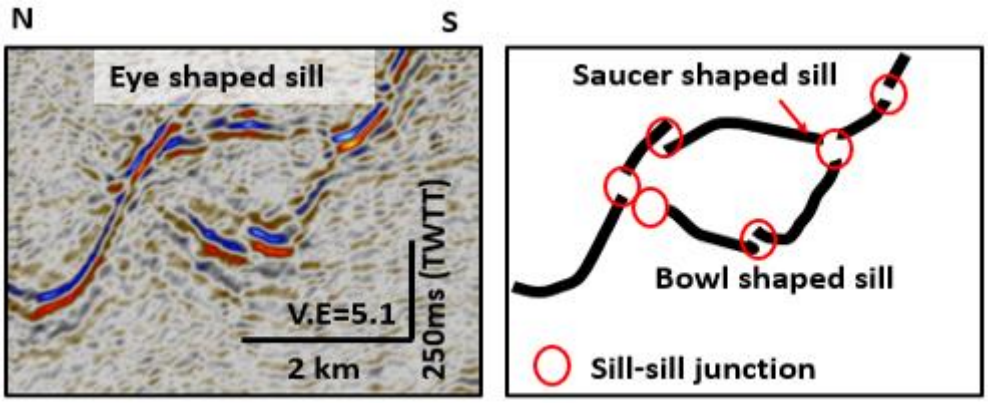


Fig. 4.13. Example of a typical eye shaped sills interpreted in the study area. It is made up of a bowl-shaped sill at the bottom, overlain by a saucer-shaped sill at the top.

Two main groups of saucer –shaped sills were identified in the area as Basin-saucer and Climbing-saucer shaped sills.

- Basin-saucer

These are high amplitude reflections characterized by smooth seismic character and a large degree of continuity are shows an overall saucer-shape defined by the basin stratigraphy (Fig. 4.14). They are found in the inner part of the area, mainly in the central region and between the intermediate and deeper levels palaeosurface and commonly marks the landward termination of the sill complex.

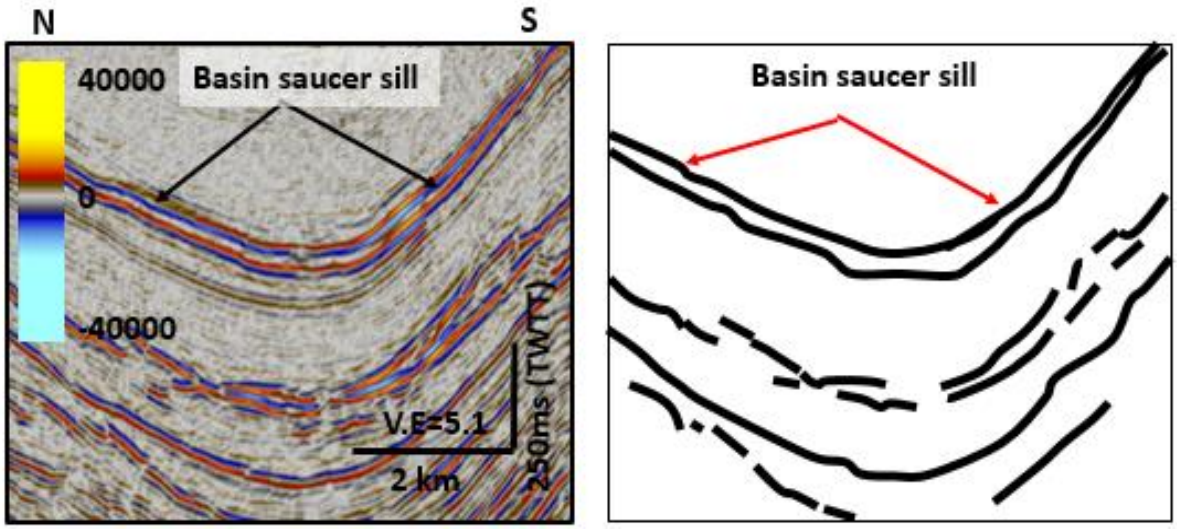


Fig. 4.14. Example of a basin-saucer interpreted in the study area.

- Climbing-saucer

These are more like saucer-shape sills transgressing the surrounding stratigraphy, therefore shows both elements of the two sill geometries (Fig. 4.15). The saucer-shaped sill is usually shallower on one side, causing it to transgress against stratigraphy.

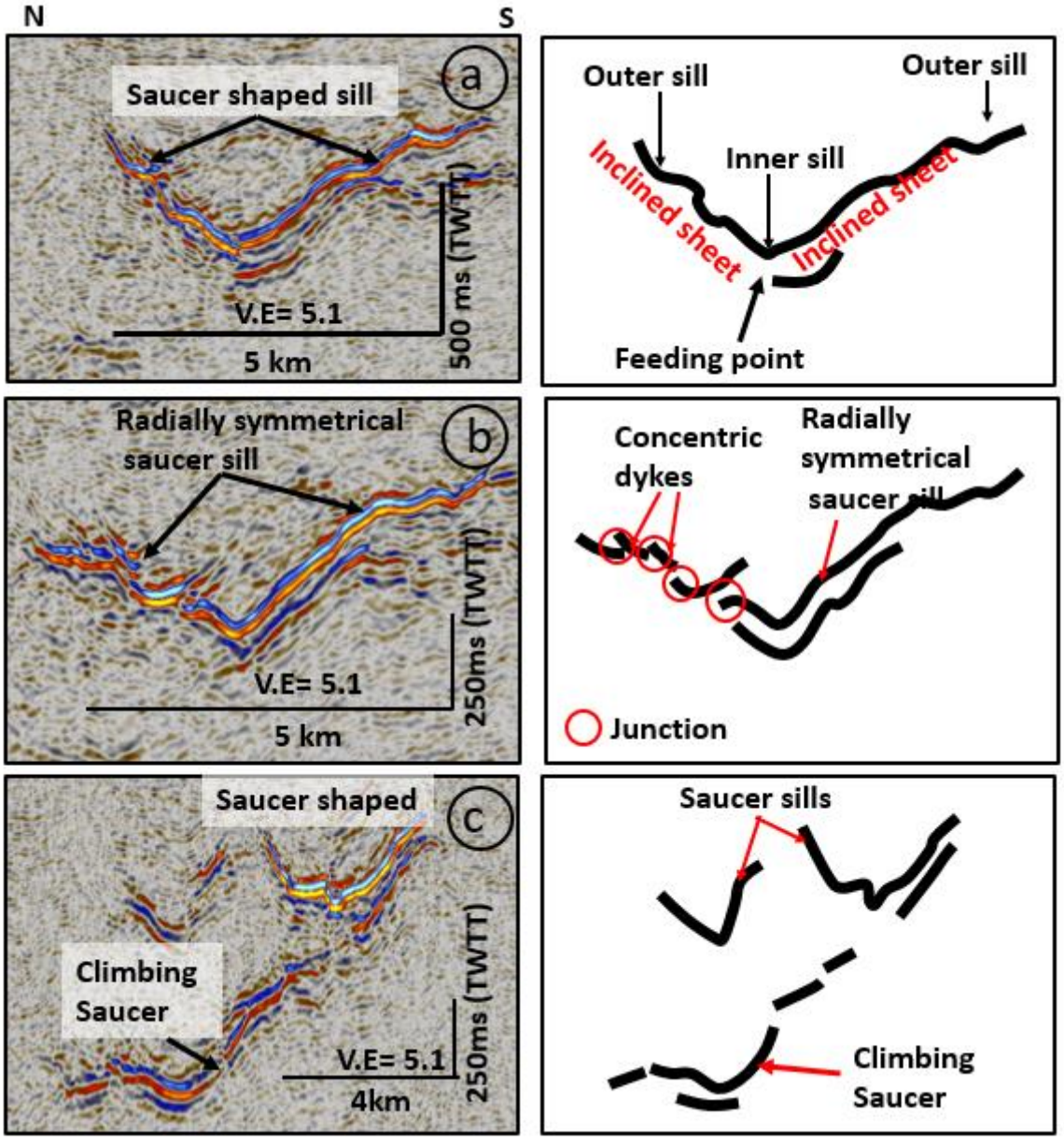


Fig. 4.15. Examples of the saucer shaped sills interpreted in the study area. (a) A well imaged saucer shaped sill made up of the inner and outer saucer and inclined sheets. (b) A radially symmetrical saucer shaped sill with concentric rings of intrusions like dykes emerging from the surface of its inner saucer. (c) Saucer shaped sills with a typical climbing saucer transgressing surrounding stratigraphy.

- Layer parallel
    - Planar - transgressive.

These are high amplitude reflection anomalies which are planar and equally rough and segmented (Fig. 4.9). They are continuous, planar and discordant to stratigraphy. The sills are found in the central parts of the sill complex in regions associated with pre-Cretaceous structural highs. Sill 7 in Fig 4.9 shows a typical transgressing sill and this is associated with Fault 1 in Fig. 4.19.

- Smooth-Layer-Parallel

They are characterized by high-amplitude, smooth seismic character which have large degree of continuity (Fig. 4.9). Mainly identified at depths ranging from the intermediate to deeper depth below the palaeosurface. Sill 3 and Sill 6 in Fig. 4.8 are typical smooth-layer parallel sill.

- Rough-Layer-Parallel

These are layer-parallel sills which are characterized by rough appearance showing high degree of discontinuity and are usually connected by local transgressing segments (Fig. 4.8). They are mainly located in the central parts of the Vøring Basin between the intermediate to deep levels below paleosurface.

- Fault Block

Sills reflection tend to follow fault planes and/or step in the stratigraphy in the vicinity of faults. They represent high-amplitude events inside fault blocks and stratigraphic weakness zones. A typical example is Sill 7 in Fig. 4.19.

## 4.3. Sill – Hydrothermal vents relationship

The hydrothermal vents / pipes located above the sills are identified on seismic data as sharp and thin vertical zones of low amplitude to chaotic reflections with either dome or crater morphology at the top with columnar structure (Fig 4.16). Almost 90% of the hydrothermal vents in the area are disconnected from the magmatic sills and have no interaction with them. Hydrothermal vents interacting with the sills are generally associated with smaller sills with varying geometries at the bottom at shallow level below the paleosurfae. Vent complexes are

mainly located in the central part of the Voring Basin. Generally, small and intermediate vent complexes dominate the southern area, whereas large vent complexes are found near the inner parts of the basin close to the north. More than 70% of all the identified hydrothermal vents complexes are small and are mostly extensive. The large vent complexes make up about 5 % of the total number.

The most dominant morphology of the vents is the crater-shaped, whereas dome-shaped upper parts are also common (Fig 4.16) and are associated with the large vents.

Hydrothermal vent complexes and fluid-flow conduits are evidences for vertically focused fluid-flow in the study area. Generally, seismic reflection above the vents are chaotic and distorted, deforming sediments within the space created by the conduits (Fig 4.16). Most reflections are dipping inwardly around the conduit zone (about 70%), whereas outward-dipping reflections are also found (about 5%). The hydrothermal vents were categorized using the Variance seismic attribute (Fig. 4.16).

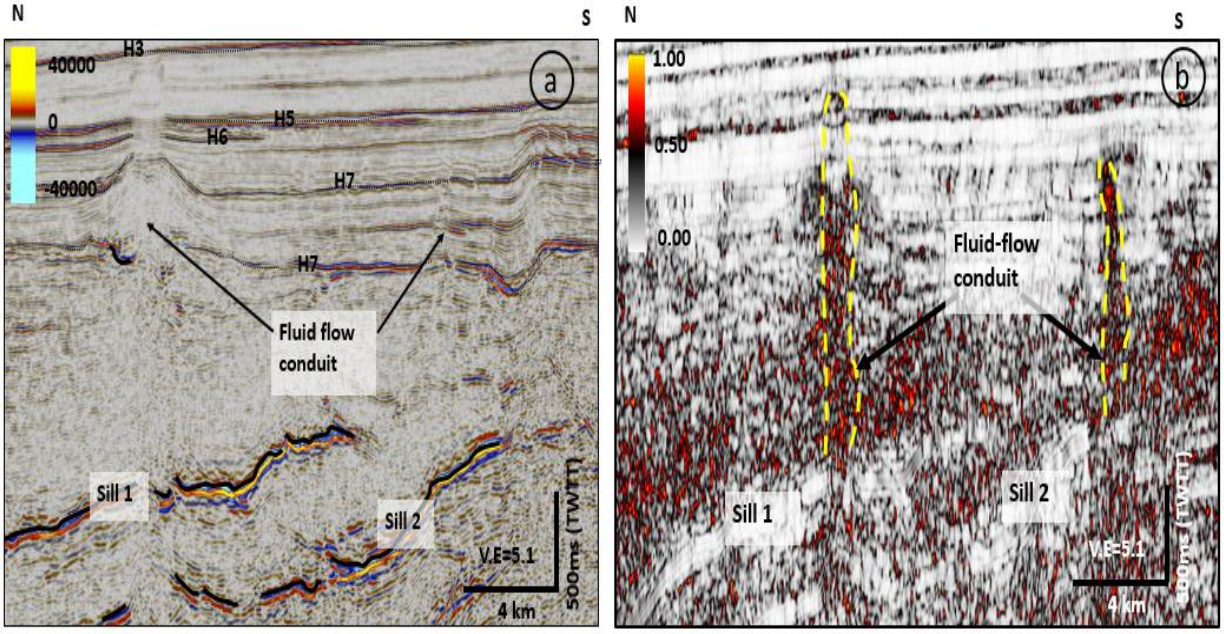


Fig 4.16. N-S seismic section through the hydrothermal vent complex. (a) At the top of the conduit (left), sediments are disturbed by the underlying sill into low amplitude reflections, the second vent to the right is not associated with any magmatic sill (b) Variance seismic section through the same hydrothermal vents in Fig. 4.16a.

4.4. Sill – Fold Relationship

Magmatic sills in the study area have less interaction with the folding, meaning that most of the folds are not influenced by sill emplacement mechanism. Nevertheless, a few forced folds in the area are influenced by the sills in Fig 4.16. Forced folds have been described by Stearns, 1978 as 'folds' in which the final overall shape and trend are dominated by the shape of some forcing member below. Most folds are identified at shallow levels of emplacement during growth of sills, showing as post depositional modification of the overlying strata. Forced folds were identified based on the thinning of the overburden strata, onlaps (seismic stratigraphic expression). The folds formed as a result of accommodation of sill emplacement as shown in the onlap refletions in H7 which is the overburden strata on H8.

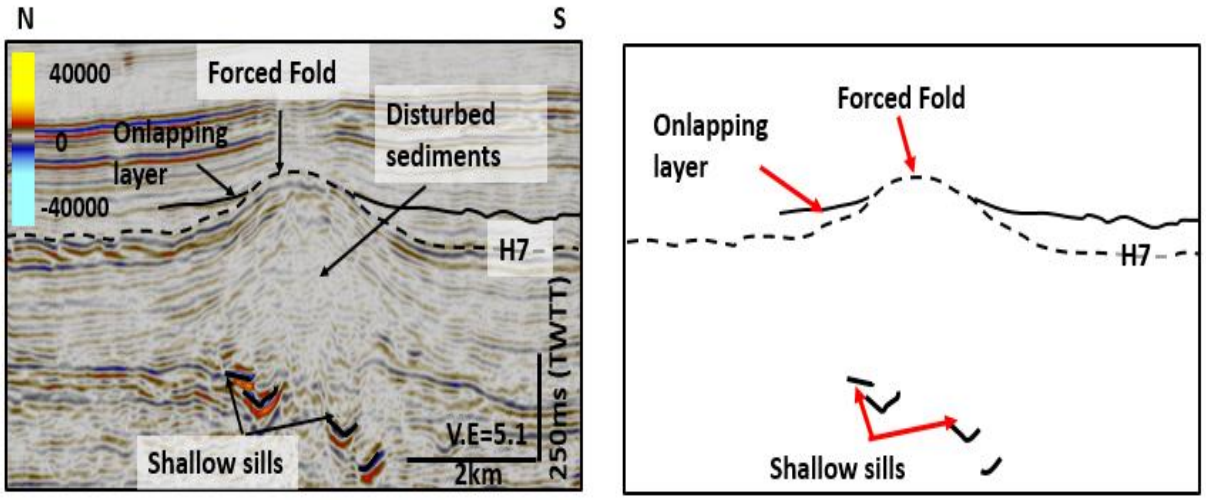


Fig. 4.17. Forced fold interpreted in seismic section of the study area. Fold formation is influenced by sill emplacement below. Sediments within the fold are chaotic and disturbed with low to medium amplitude reflections.

4.5. Fault Interpretation

Faults in the area are mainly reversed faults trending NW-SE and are mainly found between H5 to H8 and the cretaceous unit, mainly between the Brygge formation and the Tare formation and the topmost part of Tang formation and Cretaceous rocks. About 80% of the faults in the area are polygonal faults, mainly located at the shallow burial depth paleosurfae (Fig. 4.19). Fig 4.18 and Fig. 4.19 is a typical example of a deep seated faults mainly between H7, H8 and H9.The major faults are identified in the cretaceous unit and they are mainly associated with magmatic sills (Fig. 4.18).

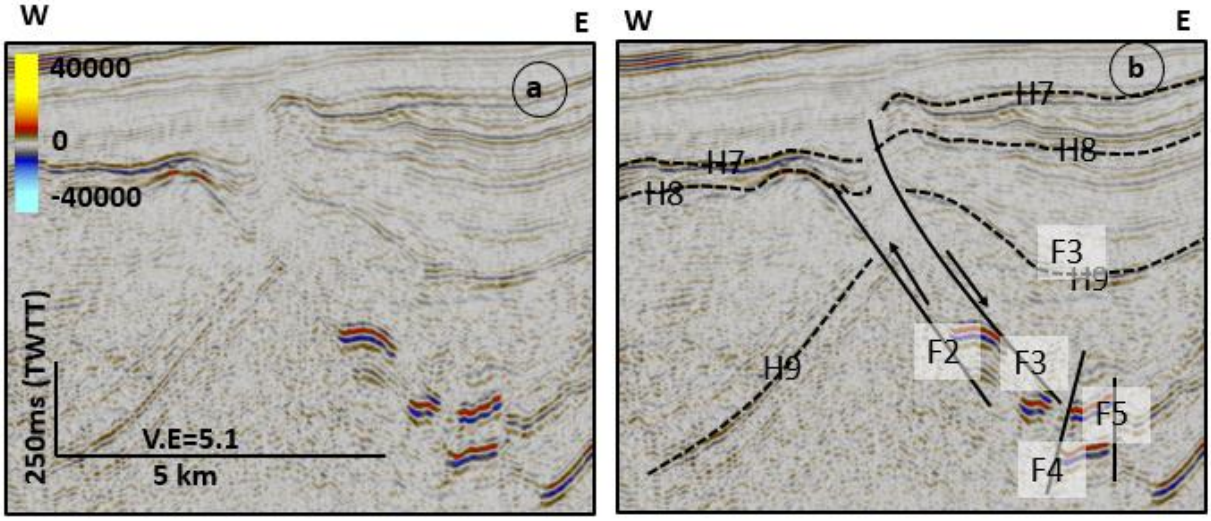


Fig 4.18. Examples of faults interpreted. These faults have no connection with the magmatic sills in the study area

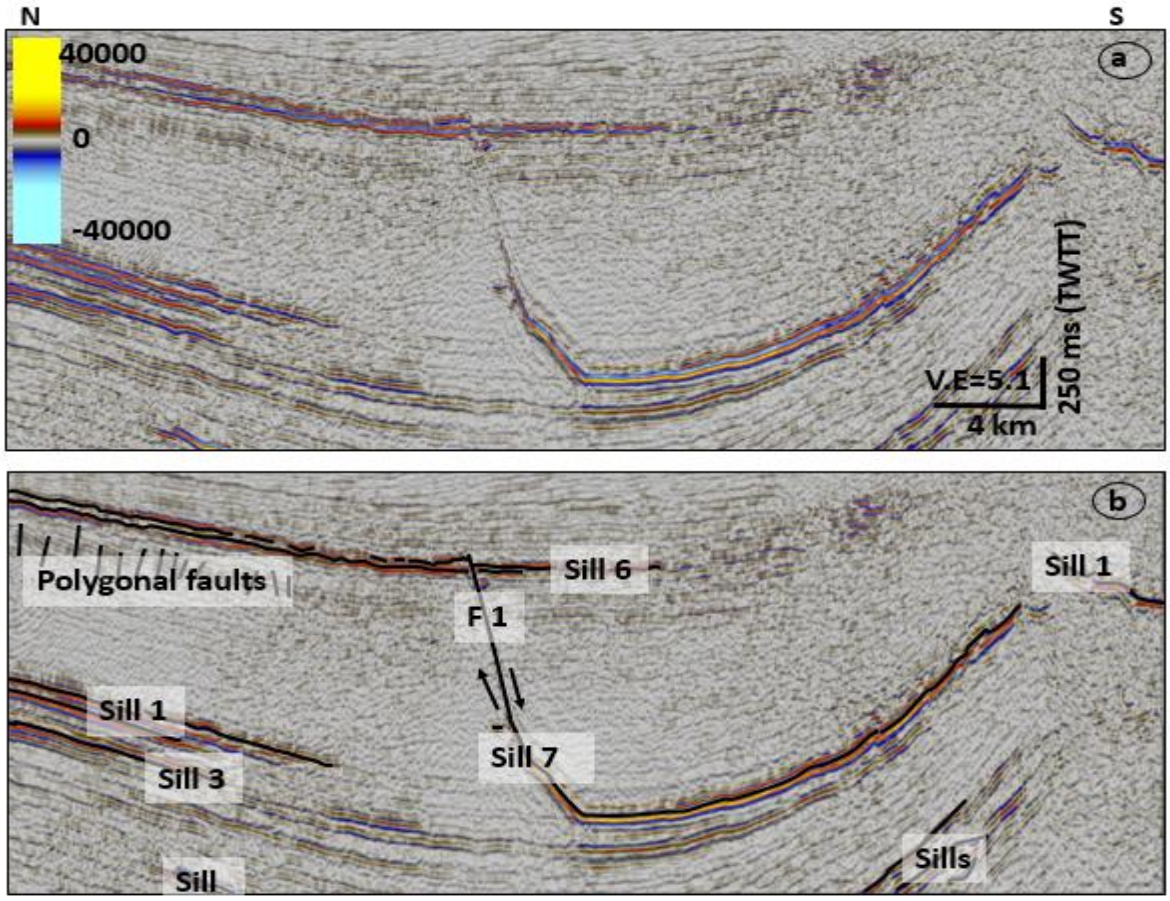


Fig 4.19. (a) Uuinterpreted seismic section through some faults in the study area. (b) Example of a major faults associated with magmatic sill emplacement interpreted in the study area. At

the shallow level are polygonal faults trending mainly southwest. The major fault is trending northeast. The geometry of the sill in the fault plane is a typical fault-plane sill.

## 4.6. Petrophysical analysis

Sills have been sampled east of the Vøring Escarpment in well 6607/5-2 on the Utgard High (Norwegian Petroleum Directorate, 1997). Three sills were penetrated by well 6607/5-2. The Uppermost sill is a 2 m thick dolerite in late Campanian claystones at a depth of 3419 m (Fig. 4.20). The Middle sill, which is 91 m thick, was reached at a depth of 3792 m, intruded into altered claystones of the Campanian Shetland Group, representing the thickest sill encountered in the well. As the well terminates, it penetrated into the third sill in the Kvitnos formation (below the Turonian sandstones) and it is about 50m thick. The middle sill is well imaged on the seismic profile because it is thicker than the vertical resolution limit unlike the upper sill. Therefore the uppermost sill in the well is not imaged properly in the seismic profile, that is, it is too thin to be imaged. The lowermost sill is poorly imaged, probably due to transmission losses of the reflected energy crossing the high-impedance boundary between the middle sill and the surrounding host rock.

The magmatic sills have distinct anomalies on the sonic and density logs from well 6607/5-2. The middle sill is obvious on the logs because of its thickness. The density log marks a velocity increase from 3.0 to 3.2 km/s in the surrounding sediments to more than 7.3km /s in the magmatic sills. The average velocity of the sill is estimated as 7.0 km/s. Adjacent velocities are high and this is a signature response from metamorphic aureoles formed in sediments close to magmatic intrusions as a results to contact metamorphism as described by Fowler and Nisbet, 1982. These metamorphic aureoles surrounding the magmatic sill form the transition zone and these are approximately 80m thick. These transition zones can be observed on the sonic log but not the density log (Fig. 4.20). The nearby wells (6607/5-1 and 6607/2-1) did not intersect any sills.

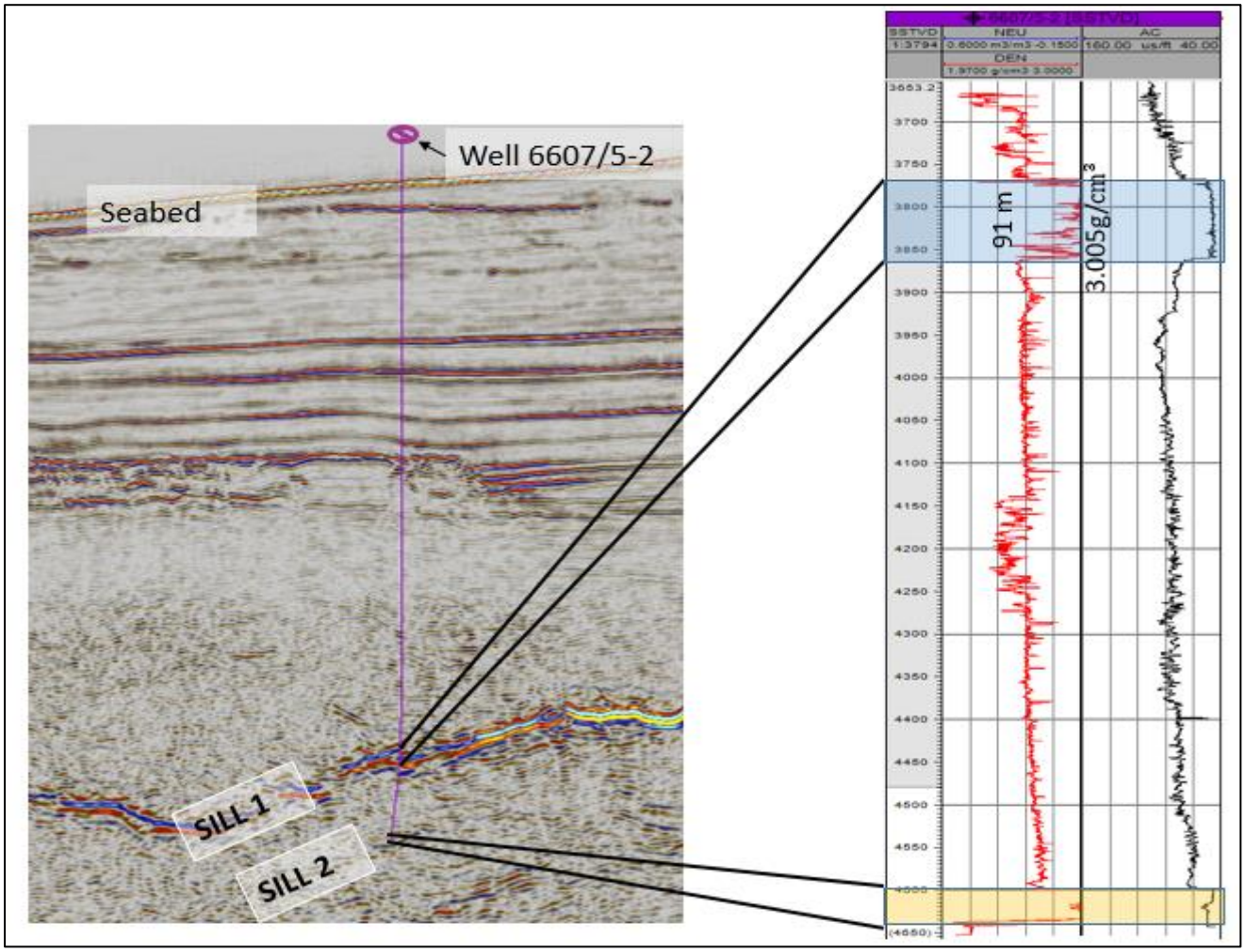


Fig 4.20. Petrophysical well log of magmatic sills found in Well 6607/5-2. The main logs featured are the density and sonic logs. Magmatic sill have high density and high velocity.

## 4.7. Statistical analysis

The morphometric character of the magmatic sills including their area, length, depth, with and orientation shows that the sills are extensive in the study area at different depths. The saucers shaped sills are predominantly at the shallow to intermediate levels whist the layer parallel sills are mostly at the deeper part of the area. Magmatic sills interpreted are mainly in the intermediate to deep levels of the study area. The intermediate sills have areas ranging from $1.20 \times 10^8 m^2$ to $6.64 \times 10^8 m^2$ and lengths of 164 km to 171km (Table 3). The area coverage and lengths of the deeper sills range from $0.52 \times 10^8\ m^2$ to $12.8 \times 10^8 m^2$and 77km to 253km respectively.

Table 3: Morphometric character of the magmatic sills in the study area. The Aspect ratio is the fraction of the length to the width of the sill

| Sill | Depth (s TWT) | Area ($\times 10^8$)$m^2$ | Length (m) | Width (m) | Aspect ratio (L/W) |
|---|---|---|---|---|---|
| 1 | 5.20 | 10.10 | 237433 | 426421.75 | 0.56 |
| 2 | 5.80 | 12.80 | 253376 | 426448.84 | 0.59 |
| 3 | 5.40 | 5.54 | 149404 | 425752.35 | 0.35 |
| 4 | 7.20 | 10.60 | 189017 | 426000.24 | 0.44 |
| 5 | 5.45 | 6.84 | 211306 | 424202.44 | 0.50 |
| 6 | 4.00 | 6.64 | 171632 | 425984.05 | 0.40 |
| 7 | 5.15 | 0.52 | 77545.2 | 416594.53 | 0.19 |
| 8 | 7.5 | 7.67 | 204372 | 424611.18 | 0.48 |
| 9 | 7.55 | 6.87 | 212152 | 425624.30 | 0.50 |
| 10 | 4.3 | 1.20 | 164441.7 | 422368.76 | 0.39 |
| 11 | 5.1 | 2.11 | 206161 | 425174.33 | 0.48 |
| 12 | 5.3 | 2.21 | 179913 | 422367.87 | 0.43 |

# CHAPTER 5: DISCUSSION AND CONCLUSION

## 5.1. Discussion

### 5.1.1. Timing of magmatic sills emplacement in the study area

Erroneous results obtained from the radiometric dating methods of constraining the timing, duration and the number of sill emplacement events makes it difficult to accurately date igneous intrusions in in sedimentary basins and this is a major challenge (Hansen, 2006). The radiometric dating can yield dating discrepancies of several million years (Jolley et al. 2002), because of alteration and poor sampling of sills penetrated by boreholes (Gibb & Kanaris-Sotiriou 1988).

Currently, new seismic-based technique that offers independent constraints on radiometric dating of the intruded material itself, has been proposed and widely applied along the NE Atlantic Margin (Hansen et al., 2008) and has been described by Smallwood and Maresh ., 2002), Trude et al., 2003 and Hansen and Cartwright., 2006b, who used post-intrusion sediment distribution and onlap relationships onto forced folds formed above igneous sills to constrain the timing of sill intrusion. This simple method can be used to seismically estimate the emplacement time and duration of igneous intrusions by dating the basal (oldest sediments onlapping the forced folds) and the upper boundary (youngest sediments) sediments deformed by the igneous intrusions (Trude et al. 2003 and Planke et al. 2005). Likewise, the method recommended that dating of the basal and upper boundaries of intrusion-related vents structures can be used to define the timing and duration of intrusion seismically as described by Davies et al. 2002; Svensen et al. 2004 and Planke et al. 2005 and Hansen., 2006.

Significantly, the method uses the application of seismic-stratigraphic principles to define the position of sill-related vent structures and forced folds and allows for the relative timing of individual intrusive events to be constrained even when the seismic data are poorly correlated with well data as is the case in the case-study areas (Hansen et al., 2008 and Hansen., 2006). Vents and/or intrusion-related forced folds developed at one stratigraphic level must logically predate similar structures formed at a stratigraphically shallower level and hence the latter must be associated with a later intrusive event (Hansen., 2006).

Hydrothermal vents and intrusion-related forced folds are developed at the seabed at the time of intrusion and hence their bounding surfaces mark the timing of the intrusive event. Interestingly, Horizon 8 forms the base to the majority of the interpreted hydrothermal vent structures (Fig 4.16) and forced folds in the study area. Horizon 7 marks the approximate upward bounding surface to the intrusion-related forced folds as shown in Fig. 4.17 and

reflections from Horizon 6 onlaps the fold. Deformed sediments within the folds or accompanying accommodation suggest post-depositional deformation of the Paleocene sediments. Onlapping stratigraphic layer on the forced fold suggest post deposition during Eocene as well as the upper boundaries of the intrusion-related vents in the study area. This suggests coeval intrusive activity across the study area around the time represented by the age of Horizon 7, 8 and 6. Seismic correlation indicates that the hydrothermal vents and forced-fold in the study area are confined at the base by the same stratigraphic layer (H8) and hence further supports the occurrence of a major intrusive phase near the Palaeocene–Eocene boundary. Hence, magmatic sill empalcement in the Vøring basin occurred during a number of discrete phases within the Paleocene and earliest Eocene.

According to Ren et al., 2003, the final rifting in the Vøring basin, culminated with complete lithospheric separation accompanied by massive igneous activity occurred at the Paleocene–Eocene transition (Eldholm et al., 1989) and intrusive activity in the upper crust was most intensed during Paleaocene. A major intrusive event near the Palaeocene–Eocene boundary has been documented on the Norwegian margin (Svensen et al. 2004; Planke et al. 2005) and in the central Faeroe–Shetland Basin (Davies et al. 2002; Trude et al. 2003) using seismicstratigraphic techniques (Hansen, 2006). The Eocene emplacement of sills corresponds with the opening of the Norwegian-Greenland Seas and the event is identified along the whole of the North Atlantic region as submarine and subaerial volcanic edifices, examples are plateaus, ridges, islands or volcanoes and large intrusions on the coast in and around the Vøring Basin, Møre Basin, and Jan Mayen (Osamanya et al., 2016).

### 5.1.2. Uncertainty of seismic method of dating sill emplacement events

According to Hansen, 2006, the uncertainty associated with seismic-based correlation of seismic reflections with well data has significant consequences for the precision of the emplacement ages and duration of emplacement events derived using the above technique. The major emplacement event close to the Palaeocene–Eocene boundary can be constrained to 55.8–55 Ma and 55.7–55 Ma for the Norwegian margin (Svensen et al. 2004; Planke et al. 2005) and the central Faeroe– Shetland Basin (Davies et al. 2002; Trude et al. 2003), respectively using the time scale of Hardenbol et al., 1998 (Hansen, 2006). Therefore, suggesting a likely maximum duration of this emplacement event of as much as 700–800 ka (Hansen, 2006).

Magmatic sill in the molten state may trigger the expulsion of hydrothermal fluids and sediments and these may occur soon after magma intruded into sedimentary strata (Jamtveit et al., 2004 and Hansen, 2006). Likewise, extrusion of sill-fed magmatic material would also require that the underlying feeder-sill was not solidified and was proficient of acting as a conduit for the magma (Hansen, 2006). Therefore, vents structures must be formed within the time interval between the intrusion and cooling of the feeder-sill, irrespective of their composition (Hansen, 2006). Jaeger, 1961 proposed that the cooling time for a magmatic sill is proportional to the square of the thickness of the sill and it is estimated that even very thick sills (>300 m) would solidify within <10 ka.

Finally, the uncertainty in dating the timing and duration of sill emplacement events based on seismic interpretations means that even if vent structures are bound by the same seismic horizons it is impossible to establish synchronicity between the associated intrusions as multiple successive events may be confined within a single seismically constrained interval (Hansen, 2006). According to Hansen, 2006, two separate sill emplacement events can to be positively distinguished based on seismic data alone, by separating them in time using an interval greater than the uncertainty of dating the individual events and this should be more than 100 ka.

### 5.1.3. Emplacement mechanism of magmatic sills

The emplacement of magma into the shallow crust has long been regarded as the result of mainly brittle processes, with the opening of a mode 1 tensile fracture ahead of the propagating tip of magma (Roberts 1970; Pollard 1973; Rubin 1993; Ernst et al. 2001; Malthe-Sørenssen et al. 2004; Kavanagh et al. 2006). In addition, brittle fracture mechanisms are often the basis for analogue modelling techniques employed in attempting to understand controls on intrusion Bunger et al. 2008; Mathieu et al. 2008). Although these models may be physically and mathematically valid, an increasing amount of evidence demonstrates that in high-level magmatic systems, intrusions (mainly sills) may preferentially exploit horizons of certain lithologies, often shale, that can more easily behave in a non-brittle fashion (Thomson 2007; Schofield et al. 2010). Assuming that brittle fracture processes operate at all points of igneous sheet intrusion into sedimentary basins may therefore be an oversimplification (Schofield et al. 2010; Schofield et al., 2012a)

Magmatic sills in the Voring Basin show different geometries in the major sill complexes observed in the study area, therefore, their mode of emplacement was complex. In the study area the most dominant sill geometry is the saucer shaped. Several models have been proposed regarding the emplacement mechanisms of magmatic sills. In the study emplacement mechanism has been described based on the model proposed by Thomson and Schofieild., 2008, which describes how the magmatic sills are generally emplaced in sedimentary basins. The model is supported by Malthe-Sørenssen et al.,2004 and Thomson and Hutton, 2004, who proposed the centrally-fed sill model. Both model assumes that the formation of saucer-shaped sills in an initially homogeneous basin may be explained by the effect of an asymmetrical stress field generated by the sill intrusion itself (Malthe-Sørenssen et al.,2004).

Furthermore the model assumes a surrounding elastic matrix as equivalent to the sedimentary basin. Thomson and Hutton, 2004, produced results on the 3-D geometries of saucer-shaped sills and sill complexes from the North Rockall Trough Volcanic continental margin. Their results lead them to propose a model to explain the geometry and growth of sill complexes. Their result generally supports the central feeder hypothesis of Malthe-Sørenssen et al. (2004). They suggest that each "radially symmetrical sill complex" is independently fed from a source located beneath the centre of the inner saucer ('T' junction, Fig 4.9.). In other words, this result suggests that sill complexes can be nested and could form in clusters of inter-feeding saucer-shaped sills as shown in Fig 4.14.

Radially symmetrical saucer shaped sills in Fig 4.15b are developed from a point source such as a steep magma tube from a deeper sill or a localised zone along a dyke (Thomson, 2007; Thomson and Hutton, 2004. Magma spreads laterally to produce the inner saucer and then steep magma tubes are developed at discrete points around the entire sill perimeter in order to eventually develop a complete inclined sheet. The inclined sheet then flattens when a shallower horizon(s) suitable for intrusion is encountered. However, all these phases of development may not take place or may only occur locally, producing a variety of partially developed morphologies based on the fully developed form.

Climbing saucers (Fig 4.15) in the study area are described as partial saucers. Based on radial symmetrical forms, the climbing saucers will develop when the feeder is located at the edge of a zone suitable for intrusion. For example, Sill 7 in Fig 4.9, likely to have exploited a pre-existing fault with Sill 1 only developing in the hanging wall due to the absence of the same horizon in the footwall. In such cases, a truncated inner saucer is developed and subsequently

the inclined sheet and outer rim with Sill 7, forming the limit to the sill. Once more, the sill may not contain all the morphological elements seen in the fully developed form such as Sill 1 in Fig 4.15a. Sill 7, demonstrate that faults can be utilised to facilitate climbing whilst Sill I shows that climbing can be restricted to a single point on a sill's periphery.

Finally, the sill emplacement mechanism in the study area was proposed to follow the Thomson and Schofield, 2008 model. According to Thomson and Schofield, 2008, the mechanism of the emplacement of sills takes place in four main stages below:

5.1.3.1. Stage 1 - Sill Initiation

A suitable horizon is feed through the sedimentary load by a steep magma feeder, a dyke or a steeply inclined part of sill as it is encountered below the level of neutral buoyancy, for sill propagation (Fig. 5.1a). Contact metamorphism of magma in contact with the shale will produce contact heating, which will enrich the country rock pore fluid pressures and reduce the effective stress, hence causing lateral magma intrusion to occur. In shale's, this process will encourage fluidization (Kokelaar 1982) and hydrothermal contraction of dewatered shales. The beginning stage of intrusion will continue until the additional pore pressures are released through fracturing of the roof and thickening of the quenched sill margin and is enough to hinder advance intrusion by partially insulating the magma from the unaltered country rock past the metamorphic aureole (Thomson and Schofield 2008).

5.1.3.2. Stage 2 - Sill lateral growth

Sill inflation occurs at this stage. The collective overburden thickness matching the magma pressure gives rise to the possible maximum sill thickness (Gilbert 1877; Corry 1988). According to analogy with Pollard et al. 1975, the lateral growth will be periodic, arising as a series of breakouts from the sill margin (Fig. 5.1 b and c). The viscosity of the magma and properties of the host rock will cause it to break out to spreading quickly to reach a finite length (cf. the fingers of Pollard et al. 1975). These properties are the ductility and pore fluid pressure of the country rock, the amount of volatilization and fluidization that may occur, and the ability to release excess pore fluid pressure by fracturing the overlying strata. Sill growth is repeated at several locations surrounding the sill boundary until a limiting sill width is achieved. Growth may be controlled by variations in the country rock properties, decreasing the easiness with which magma can be intruded and/or the thickness of the sill chilled margin, and prevent advance break-out and intrusion when the metamorphic aureole is enough. Instead, the magma

is averted into a steeper orientation (Stage 3) instead of following the suitable horizon for intrusion (Thomson et al., 2008).

5.1.3.3. Stage 3 - Sill climbing

Force-folding and fracturing occur in the overburdened rock due to the thickening of the sill resulting in roof uplift (Fig. 5.1d and j) (Pollard 1973; Johnson and Pollard 1973; Pollard and Johnson 1973; see also Hansen and Cartwright 2006b). Depth of sill during deformation is an important factor in this stage (Stearns, 1978), since low cohesive strength along bedding planes, essential for flexural-slip folding, becomes less of a mechanical advantage with increasing depth. The extent of shear required for slip takes place along the bedding planes increases when burial causes the normal stresses perpendicular bedding planes to increase. Subsequently, at deeper depth fracturing occurs and folding is more probable at shallow burial depths (Stearns 1978). Structures formed from the emplacement of sills depend on the depth of intrusion and the elastic nature of the host rock. Sills grow to form different structures, as at shallow depths the bending moments at the fold hinges will increase significantly forming fractures that dip towards the sill. Furthermore, at deeper depth, steep reverse faulting dipping towards the sill may be dominant. Magma climbs and exploits these fractures as the sill will normally be below the level of neutral buoyancy, magma will climb exploiting these fractures (Fig. 5.1e–g and k–m).

The whole sill boundary is not likely to ascend as one coherent sheet. Rather, fractures developing will spread individually, hence the magma is seen as a series of distinct events. This will result in the formation of a semi-continuous sheet as the individual steeply ascending magma trails merge. Note that it is likely some parts of the will not develop a climbing section. Likewise, pre-existing fractures may be exploited by the sills when they encounter them and this is the mechanically easier preference (Weertman 1980). Sill thickening is stopped when the pathway is developed since the magma has other trails to exploit and this will prevent the likelihood for inclined sheets from developing along the sill boundary where there are no development.

5.1.3.4. Stage 4: Sill flattening

This stage is similar to the sill ignition stage, where the outer rim is allowed to develop and sometimes a new concave-upward sill is formed. This stage also depends on level of the neural buoyancy or level below of the host rock and a candidate horizon with appropriate properties. This may occur at the level of neutral buoyancy or at a level below this provided that a

candidate horizon with appropriate properties is present (seen in stage one). The steep magma trails form branching network as a results of break-outs at the new level as they grow at limited number of locations during the climbing phase. These could be at a smaller scale to produce small lobes in the sill outer rim (Fig. 5.1h and n) (cf. Thomson and Hutton 2004) or a complete inner saucer for a new large sill.

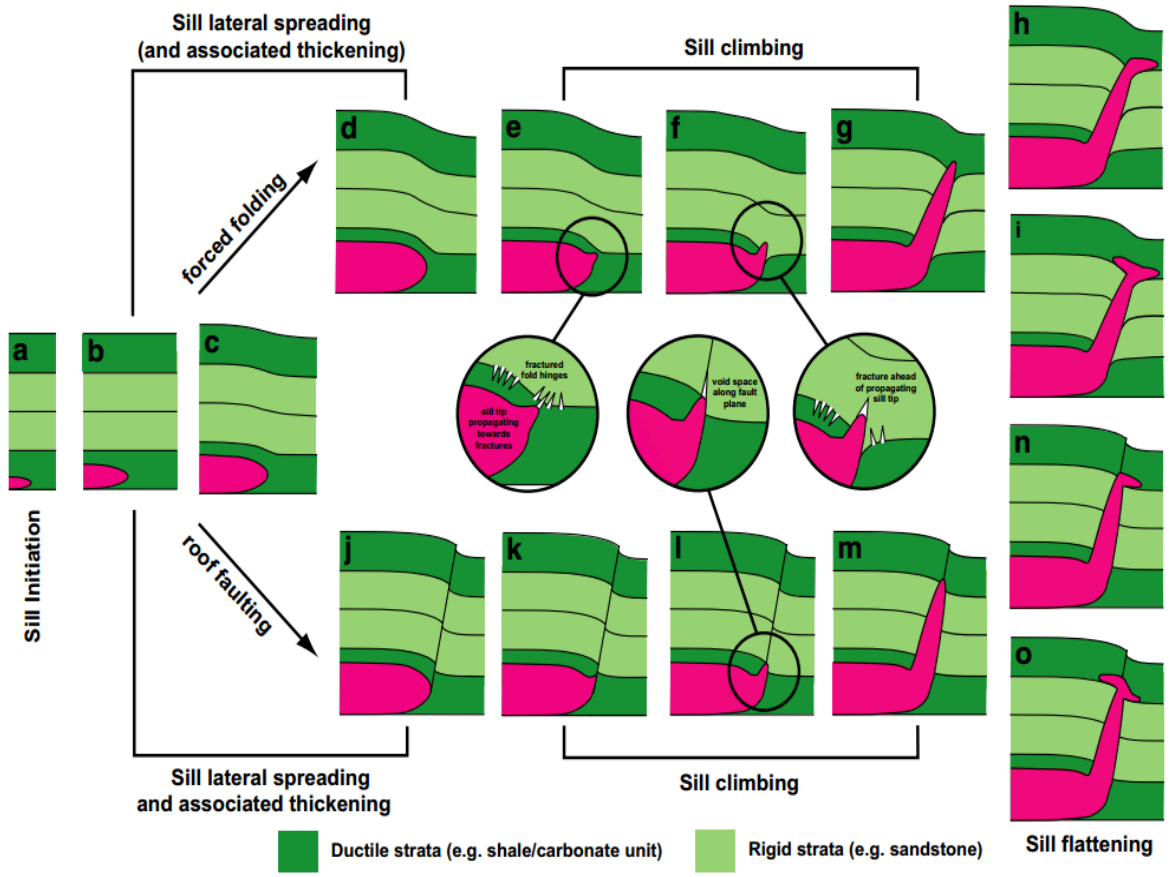


Fig. 5.1. Schematic model for the development of sill intrusions within sedimentary basins. (a) A sill initiates when magma encounters a ductile horizon such as shale. (b–d; b–j) Lateral spreading and associated thickening occur. Contact of magma with shales results in lowering the effective stress within the horizon and with potential fluidization permit spreading. Note that contact of the magma with shale will result in porosity loss thus providing some space for the intrusion to develop without the need for roof uplift. As the intrusion expands and thickens forced folding and/or faulting of the overburden occurs. (e–g; k–m) Sill climbing is initiated at discrete localities along the sill periphery when magma makes contact with either open fractures associated with forced fold hinges or a fault. (h–i; n,o) On reaching a shallower horizon suitable for intrusion the sill will flatten. This may result in the development of a flat outer rim (h and n) or symmetrical intrusion about the steep feeder (n and o) and ultimately a new radially symmetrical saucer may develop (Thomson and Schofield, 2008)

### 5.1.4. Implication of magmatic sills on hydrocarbon system

Identifying and constraining the timing of igneous intrusive bodies in sedimentary basins is critical in relation to any hydrocarbon exploration and development activities (Hansen et al., 2008). Interruption of hot magma, causing the initiation of hydrothermal systems introduce a major heat source into sedimentary basins and supplied heat may induce early maturation of hydrocarbons (Raymond and Murchison, 1988, 1991; Didyk and Simoneit, 1989; Kennish et al., 1992; Svensen et al., 2004; Hansen et al., 2008).

According to Senger et al., 2014, the melt temperature from magmatic sill emplacement is usually higher than 100°C, and sills influence the sedimentary host rock by developing contact metamorphic aureoles (Jaeger, 1959; Simoneit et al., 1978; Aarnes et al., 2010). The contact metamorphism on a local scale can change the properties of the reservoir (host rock) through a series of physical-chemical reactions (Senger et al., 2014). These reactions involve the loss of total organic carbon content (TOC) and devolatilisation, compaction and density changes, increased aromatisation and changes in the carbon isotope compositions of the residual organic material towards the contact (Aarnes et al. 2010 and Senger et al., 2014).

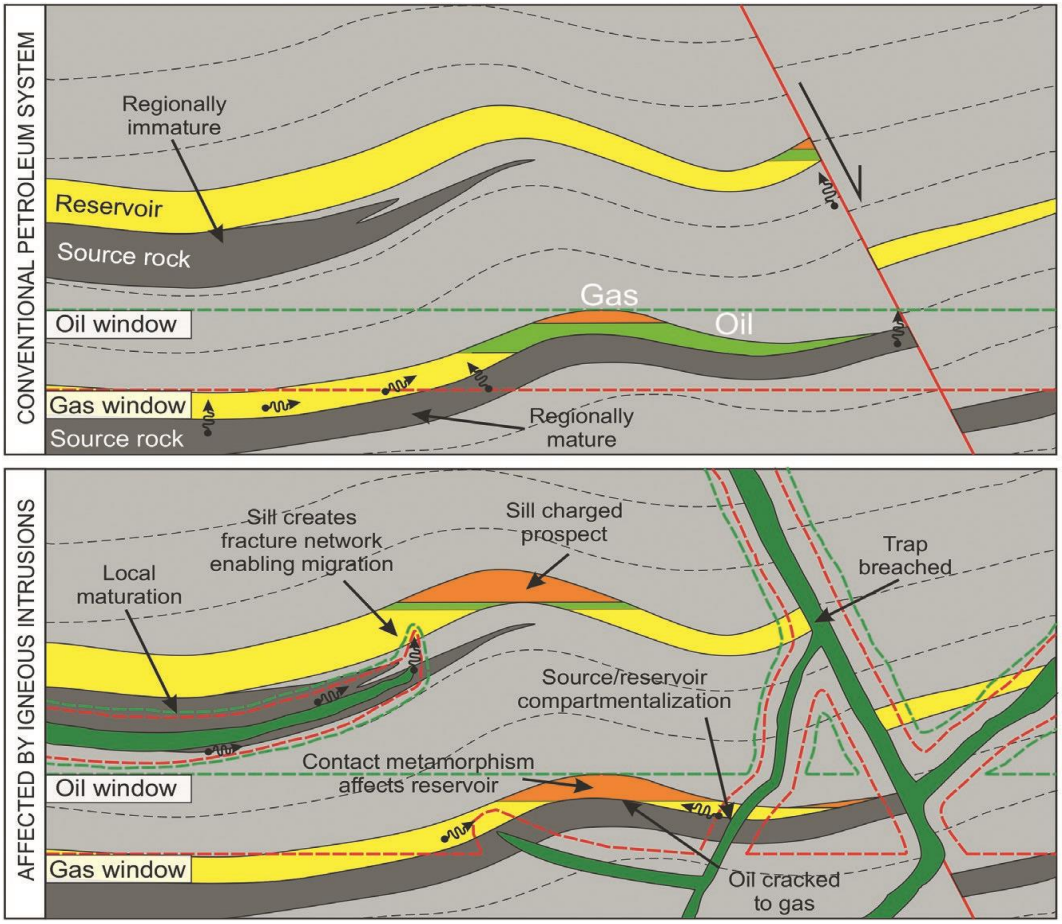


Fig. 5.2. Conventional petroleum system in the sketch above against the affected area by igneous intrusions (Senger et al., 2017)

5.1.4.1. Maturation of source rock

Magmatic sill emplacement may influence the maturation of organic matter by providing almost instantaneous high geothermal flow to the sedimentary basin (e.g. George, 1992, Aarnes et al., 2010 and Cukur et al., 2010). The quantity of heat transferred from any type of cooling of igneous intrusion whether conductive or convective of a magmatic intursion depends on the size and temperature of the igneous body (Jaeger, 1964 and Cukur et al., 2010). This is supported by an example from the modelling of the effect of intrusions in the northern Taranaki Basin, which demonstrates that the area over which hydrocarbons are produced will be influenced by the temperature, thickness and lateral extent of the magmatic intrusion, rather than by the regional geothermal gradient (Stagpoole and Funnell 2001 and Cukur et al., 2010). Nevertheless, Clift, 1999, based on modelling studies in the Faore-Shetland-Rockall region,

suggest that that regional underplating has the greatest effect on regional heat flow and the sills are only important locally.

According to Eliassen et al., 1999, four possible source rocks in the Vøring Basin are shales of Upper Jurassic, Barremian, Cenomanian / Turonian and Paleocene age and the Upper Jurassic source rock is most likely of the four to be present, but the generally great depth of burial suggests that it is likely to be post-mature with respect to oil generation. Other possible active source rocks are considered rare, with Barremian shales representing the most promising of these, while the Cenomanian/Turonian shales are the least probable (Eliassen et al., 1999). Based on basin modeling done by Eliassen et al., 1999, the main phase of structural trap development of the reservoirs (with exception of the Gjallar Ridge area to the west) occurred during the Eocene/Miocene (earlier in the Vema Dome area) and any hydrocarbon supply prior to this stage would have been lost.

An underplated body has been identified west of the Vøring Escarpment (Eliassen et al., 1999). 2D modelling and sensitivity analysis (with respect to volume of intruded material and depth of intrusion) were performed along the western margin of the basin to evaluate the degree of degree of perturbation in heat-flow associated with the emplacement of this body and the implications for the maturation history of the source rock candidates (Eliassen et al., 1999). Results from the modelling showed that the thermal anomaly associated with the underplating appeared to have been short live, hence, was reduced to about 25% of the original magnitude within 10 Ma after the emplacement of the underplated body (Eliassen et al., 1999). According to Eliassen et al., 1999, the analysis assumes instantaneous emplacement of the underplated body and may thus overestimate the thermal effect of the underplating. However, modelling of source rock maturity concluded that the thermal effects of the underplated body did not significantly influence the prospectiviity in the investigated area, therefore suggesting that the prospectivity of the Vøring basin is very poor and this is evident in the three dry wells (6607/5-2, 6607/5-1 and 6607/2-1) drilled in the study area.

#### 5.1.4.2. Reservoir and Seal

Magmatic sills, like sedimentary rocks, can develop primary and secondary porosity. Primary porosity can include cavities and fractures (Cukur et al., 2010). Emplacement, cooling and petrological properties of the magmatic sills influence the formation of primary property in these igneous bodies (Cukur et al., 2010). Secondary porosity develops by post-cooling tectonic and alteration processes (Chevallier et al., 2001, Cukur et al., 2010 and Senger et al., 2014).

These fractured magmatic sills serve as spaces for hydrocarbon entrapment and they are the most common igneous traps. A good example is the Dineh-bi-Keyah oil Field in northeastern Arizona, which relates to sill intrusion of source rock facies (Cukur et al., 2010).

Furthermore, magmatic sills can act as seals because of the alteration process that induces the filling of fractures and cavities so that the degree of primary porosity and permeability is drastically reduced (Cukur et al., 2010). Impermeable magmatic sills (fracture-free sills) intruded or penetrated into permeable sedimentary beds, block transport of hydrocarbons in these beds, resulting in the accumulation of the hydrocarbons outside the boundary of the sills (Wu et al. 2006 and Cukur et al., 2010).

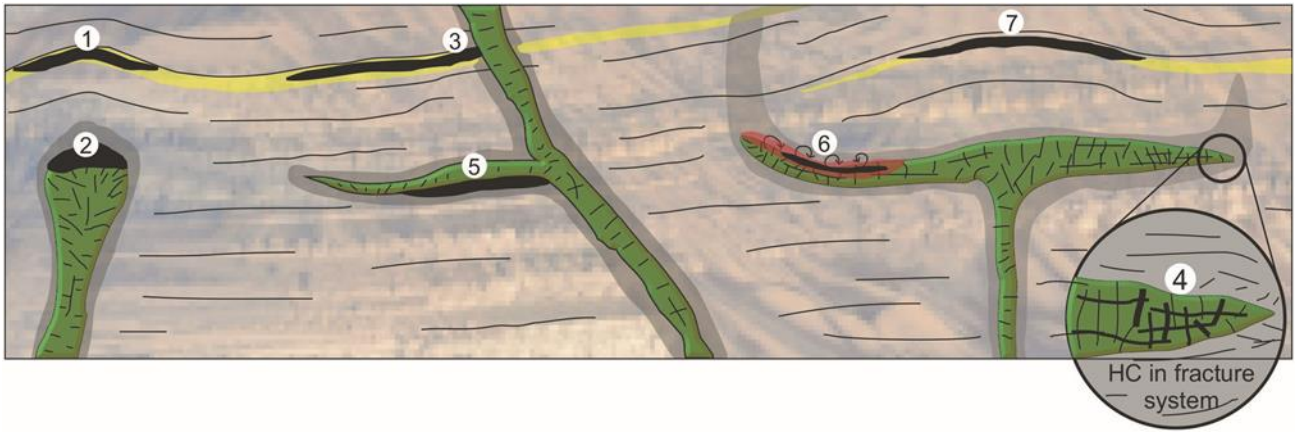


Fig. 5.3. Fractured igneous intrusion acting as a reservoir for hydrocarbon accomulation in a sedimentary basin (Senger et al., 2017)

5.1.4.3. Volcanic edifice acting as reservoirs

Generally, volcanic edifice in sedimentary basins are likely to have experienced long-term weathering that probably resulted in considerable fracture porosity (Cukur et al., 2010). Abundant cavities and fissures develop in the residues due to weathering of these volcanic rocks (Li and Kang, 1999; Cukur et al., 2010). As the weathered volcanic rocks being buried by new strata, the cavities and fissures usually occupied by diagenetic materials. Nevertheless, most of these materials are water-soluble, hence, can easily be removed by late-stage fluids, causing the recovery or even enlargement of these cavities and fissures and, thus providing significant reservoir spaces (Luo et al., 1996; Cukur et al., 2010).

According to Cukur et al., 2010, most fractured igneous or metamorphic basement rocks in many regions throughout the world have produced hydrocarbon (Aguilera, 1995; Nelson, 2001; Schutter, 2003b) and these basement reservoirs underlie a regional unconformity and almost

all lie on an uplift or high (Sircar, 2004). This uplift or high was generally continuously uplifted for long periods of geologic time and was subject to a long period of weathering and erosion (Sircar, 2004; Cukur et al., 2010). Younger sediments acting as hydrocarbon source rocks, either flank or directly overlie the basement, providing an opportunity for entrapment of hydrocarbons in basement reservoirs (Sircar, 2004; Cukur et al., 2010). Nevertheless, this is not likely in the study area because the basement complexes that underlie the regional unconformities occur at very shallow level and does not show any signs of possible weathering as shown in Fig. 4.16.

#### 5.1.4.4. Traps

Intrusion-related forced folds above saucer-shaped sills represent new potential hydrocarbon traps, developing into four-way dip closures in the overlying sediments (Hansen and Cartwright, 2006b; Jackson et al., 2013; Senger et al., 2017; Hansen, 2006). If sandstone units develop folds as part of the deformation process, these structures have the potential to form hydrocarbon traps that may subsequently be charged (Hansen and Cartwright, 2006b; Hansen, 2006). Nevertheless, the level of cementation by hydrothermal fluids is essential concerning the preserved reservoir potential in these overlying folded units, and it may be that the best play potential related to these structures are available in post-intrusion deep-water clastics that pinch-out against the folds rather than within the folded strata (Hansen, 2006).

According to Senger et al., 2017, in a given basin, intrusion-related traps are not essentially related to the overall tectonic regime, and are more locally controlled by igneous processes and subsequent geometries of intrusive bodies; therefore, different exploration strategy must be engaged when targeting such traps. Nevertheless, intrusions may also destroy pre-existing traps, deeply modifying the geologic framework. For example, migrating magma may exploit fault zones and eventually destroying fault-related structural traps (e.g., Magee et al., 2013; Schofield et al., 2016; Senger et al., 2017).

#### 5.1.4.5. Implication of hydrothermal vents

According to Hansen et al., 2008, the width of the hydrothermal aureole and thus the volume of heat-affected host-rock surrounding a magmatic sill from which hydrocarbons may be produced is approximately twice the thickness of the sill (Raymond and Murchison, 1991; Svensen et al., 2004). Hence, the movement of hydrothermal fluids implies that not only the

host sediments directly surrounding individual intrusions are affected, but any sandstone units with reservoir potential found within the affected area may have been indurated by the heat from the fluids (Hansen et al, 2008). Magmatic sill emplacement is likely to be coincident with increased heat flow within the Vøring basin as a whole.

Nevertheless, hydrothermal vent structures formed above magmatic sills may have reservoir potential since some may be made up of remobilized sands (Svensen et al., 2003; Jamtveit et al., 2004; Hansen, 2006 and Hansen et al., 2008). However, the fluid that leads to the entrainment of the sediments found within such vents is hydrothermal in origin, and normally supersaturated, and the vent sediments are hence likely to be cemented (Hansen et al., 2008).

Generally, the Norwegian Margin conduits that connect hydrothermal vents to the underlying sill complex have been found to act as fluid conduits long after (up to as much as 50 My) hydrothermal activity has ceased (Svensen et al., 2003 and Hansen et al., 2008). Therefore, most important implication of hydrothermal vent for petroleum systems may be as migration pathways for hydrocarbons (Hansen et al., 2008).

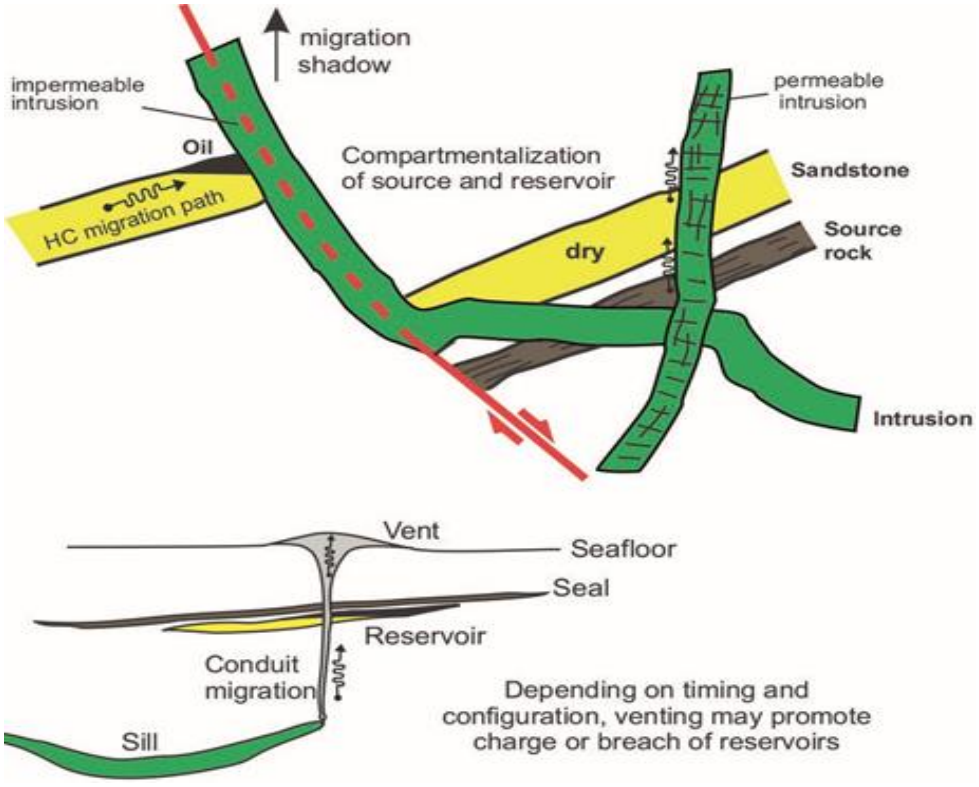


Fig. 5.4. A typical hydrothermal vent system associated with magmatic emplacement of sills. Depending on the timing and configuration, the vent may promote charge or breach reservoir (Senger et al., 2017)

## 5.2. Conclusion

The Cretaceous sediments of the Vøring Basin, Norwegian Sea, are locally intruded by several igneous sills, which are mainly Doleritic. 12 magmatic sills were interpreted in the on high resolution 3D seismic data, together with petrophysical data form wells located in the area. Sills were inrterpreted mainly in the intermediate and deep parts of the area and they were characterized based on their geometries.

Seismic-high amplitude anomalies were necessary for interpreting and characterizing the magmatic sills in the study area. Magmatic sills also show saucer-shaped geometries, transgression across strata and abrupts terminations. Magmatic sills showed complex geometries such as saucer-shape, eye-shape, layer-parallel, transgressive and fault-plane. The saucer-shaped sills dominate the intermediate levels whereas the layer-parallel dominate the deeper parts of the Vøring Basin.

Brittle fracture and ductile mechanisms were the techniques employed in attempting to understand controls on intrusions in the study area. Brittle deformation such as steps and hydrothermal vents are evident in the area, likewise, ductile deformation such as folding. Magmatic sills have preferentially exploited weak zones such as faults planes. Sills growth was through feeding of sills from a point source to form mainly radially symmetrical morphologies. Sill have exploited faults zones to form transgressive sills in the study area.

Hydrothermal vents and intrusion-related forced folds are found associated with the interpreted igneous sills and interpretation of their stratigraphic context constrains the timing of intrusion to the Late Paleocene to Earliest Eocene. The intrusive event is coincident in time with the final rifting in the Vøring basin, culminated with complete lithospheric separation accompanied by massive igneous activity occurred at the Paleocene–Eocene transition, where, intrusive activity was intensive during the Paleocene age.

Circulation of hydrothermal fluids following intrusion is likely to have affected reservoir units and have influenced fluid migration pathways within the basin. Hydrothermal vents and gas-charged sediments are proof of vertically focused and active fluid-flow in the study area. The forceful intrusion of igneous sills has produced forced folds forming potential four-way-dip traps in the overlying section and potential stratigraphic traps in the form of pinch-out of post-intrusion deep-water clastics against the folds.

**References**

Aarnes, I., Svensen, H., Connolly, J.A.D. and Podladchikov, Y.Y. 2010. How contact metamorphism can trigger global climate changes: Modeling gas generation around igneous sills in sedimentary basins. Geochimica et Cosmochimica Acta 74, 7179–7195

Allaby, A, and Allaby, M. 1999. Dictionary of Earth Sciences. Oxford University Press.

Bradley, J., 1964. Intrusion of major dolerite sills: Royal Society of New Zealand Transactions, v.3, p. 27–54.

Brooks, J., and Glennle. K. W. (eds) Petroleum Geology of NW Europe. Heyden, London, 751-763.

Badley, M. E., 1985. Practical seismic interpretation

Brekke, H., 2000. The tectonic evolution of the Norwegian Sea continental margin, with emphasis on the Voring and More basins. Special Publication-Geological Society of London, 167, 327-378.

Brekke, H., Dahlgren, S., Nyland, B., and Magnus, C., 1999. The prospectivity of the Vøring and Møre basins on the Norwegian Sea continental margin. In Geological Society, London, Petroleum Geology Conference series (Vol. 5, No. 1, pp. 261-274). Geological Society of London.

Blystad, P., Brekke, H., Færseth, R. B., Larsen, B. T., Skogseid, J., and Torudbakken, B., 1995. Structural elements of the Norwegian continental shelf. Part II: The Norwegian Sea Region. NPD-Bulletin, 8. The Norwegian Petroleum Directorate, Stavanger.

Brouwer, F. and Huck, A., 2011. An integrated workflow to optimize discontinuity attributes for the imaging of faults. Attributes: New views on seismic imaging—Their use in exploration and production: 31st Annual, pp.496-533.

Brown, A.R., 2004. AAPG Memoir 42 and SEG Investigations in Geophysics, No. 9, Chapter 6: Tuning Phenomena in Reservoirs.

Brown, L. F. and Fisher, W. L. 1980. Seismic stratigraphic interpretation and petroleum exploration, AAPG Department of Education.

Bukovics, C., and Ziegler, P. A., 1985. Tectonic development of the Mid-Norway continental margin. Marine and Petroleum Geology, 2(1), 2-22.

Chevallier, L., Goedhart, M., and Woodford, A.C., 2001. The influences of dolerite sill and ring complexes on the occurrence of groundwater in Karoo fractured aquifers: a morpho-tectonic approach. Water Resource Commission Reports, WRC Report No. 937/1/01

Chopra, S. and Marfurt, K.J., 2005. Seismic attributes for prospect identification and reservoir characterization: SEG Geophysical Development Series No. 11, 464 p.

Coffin, M. F., and Eldholm, O., 1994. Large igneous provinces: crustal structure, dimensions, and external consequences. Reviews of Geophysics, 32(1), 1-36.

Cukur, D., Horozal, S., Kim, D.C., Lee, G.H., Han, H.C. and Kang, M.H., 2010. The distribution and characteristics of the igneous complexes in the northern East China Sea Shelf Basin and their implications for hydrocarbon potential. Marine Geophysical Researches, 31(4), pp.299-313.

Dalland, A., Worsley, D. and Ofstad, K. (eds.) 1988: A lithostratigraphic scheme for the Mesozoic and Cenozoic succession offshore mid- and northern Norway. NPD-Bulletin No. 4, 65 pp.

Davies, R., Bell, B.R., Cartwright, J.A. and Shoulders, S. 2002. Three-dimensional seismic imaging of Paleogene dike-fed submarine volcanoes from the northeast Atlantic margin. Geology, 30, 223–226.

Didyk, B.M., and Simoneit, B.R.T., 1989. Hydrothermal oil of Guaymas Basin and implications for petroleum formation mechanisms. Nature 342, 65–342.

Du Toit, A.L., 1920, The Karoo Dolerites of South Africa: A study in hypabyssal injection: Geological Society of South Africa Transactions, v. 23, p. 1–42.

Eldholm, O., Thiede, J., and Taylor, E., 1989. Evolution of the Vøring volcanic margin. In O. Eldholm, J. Thiede, and E. Taylor (Eds.), (pp. 1033–1065). Proceedings of Ocean Drilling Program (ODP), Scientific Results, 104.

Eliassen P. E., Christian H., Hege M. Nordgård B. and Eirik V., 1999. Petroleum Systems of the Vøring Basin - Constraints from Basin Modelling. AAPG Search and Discovery Article International Conference and Exhibition.

George, S.C., 1992. Effect of igneous intrusion on the organic geochemistry of a siltstone and an oil shale horizon in the Midland Valley of Scotland. Organic Geochemistry, 18(5), pp.705-723.

Gernigon, L., Ringenbach, J. C., Planke, S., Le Gall, B., and Jonquet-Kolstø, H., 2003. Extension, crustal structure and magmatism at the outer Vøring Basin, Norwegian margin. Journal of the Geological Society, 160(2), 197-208.

Gibb, F.G.F., and Kanaris-Sotiriou, R., 1988, The geochemistry and origin of the Faeroe-Shetland sill complex, in Morton, A.C., and Parson, L., eds.,Early Tertiary volcanism and the opening of the northeast Atlantic: Geological Society [London] Special Publication 39, p. 241–252.

Hansen, D.M., 2006. The morphology of intrusion-related vent structures and their implications for constraining the timing of intrusive events along the NE Atlantic margin. Journal of the Geological Society, 163(5), pp.789-800.

Hansen, D.M., Cartwright, J., 2006b. The three-dimensional geometry and growth of forced folds above saucer-shaped igneous sills. Journal of Structural Geology 28, 1520–1525.

Hansen, D.M., Cartwright, J.A., and Thomas, D., 2004, 3D seismic analysis of the geometry of igneous sills and sill junction relationships, in Davies, R.J., et al., eds., 3D seismic technology: Application to the exploration of sedimentary basins: Geological Society of London Memoir 29, p. 199–208

Hansen, D.M., Redfern, J., Federici, F., Di Biase, D. and Bertozzi, G., 2008. Miocene igneous activity in the Northern Subbasin, offshore Senegal, NW Africa. Marine and Petroleum Geology, 25(1), pp.1-15.

Hardenbol, J.A.N., Thierry, J., Farley, M.B., Jacquin, T., De Graciansky, P.C. and Vail, P.R., 1998. Mesozoic and Cenozoic sequence chronostratigraphic framework of European basins.

Herron, D. A. First Steps in Seismic Interpretation

Holford, S., Schofield, N., MacDonald, J., Duddy, I. and Green, P., 2012. Seismic analysis of igneous systems in sedimentary basins and their impacts on hydrocarbon prospectivity: Examples from the southern Australian margin. The APPEA Journal, 52(1), pp.229-252.

Isaksen, D. and Tonstad, K. (eds.) 1989: A revised Cretaceous and Tertiary lithostratigraphic nomenclature for the Norwegian North Sea. NPD-Bulletin No. 5, 59 pp.

Jaeger, J.C. 1959: Temperatures outside a cooling intrusive sheet. American Journal of Science 257, 44–54.

Jamtveit, B., Svensen, H., Podladchikov, Y.Y., Planke, S., 2004. Hydrothermal vent complexes associated with sill intrusions in sedimentary basins. In: Breitkreuz, C., Petford, N. (Eds.), Physical Geology of High-Level Magmatic Systems, Geological Society, London, Special Publications 234, pp. 233–241.

Jinglan, L., Zhihao, Q., Wei, S. and Fazhan, S., 1996. The relations between lithofacies, reservoir lithology and oil and gas of volcanic rocks in Fenghuadian area. Acta Petrolei Sinica, 17(1), pp.32-39.

Jolley, D.W., Clarke, B., and Kelley, S., 2002. Paleogene time scale miscalibration: evidence from the dating of North Atlantic igneous province. Geology, 30, 7–10.

Jones, S.F., Wielens, H., Williamson, M.C. and Zentilli, M., 2007. Impact of magmatism on petroleum systems in the Sverdrup Basin, Canadian Arctic Islands, Nunavut: a numerical modelling study. Journal of Petroleum Geology, 30(3), pp.237-256.

Kennish, M.J., Lutz, R.A., Simoneit, B.R.T., 1992. Hydrothermal activity and petroleum generation in the Guaymas Basin. Reviews in Aquatic Sciences 6, 467–477.

Li, C. and Kang, R.H., 1999. Genetic types of reservoir spaces of igneous rocks in the Luo 151 block. Jiyang sag (in Chinese with English abstract): Geological Review, 45, pp.599-604.

Lister, J. and Kerr, R. 1991. Fluid-mechanical models of crack propagation and their application to magma transport in dykes. Journal of Geophysical Research, 96, 10049-10077

Lundin, E. R. and Dore, A. G. 1997. A tectonic model for the passive margin between the Rockall Trough and the Lofotens: Early Cretaceous to break-up. Journal of the Geological Society, London, **154,** 545-550.

Magee, C., Jackson, C.A.L., and Schofield, N., 2013c, The influence of normal fault geometry on igneous sill emplacement and morphology: Geology, v. 41, p. 407–410

Magee, C., Maharaj, S.M., Wrona, T., and Jackson, C.A.L., 2015, Controls on the expression of igneous intrusions in seismic reflection data: Geosphere, v. 11, p. 1024–1041

Magee, C., Muirhead, J.D., Karvelas, A., Holford, S.P., Jackson, C.A., Bastow, I.D., Schofield, N., Stevenson, C.T., McLean, C., McCarthy, W., 2016. Lateral magma flow in mafic sill complexes. Geosphere 12, 809-841.

Malthe-Sørenssen, A., Planke, S., Svensen, H., and Jamtveit, B., 2004. Formation of saucer shaped sills. In: Breitkreuz, C. & Petford, N. (eds) Physical Geology of High-Level Magmatic Systems. Geological Society, London, Special Publications, 234, 215–227.

Mathieu, L., Burchardt, S., Troll, V.R., Krumbholz, M., and Delcamp, A., 2015, Geological constraints on the dynamic emplacement of cone-sheets—The Ardnamurchan cone-sheet swarm, NW Scotland: Journal of Structural Geology, v. 80, p. 133–141

Monreal, F. R., Villar, H. J., Baudino, R., Delpino, D., and Zencich, S., 2009. Modeling an atypical petroleum system: a case study of hydrocarbon generation, migration and accumulation related to igneous intrusions in the Neuquen Basin, Argentina. Marine and Petroleum Geology, 26(4), 590-605.

Mudge. D. C. and Rashid. B. 1987. The geology of the Faroe Basin area

NPD, 2017. NPD fact page.

Njone, I, 2014. Hydrothermal vent Activities At the Gjallar Ridge In the Vøring Basin, mid-Norway (Master's thesis, UiT Norges arktiske universitet).

Omosanya, K., Johansen, S., Abrahamson, P., 2016. Magmatic activity during the breakup of Greenland-Eurasia and fluid-flow in Stappen High, SW Barents Sea. Marine and Petroleum Geology 76, 397-411.

Omosanya, K.O., Johansen, S.E., Eruteya, O.E., Waldmann, N., 2017. Forced folding and complex overburden deformation associated with magmatic intrusion in the Vøring Basin, offshore Norway. Tectonophysics 706, 14-34.

Patel, D., Bruckner, S., Viola, I. and Gröller, E.M., 2010, March. Seismic volume visualization for horizon extraction. In Visualization Symposium (PacificVis), 2010 IEEE Pacific (pp. 73-80). IEEE.

Pigott, J.D., Kang, M.H., and Han, H.C., 2013. First order seismic attributes for clasticseismic facies interpretation: Examples from the East China Sea. Journal of Asian Earth Sciences, v.66, 34-54

Planke, S., Jamtveit, B., Malthe-Sørenssen, A., Myklebust, R., Svensen, H., Rasmussen, T., and Berndt, C., 2003. Volcanic Processes and Deposits on Rifted Margins and in Sedimentary Basins. In 8th International Congress of the Brazilian Geophysical Society.

Planke, S., Rasmussen, T., Rey, S., Myklebust, R., 2005. Seismic characteristics and distribution of volcanic intrusions and hydrothermal vent complexes in the Vøring and Møre basins, Geological Society, London, Petroleum Geology Conference series. Geological Society of London, pp. 833- 844.

Planke, S., Alvestad, E. and Eldholm, O., 1999. Seismic characteristics of basaltic extrusive and intrusive rocks. The Leading Edge, 18(3), pp.342-348.

Pollard, D.D., and Johnson, A.M., 1973, Mechanics of growth of some laccolithic intrusions in the Henry Mountains, Utah: II. Bending and failure of overburden layers and sill formation: Tectonophysics, v. 18, p. 311–354

Raum, T., Mjelde, R., Digranes, P., Shimamura, H., Shiobara, H., Kodaira, S., and Thorbjørnsen, T. (2002). Crustal structure of the southern part of the Vøring Basin, mid-Norway margin, from wide-angle seismic and gravity data. Tectonophysics, 355(1), 99-126.

Raymond, A.C., Murchison, D.G., 1988. Development of organic maturation in the thermal aureoles of sills and its relation to sediment compaction. Fuel 67, 1599–1608.

Ren, S., Faleide, J. I., Eldholm, O., Skogseid, J., and Gradstein, F., 2003. Late Cretaceous–Paleocene tectonic development of the NW Vøring basin. Marine and Petroleum Geology, 20(2), 177-206.

Rohrman, M., 2007. Prospectivity of volcanic basins: Trap delineation and acreage de-risking. AAPG bulletin, 91(6), pp.915-939.

Schofield, N., 2009. Linking sill morphology to emplacement mechanisms (Doctoral dissertation, University of Birmingham

Schofield, N., Stevenson, C. and Reston, T. 2010. Magma fingers and host rock fluidization in the emplacement of sills. Geology, 38, 63–66.

Schofield, N.J., Brown, D.J., Magee, C. and Stevenson, C.T., 2012. Sill morphology and comparison of brittle and non-brittle emplacement mechanisms. Journal of the Geological Society, 169(2), pp.127-141.

Schutter, S.R., 2003. Hydrocarbon occurrence and exploration in and around igneous rocks, in Petford, N., and Mccaffrey, K.J.W. (Eds), Hydrocarbons in Crystalline Rocks: Geological Society of London Special Publication, 214, 7–33.

Schutter, S.R. 2003a. Hydrocarbon occurrence and exploration in and around igneous rocks. In Petford, N., and McCaffrey, K.J.W. (eds), Hydrocarbons in Crystalline Rocks. Geological Society of London Special Publications, 214, 7-33. In Petford, N. & McCaffrey, K.J.W. (eds), Hydrocarbons in Crystalline Rocks. Geological Society of London Special Publications, 214, 7-33.

Schutter, S.R. 2003b. Occurrences of hydrocarbons in and around igneous rocks. In Petford, N. & McCaffrey, K.J.W. (eds), Hydrocarbons in Crystalline Rocks. Geological Society of London Special Publications, 214, 35-68.

Senger, K., Planke, S., Polteau, S., Ogata, K. and Svensen, H., 2014. Sill emplacement and contact metamorphism in a siliciclastic reservoir on Svalbard, Arctic Norway. Norwegian Journal of Geology/Norsk Geologisk Forening, 94.

Senger, K., Millett, J., Planke, S., Ogata, K., Eide, C.H., Festøy, M., Galland, O. and Jerram, D.A., 2017. Effects of igneous intrusions on the petroleum system: a review. First Break, 35(6), pp.47-56.

Sheriff, R. E. 2002. Encyclopedic dictionary of applied geophysics. Society of Exploration Geophysicists Tulsa, OK.

Sheriff, Robert E., and Lloyd P. Geldart. Exploration seismology. Cambridge university press, 1995.

Simm, R., Bacon, M. and Bacon, M. 2014. Seismic Amplitude: An interpreter's handbook, Cambridge University Press.

Simoneit, B.R.T., Brenner, S., Peters, K.E. & Kaplan, I.R. 1978: Thermal alteration of cretaceous Black Shale by basaltic intrusions in Eastern Atlantic. Nature 273, 501–504.

Skogly, O. P., 1998. Seismic characterization and emplacement of intrusives in the Vøring Basin [Ph. D. thesis]. University of Oslo.

Skogseid, J., Pedersen, T., Eldholm, O., Larsen, B.T., 1992. Tectonism and magmatism during NE Atlantic continental break-up: the Vøring Margin. Geological Society, London, Special Publications 68, 305-320.

Smallwood, J.R., Maresh, J., 2002. The properties, morphology and distribution of igneous sills: modelling, borehole data and 3D seismic from the Faroe-Shetland area. Geological Society, London, Special Publications 197, 271-306.

Spacapan, J. B., Galland, O., Leanza, H. A., and Planke, S., 2016. Igneous sill and finger emplacement mechanism in shale-dominated formations: a field study at Cuesta del Chihuido, Neuquén Basin, Argentina. Journal of the Geological Society, 174(3), 422-433.

Stagpoole, V. and Funnell, R., 2001. Arc magmatism and hydrocarbon generation in the northern Taranaki Basin, New Zealand. Petroleum Geoscience, 7(3), pp.255-267.

Stearns, D.W., 1978, Faulting and forced folding in the Rocky Mountain foreland, in Matthews, V.I., ed., Laramide folding associated with basement block faulting in the western United States: Geological Society of America Memoir 151, p. 1–38.

Subrahmanyam, D., Rao, P., 2008. Seismic attributes–A review, 7th International Conference & Exposition on Petroleum Geophysics, Hyderabad, pp. 398-404.

Svensen, H., Jamtveit, B., Planke, S., Chevallier, L., 2006. Structure and evolution of hydrothermal vent complexes in the Karoo Basin, South Africa. Journal of the Geological Society 163, 671-682.

Svensen, H., Planke, S., Jamtveit, B., Pedersen, T., 2003. Seep carbonate formation controlled by hydrothermal vent complexes: a case study from the Vøring Basin, the Norwegian Sea. GeoMarine Letters 23, 351-358.

Svensen, H., Planke, S., Malthe-Sørenssen, A., Jamtveit, B., Myklebust, R., Eidem, T.R., and Rey, S.S., 2004. Release of methane from a volcanic basin as a mechanism for initial Eocene global warming. Nature 429, 542-545.

Thomson, K., 2007. Determining magma flow in sills, dykes and laccoliths and their implications for sill emplacement mechanisms. Bulletin of Volcanology, 70(2), pp.183-201.

Thomson, K., and Hutton, D., 2004. Geometry and growth of sill complexes: Insights using 3D seismic from the North Rockall Trough. Bulletin of Volcanology, 66, 364–375

Thomson, K., and Schofield, N., 2008. Lithological and structural controls on the emplacement and morphology of sills in sedimentary basins. In: Thomson, K. & Petford, N. (eds) Structure and emplacement of high-level magmatic systems. Geological Society, London, Special Publications, 302, 31–44.

Trude, J., Cartwright, J., Davies, R.J. and Smallwood, J., 2003. New technique for dating igneous sills. Geology, 31(9), pp.813-816.

Walker, G. P. L. 1975. A new concept of the evolution of the British intrusive centres. Journal of the Geological Society', London, 131, 121-141.

Widess, M., 1973, How thin is a thin bed?: Geophysics, v. 38, p. 1176–1180, doi: 10 .1190 /1 .1440403

Wu, C., Gu, L., Zhang, Z., Ren, Z., Chen, Z. and Li, W., 2006. Formation mechanisms of hydrocarbon reservoirs associated with volcanic and subvolcanic intrusive rocks: Examples in MesozoicCenozoic basins of eastern China. AAPG bulletin, 90(1), pp.137-147.

Vail, P. R. & Mitchum, R. M. 1977. Seismic stratigraphy and global changes of sea level, 1, Overview. In: American Association of Petroleum Geologists, Memoir, 26, 21–52.

Yilmaz, Öz. Seismic data analysis: Processing, inversion, and interpretation of seismic data. Society of exploration geophysicists, 2001.